

Applications of Heavy Quark Methods

DISSERTATION

zur Erlangung des akademischen Grades eines
Doktor der Naturwissenschaften
(Dr. rer. nat.)

vorgelegt von
Rebecca Klein, M.Sc.

eingereicht bei der
Naturwissenschaftlich-Technischen Fakultät
der Universität Siegen

Siegen, Januar 2018

Gutachter der Dissertation: Prof. Dr. Thomas Mannel
Prof. Dr. Alexander Khodjamirian
Datum der Disputation: 16.02.2018

gedruckt auf alterungsbeständigem holz- und säurefreiem Papier

Zusammenfassung

Zur Berechnung von Prozessen im Standardmodell der Elementarteilchenphysik (SM) werden sogenannte Effektive Feldtheorien (EFT) verwendet. Somit ist es möglich Korrekturen systematisch zu behandeln. Eine EFT ist die Heavy Quark Effective Theory (HQET), welche ausnutzt, dass im Grenzwert der schweren Quarkmasse $m_Q \rightarrow \infty$ eine Spin- sowie Flavor-Symmetrie auftritt. In dieser Arbeit werden drei Anwendungen von HQET präsentiert.

Zuerst wird das ‘1/2 vs. 3/2’-Puzzle behandelt. Hier wird eine Spannung zwischen den Vorhersagen in der Theorie und den experimentellen Messungen von semileptonischen Zerfällen von B -Mesonen in orbital angeregte D -Mesonen beobachtet. Für letztere existieren vier verschiedene Zustände, die in zwei Spin-Symmetrie-Doublets angeordnet werden können, welche durch den Gesamtdrehimpuls ihrer leichten Freiheitsgrade $j = 1/2$ und $j = 3/2$ klassifiziert werden können. Zieht man den Spin des schweren Quarks in Betracht, so können die Zustände im $j = 1/2$ Doublet einen Gesamtdrehimpuls von 0 und 1 erhalten und die Zustände im $j = 3/2$ Doublet 1 und 2. Von Seiten der Theorie erwartet man, dass die Zerfallsraten der Zustände mit $j = 3/2$ signifikant größer sind als die für $j = 1/2$. Im Experiment werden jedoch Zerfallsraten gemessen die ungefähr gleich groß sind. In dieser Arbeit wird untersucht, ob eine Mischung der beiden Zustände mit einem Gesamtdrehimpuls von 1 diese Spannung auflösen kann.

Ein anderer Aspekt von Mischung kann im B - \bar{B} -System beobachtet werden. Hier wird die Massendifferenz zwischen den B - und \bar{B} -Zuständen durch das Matrixelement des effektiven lokalen Vier-Quark-Operators bestimmt. Für die Berechnung dieses Matrixelements wird ein ‘Bag-Parameter’ eingeführt der in naiver Faktorisierung Eins ist. Jede Abweichung von Eins rührt von nicht-faktorisierenden Beiträgen her. Der Bag-Parameter kann mit Hilfe der etablierten Methode der Summenregeln im Kontext von HQET bestimmt werden. Im Falle der nicht-faktorisierenden Beiträge erfordert dies die Berechnung von Drei-Schleifen-Diagrammen. Die präsentierte Rechnung komplettiert das Next-to-Leading-Order-Resultat für den Bag-Parameter.

Eine weitere Anwendung von HQET ist QCD-Faktorisierung, welche kürzlich auf Dreikörper-Zerfälle erweitert wurde. In dieser Arbeit wird CP-Verletzung im Zerfall $B \rightarrow \pi\pi\pi$ in diesem Rahmen untersucht. In experimentellen Daten wird eine komplexe Struktur von großen lokalen CP-Asymmetrien beobachtet. Es wird ermittelt, ob diese Struktur mit der Methode der QCD-Faktorisierung erklärt werden kann. Auch wenn ein paar Verfeinerungen nötig sind, können die groben Merkmale der gemessenen CP Asymmetrie innerhalb des Modells reproduziert werden.

Abstract

For the computation of processes in the Standard Model of Elementary Particle Physics (SM), so-called effective field theories (EFTs) are used. In this way, it is possible to treat corrections systematically. One EFT is the Heavy Quark Effective Theory (HQET), which exploits the fact that in the heavy quark mass limit $m_Q \rightarrow \infty$, a spin as well as a flavor symmetry appears. In this thesis, three applications of HQET are presented.

First, the ‘ $1/2$ vs. $3/2$ ’ puzzle is addressed. Here, a tension between the theory prediction and the experimental measurement of semileptonic decays of B mesons into orbitally excited D mesons is observed. For the latter, four different states exist that can be arranged into two spin-symmetry doublets, which are classified by the total angular momentum of their light degrees of freedom $j = 1/2$ and $j = 3/2$, respectively. Taking into account the spin of the heavy quark, the states in the $j = 1/2$ doublet can have a total angular momentum of 0 and 1 and the states in the $j = 3/2$ doublet 1 and 2. From theory, it is expected that the rates for the decays into the states with $j = 3/2$ are significantly larger than the ones for $j = 1/2$. In experiments, however, the measured decay rates are roughly the same. In this thesis, it is investigated if a mixing of the two states with a total angular momentum of 1 can ease this tension.

Another aspect of mixing can be observed in the B - \bar{B} system. Here, the mass difference between the B and \bar{B} states is determined by the matrix element of the effective local four-quark operator. For the computation of this matrix element a ‘bag parameter’ is introduced which is unity in naive factorization. Any deviation from unity stems from non-factorizable contributions. The bag parameter can be obtained using the established method of sum rules in the context of HQET, which requires the calculation of three-loop diagrams in the case of the non-factorizable contributions. The presented computation completes the next-to-leading order result for the bag parameter.

A further application of HQET is QCD factorization, which has recently been extended to three-body decays. In this thesis, CP violation in the decay $B \rightarrow \pi\pi\pi$ is studied in that framework. In experimental data, a rich structure of large local CP asymmetries has been observed. It is investigated if this structure can be explained within the QCD factorization approach. Even though some refinement is required, the rough features of the observed CP asymmetry can be reproduced within this model.

Contents

1	Introduction	1
2	Standard Model of Particle Physics	5
2.1	Gauge Group of the Standard Model	5
2.2	The CKM Matrix	7
2.3	CP Violation	11
2.4	Quantum Chromodynamics	11
3	Heavy Quark Expansion	15
3.1	Heavy Quark Limit	16
3.1.1	Derivation of the Effective Lagrangian	16
3.1.2	Feynman Rules in HQET	19
3.2	Heavy Quark Symmetry	19
3.2.1	Form Factors in Weak Decays	20
3.2.2	Further Features in HQET	22
3.3	Renormalization	23
3.3.1	On-Shell Renormalization	23
3.3.2	Quark Self-Energy	25
3.3.3	Composite Operators	27
3.4	Matching of the Four-Quark Operator	30
3.4.1	Four-Quark Operator	30
3.4.2	Perturbative Corrections	32
3.4.3	Matching	33
3.4.4	Running of the Four-Quark Operator	34
4	D^{**} Spectroscopy and $B \rightarrow D^{**}\ell\nu$	35
4.1	Spectroscopy	36
4.2	Power Corrections to the HQET Hamiltonian	37
4.3	Extracting the Mixing Angle	39
4.4	Fitting the Mixing Angle	42
4.5	Effects on Semileptonic Decays $B \rightarrow D^{**}\ell\nu$	43
4.6	Effects on the Widths of the Orbitaly Excited States	48
4.7	Discussion	49

5	$B - \bar{B}$-Mixing	51
5.1	Overview	52
5.2	Bag Parameter	55
5.2.1	Matching of the Bag Parameter	55
5.2.2	Running of the Bag Parameter	57
5.3	Calculation	58
5.3.1	Perturbative Contribution	58
5.3.2	Quark Condensates	63
5.3.3	Sum Rule	66
5.4	Result	70
5.5	Discussion	71
6	CP Violation in Three-Body Decays	73
6.1	QCD Factorization	74
6.1.1	Two-Body Decays	74
6.1.2	Three-Body Decays	76
6.2	QCD-factorized Effective Hamiltonian	79
6.3	Non-Perturbative Input	79
6.3.1	Pion Decay Constant and Pion Form Factor	80
6.3.2	$B \rightarrow \pi$ Form Factors	81
6.3.3	$B \rightarrow \pi\pi$ Form Factors	81
6.4	Calculation of the Amplitude	86
6.5	CP Violation	88
6.6	Charm Resonance Model	89
6.7	Discussion	92
7	Summary and Conclusion	95
	Appendix	97
A	Fierz Transformations	99
B	Details on D^{**} Spectroscopy and $B \rightarrow D^{**}\ell\nu$	101
B.1	Spin Wave Functions	101
B.2	Mixing of the 1^+ States	103
B.3	Details On The Fit	105
C	Details on $B-\bar{B}$ Mixing	109
C.1	Loop Integrals	109
C.2	Master Integrals	109
C.2.1	Perturbative Contribution	109
C.2.2	Quark Condensate Contribution	112

D	Details on CP Violation in Three-Body-Decays	113
D.1	Dalitz Distribution	113
D.2	Calculation of the QCD-Factorized Effective Hamiltonian	116
D.3	New Non-Perturbative Input	118
D.3.1	Generalized Form Factor	119
D.3.2	Two-Pion Generalized Distribution Amplitude (GDA)	119
D.4	Calculation of the Amplitude for $B \rightarrow \pi\pi\pi$	120
D.5	Computation of the Helicity Angle θ_π	122
	Bibliography	125

1. Introduction

Already the ancient Greek engaged with the question what we are made of and why we are here. Nowadays, we have come a long way to answer these questions. We have a much more profound understanding what matter is made of, namely a small number of fundamental particles. The beginning of elementary particle physics can be dated back to 1897 when Thomson discovered the electron [1]. A further milestone was the realization by Gell-Mann and Zweig in 1964 that hadrons are composed of quarks [2, 3]. Today, a whole zoo of particles is known that are composed of these fundamental building blocks.

Not only the composition of matter is of interest, but also the way the fundamental particles interact. In the 1960s, the Glashow-Salam-Weinberg model [4–6] was established which unifies electromagnetic and weak interactions. From this model, together with the quantum-field-theoretical description of strong interactions, the Standard Model of Particle Physics (SM) emerged. It became widely accepted after the discovery of the W and Z bosons at CERN in 1983. Predictions for decays and scattering processes can be made using the SM which can be investigated by experiments. In turn, experimental observations are subject to be explained by theory.

Some of the parameters in the SM cannot be predicted by theory, though. Neglecting neutrino masses and thus mixing in the lepton sector, there are 18 free parameters that need to be determined experimentally: 6 quark masses, 3 charged-lepton masses, 3 gauge couplings, 2 parameters from the Higgs potential and finally 4 Cabibbo-Kobayashi-Maskawa (CKM) quark flavor mixing parameters. The latter only occur in weak transitions of quarks and can be over-constrained by different independent processes. This is necessary to test the SM. Discrepancies would be a sign for physics beyond the SM (BSM), so-called “new physics” (NP).

The SM admittedly has some limitations. Even though there are four fundamental interactions, only three of them are implemented. Gravity is missing, which is due to the lack of an adequate description of general relativity as a quantum field theory (QFT). Moreover, neutrinos are massless in the SM. This is in contradiction with the observation of neutrino oscillation, which is only possible when neutrinos have a non-zero mass. Furthermore, from cosmological studies we assume that our universe consists only to about 5% of our known matter. The SM cannot explain the remaining 95%, namely dark matter and dark energy. In addition, the amount of matter in the universe greatly exceeds the one of anti-matter, the so-called baryon asymmetry. They should have been produced in equal amounts at the big bang,

though. Sakharov [7] formulated three conditions for an asymmetry to occur: thermal disequilibrium, violation of Baryon number and the violation of invariance under charge conjugation (C) as well as combined with parity (P) transformations. The SM does provide an explanation for the latter. However, the only established source of CP violation in the SM, the phase of the CKM matrix, cannot predict the required size of this asymmetry. This issue could be solved by possible additional sources of CP violation in BSM models. Another essential question is, why we particularly observe three generations of leptons and quarks and why their masses span so many orders of magnitude. Moreover, the origin of the hierarchy problem, that the electroweak scale is much smaller than the Planck scale, is unexplained.

After the discovery of the b quark in 1977, the CKM mixing matrix became an established component of the SM. The B mesons, which consist of one b quark, turned out to be quite heavy compared to the quarks which were already known. They have a long lifetime and in 1987 a substantial $B - \bar{B}$ mixing rate was found by ARGUS at DESY. The mixing induces a CP asymmetry which is about two orders of magnitudes higher than in the K system. To observe CP violation in B decays much larger data samples on B mesons were required which called for B factories such as BaBar and Belle. Until then, experiments concentrated on the gauge sector of the SM. The greatest achievement of the LEP collider at CERN was the measurement of the Z -line shape and the consequential number of 3 neutrinos with vanishingly small masses. Nowadays, a great focus lies on the Yukawa sector and, with the LHC put into operation, high p_T and the search for new physics.

In this thesis we will present three different projects with a technical, phenomenological or conceptual focus. The former is related to the fact that we have reached an era of high experimental precision, especially with LHC Run II and Belle II starting soon. Therefore, also precise SM predictions are required. In this context, we will compute the missing non-factorizable next-to-leading order results for the bag factor for $B - \bar{B}$ mixing. This requires the computation of three-loop diagrams. These are computed in Heavy Quark Effective Theory (HQET) which simplifies the calculation a lot.

In the SM there are a couple of more soft spots where tensions between experimental measurements and theoretical predictions are observed, all of them in the quark and lepton flavor sector. One example is the ‘1/2 vs. 3/2’ puzzle. Here, we would expect a significant difference of the branching fraction for semileptonic decays of a B meson into the respective orbitally excited D mesons with total angular momentum of 1^+ . This is in contradiction to experimental results, where the two branching fractions are roughly equal. This does not necessarily need to be a sign for new physics. In this thesis we attempt to explain the data by investigating the impact of the mixing of these two states on the branching fraction.

Another puzzling experimental observation which requires theoretical attention are

large local CP asymmetries especially in the decay $B \rightarrow \pi\pi\pi$. Theoretical approaches are still in their infancy. We use a recently developed approach in the framework of QCD (Quantum Chromodynamics) factorization in order to obtain a data-driven model. From this we obtain a Dalitz distribution for the CP asymmetry to see if we can reproduce the rough features that were observed by the experiment.

The thesis is organized as follows. First, we will give a brief introduction to the Standard Model of Particle Physics in Chapter 2. Then, we will roughly outline the aspects of Heavy Quark Effective Theory in Chapter 3. Chapter 4 will deal with the $1/m$ corrections for orbitally excited D mesons, the resulting mixing of the states with total angular momentum 1^+ and its effect on the semileptonic branching fractions and their widths. Non-factorizable contributions to the bag parameter, which are of interest when dealing with $B - \bar{B}$ mixing are computed in the next Chapter 5. In the following Chapter 6, we investigate the local CP asymmetries in the decay $B \rightarrow \pi\pi\pi$ within the QCD factorization framework. In the last Chapter 7 we summarize and draw our conclusions.

2. Standard Model of Particle Physics

The elementary particles and their electromagnetic, strong and weak interactions are described within the Standard Model of Particle Physics. Here, we distinguish between fundamental fermions and bosons. For the former we differentiate between leptons and quarks whose different types we call flavor. There are six of them, respectively, which are assigned to three different generations (or families) as shown in Table 2.1. For the quarks we have the flavors up (u), down (d), strange (s), charm (c), bottom (b) and top (t). The six leptons are the electron (e), muon (μ) and tau (τ) with the corresponding massless neutrinos ν_e , ν_μ and ν_τ . In addition, there exist anti-particles to the fundamental fermions with equal mass but opposite internal quantum numbers compared to the respective particle.

The interactions are described through local gauge symmetries and are mediated by gauge bosons which are vector particles. The weak interaction is mediated by the Z^0 and the W^\pm bosons. All fermions in the SM are subject to the weak interaction. Electromagnetic interactions are mediated by photons γ which couple only to the electrically charged particles. Solely the quarks interact strongly since they are the only fundamental fermions that carry color charge. Strong interactions are mediated by 8 gluons g . As a consequence of spontaneous symmetry breaking we also obtain the Higgs boson H . It was the last missing piece of the SM for quite some time until its discovery in 2012 and to date it is the only known fundamental scalar particle.

A general overview of quantum field theory and the standard model can be found in the pertinent literature [8–12]. For further details on the group theoretical approach we refer to [13]. A nice overview of the historic development of particle physics and an introduction to the SM from the experimental point of view can be found in [14, 15]. In the following we will give a rough overview over some of the aspects of the SM based on [8, 10, 16].

2.1. Gauge Group of the Standard Model

The SM is a gauge theory which means that it has a local gauge symmetry. It can be constructed as the direct product of the local gauge symmetry groups of the fundamental interactions

$$SU(3)_C \otimes SU(2)_L \otimes U(1)_Y. \tag{2.1}$$

Generations				
1	2	3	Charge Q [e]	Spin s
Quarks				
$\begin{pmatrix} u \\ d \end{pmatrix}$	$\begin{pmatrix} c \\ s \end{pmatrix}$	$\begin{pmatrix} t \\ b \end{pmatrix}$	$+\frac{2}{3}$	$\frac{1}{2}$
			$-\frac{1}{3}$	$\frac{1}{2}$
Leptons				
$\begin{pmatrix} \nu_e \\ e \end{pmatrix}$	$\begin{pmatrix} \nu_\mu \\ \mu \end{pmatrix}$	$\begin{pmatrix} \nu_\tau \\ \tau \end{pmatrix}$	0	$\frac{1}{2}$
			-1	$\frac{1}{2}$
Gauge Bosons				
	Photon γ		0	1
	8 Gluons g		0	1
	Z^0, W^\pm		$0, \pm 1$	1
	Higgs H		0	0

Table 2.1.: Particles of the Standard Model and their charge and spin.

Here, $SU(3)_C$ is the symmetry group of Quantum Chromodynamics (QCD) and describes strong interactions. The corresponding internal quantum number is the color charge. $SU(2)_L$ is the gauge group associated with the weak isospin I . The quantum number linked to the unitary group $U(1)_Y$ is the hypercharge Y .

The number of generators of a gauge group determines the number of gauge bosons that mediate the corresponding interaction. For special unitary groups $SU(N)$ we obtain $N^2 - 1$ generators. This means, that in QCD we get 8 gauge bosons, namely the gluons g , and for the weak interaction there are three generators T^a , $a = 1, 2, 3$. For the unitary group $U(1)$ we only obtain one generator Y . Since a mass-term is not allowed by gauge invariance, the gauge fields are massless which is in contradiction to phenomenological observations. Since the weak force is short-ranged, the corresponding mediators ought to be quite massive.

Masses for gauge bosons require the breaking of gauge symmetry, which is achieved by the Higgs mechanism [17, 18] through spontaneous symmetry breaking (SSB). Here, the electroweak gauge group is broken down to a single $U(1)$ symmetry

$$SU(3)_C \otimes SU(2)_L \otimes U(1)_Y \xrightarrow{\text{SSB}} SU(3)_C \otimes U(1)_Q. \quad (2.2)$$

The SSB is induced by the scalar Higgs field and its vacuum expectation value (vev)

$$\phi = \begin{pmatrix} \phi^+ \\ \phi^0 \end{pmatrix}, \quad \langle \phi \rangle = \frac{1}{\sqrt{2}} \begin{pmatrix} 0 \\ v \end{pmatrix}, \quad (2.3)$$

where the Higgs field transforms under $SU(2)_L \otimes U(1)_Y$. The vev leads to the breaking of the generators which do not leave the ground state invariant. In this case these are the generators T^1, T^2 and the combination $T^3 - Y/2$ which eventually lead to the massive weak gauge bosons W^\pm and Z^0 . The unbroken combination $Q = T^3 + Y/2$ leads to the $U(1)_Q$ gauge group of the Quantum Electrodynamics (QED) where the conserved quantity is now the electromagnetic charge Q . The massless gauge boson field is then the photon γ . In 2012, the Higgs boson was found at CERN [19, 20] and since the Higgs mechanism seems to be realized in nature, Englert and Higgs were awarded the Nobel Prize in Physics in 2013.

For the fermions we have different chiralities, namely left-handed and right-handed fields where we have the projection

$$\psi_{L/R} = \frac{1}{2}(1 \mp \gamma_5)\psi. \quad (2.4)$$

Under the weak symmetry group $SU(2)_L$ the left-handed fields transform as doublets, whereas the right-handed fields transform as singlets. Thus, the W^\pm bosons solely couple to fields with a left-handed chirality. This has been confirmed experimentally in [21].

Schematically, the Lagrangian of the Standard Model is given by

$$\mathcal{L}_{\text{SM}} = \mathcal{L}_{\text{Yukawa}} + \mathcal{L}_{\text{kin}} + \mathcal{L}_{\text{Higgs}}. \quad (2.5)$$

Here, the fundamental fermions acquire their mass through the $\mathcal{L}_{\text{Yukawa}}$ term. This will be subject to the next section. The kinetic terms are encoded in \mathcal{L}_{kin} and $\mathcal{L}_{\text{Higgs}}$ denotes the Lagrangian for the Higgs potential.

2.2. The CKM Matrix

As already mentioned, we obtain the masses of the quarks via a Yukawa interaction term which is gauge invariant

$$\mathcal{L}_{\text{Yukawa}} = -\bar{Q}'_L Y_u \phi^c u'_R - \bar{Q}'_L Y_d \phi d'_R. \quad (2.6)$$

Here, the quark fields are coupled to the Higgs field ϕ and its charged conjugated field ϕ^c via the Yukawas $Y_{u,d}$. The left-handed quarks are denoted by $Q'_L = (u'_L, d'_L)^T$ and u'_R, d'_R are right-handed up- and down-type quarks. The Yukawa couplings are actually matrices in flavor space. We drop flavor indices for transparency, though.

Via the Higgs mechanism we find a mass term proportional to the Higgs vev and the Yukawa couplings

$$\begin{aligned} \mathcal{L}_{\text{Yukawa}} &= -\frac{v}{\sqrt{2}} \bar{u}'_L Y_u u'_R - \frac{v}{\sqrt{2}} \bar{d}'_L Y_d d'_R \\ &= -\bar{u}'_L M_u u'_R - \bar{d}'_L M_d d'_R, \end{aligned} \quad (2.7)$$

which acts as a coupling between the left- and right-handed components of the quarks. In order to obtain the physical states we ought to diagonalize the quark mass matrices $M_{u,d}$

$$\begin{aligned}\mathcal{L}_{\text{Yukawa}} &= -\bar{u}'_L V_u^{L\dagger} M_u^{\text{diag}} V_u^R u'_R - \bar{d}'_L V_d^{L\dagger} M_d^{\text{diag}} V_d^R d'_R \\ &= -\bar{u}_L M_u^{\text{diag}} u_R - \bar{d}_L M_d^{\text{diag}} d_R,\end{aligned}\tag{2.8}$$

where the matrices V_u^L , V_d^L , V_u^R and V_d^R are unitary. In the last step we redefined the quark fields

$$u_{L/R} = V_u^{L/R} u'_{L/R}, \quad d_{L/R} = V_d^{L/R} d'_{L/R}\tag{2.9}$$

Technically, this is a transition of the weak eigenstates, which are denoted with a prime, to their mass eigenstates. We can now apply the redefinition to all terms of the weak Lagrangian. The unitary matrices cancel in almost every term. Only in the weak interaction charged current term

$$\begin{aligned}\mathcal{L}_{\text{int}} \supset \mathcal{L}_{\text{CC}} &= \frac{g_2}{\sqrt{2}} \left(\bar{u}'_L \gamma^\mu W_\mu^+ d'_L + \bar{d}'_L \gamma^\mu W_\mu^- u'_L \right) \\ &= \frac{g_2}{\sqrt{2}} \left(\bar{u}_L \gamma^\mu V_{\text{CKM}} W_\mu^+ d_L + \bar{d}_L V_{\text{CKM}}^\dagger \gamma^\mu W_\mu^- u_L \right)\end{aligned}\tag{2.10}$$

the combination

$$V_{\text{CKM}} \equiv V_u^L V_d^{L\dagger}\tag{2.11}$$

survives. This is the so-called Cabibbo-Kobayashi-Maskawa (CKM) matrix [22, 23]. It can be chosen such that the weak and mass eigenstates of the up-type quarks are identical. This on the other hand results in a direct connection between the eigenstates of the down-type quarks via the CKM matrix

$$\begin{pmatrix} d' \\ s' \\ b' \end{pmatrix} = V_{\text{CKM}} \begin{pmatrix} d \\ s \\ b \end{pmatrix} = \begin{pmatrix} V_{ud} & V_{us} & V_{ub} \\ V_{cd} & V_{cs} & V_{cb} \\ V_{td} & V_{ts} & V_{tb} \end{pmatrix} \begin{pmatrix} d \\ s \\ b \end{pmatrix}.\tag{2.12}$$

As a consequence, interactions that involve a charged weak vector boson can change the quark flavor even among different generations. Transitions of down-type quarks into up-type quarks and vice versa are then proportional to the corresponding matrix element of the respective V_{CKM} or V_{CKM}^\dagger matrix.

In the case of n generations the unitary CKM matrix would have n^2 real parameters. However, we are free to choose the relative phases between the individual quark fields whereas a global phase would not be observed. This leaves us with $n^2 - 2n + 1 = (n-1)^2$ free parameters. These parameters are split up into $n(n-1)/2$ angles and $(n-1)(n-2)/2$ phases. Hence, our CKM matrix can be expressed through three real angles and one phase which induces CP violation.

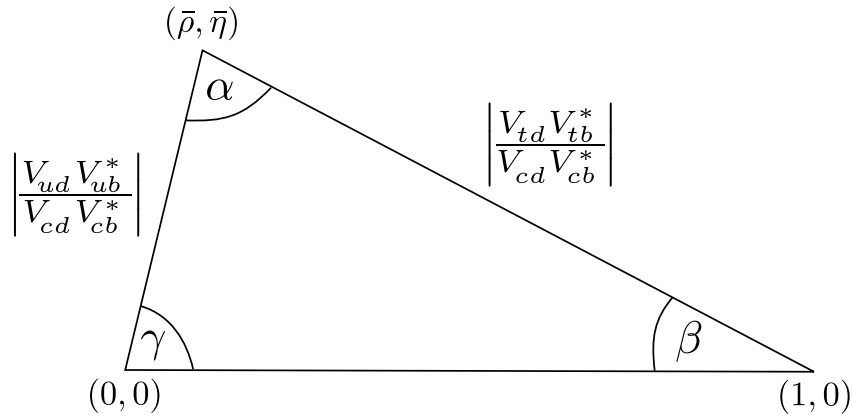


Figure 2.1.: Unitarity Triangle.

It has been observed that the entries of the CKM matrix follow a certain hierarchy. Being almost a unit matrix, the matrix elements decrease in size with increasing distance to the diagonal. In the Wolfenstein parameterization [24]

$$V_{\text{CKM}} = \begin{pmatrix} 1 - \frac{\lambda^2}{2} & \lambda & A\lambda^3(\rho - i\eta) \\ -\lambda & 1 - \frac{\lambda^2}{2} & A\lambda^2 \\ A\lambda^3(1 - \rho - i\eta) & -A\lambda^2 & 1 \end{pmatrix} + \mathcal{O}(\lambda^4), \quad (2.13)$$

with the free Wolfenstein parameters λ , A , ρ and η , this is expressed in an expansion in the parameter $\lambda \approx 0.22$.

A further advantage of the unitarity of the CKM matrix is, that it can be displayed as a triangle. The commonly used unitarity relation is

$$V_{ud}V_{ub}^* + V_{cd}V_{cb}^* + V_{td}V_{tb}^* = 0 \quad \Rightarrow \quad 1 + \frac{V_{ud}V_{ub}^*}{V_{cd}V_{cb}^*} + \frac{V_{td}V_{tb}^*}{V_{cd}V_{cb}^*} = 0. \quad (2.14)$$

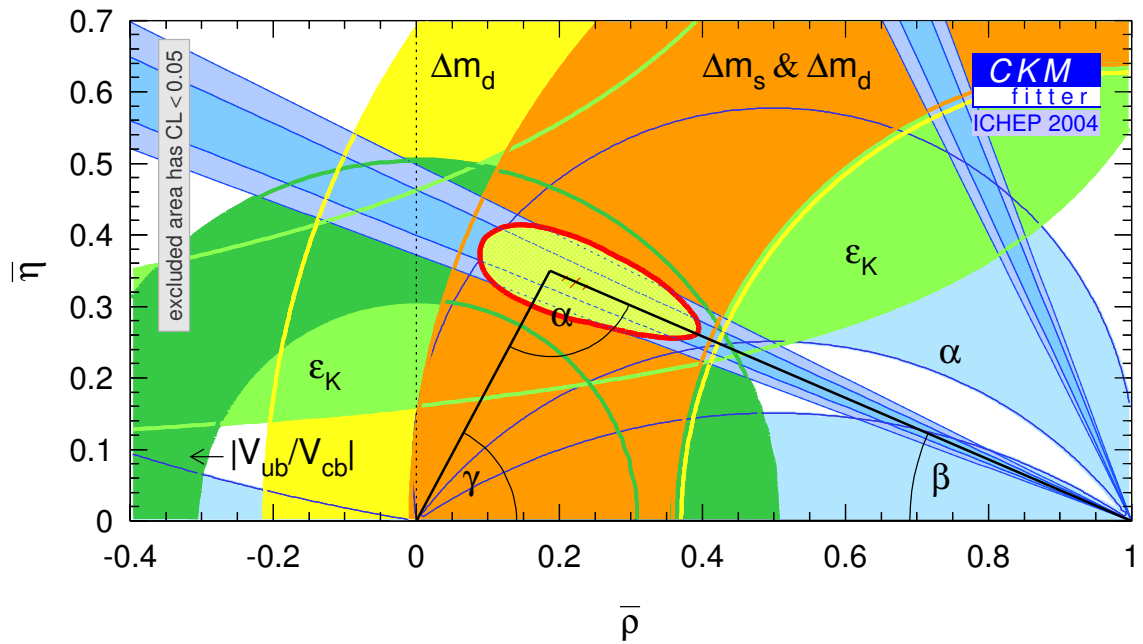
which is schematically pictured in Figure 2.1. One goal is to more and more constrain the apex of this triangle, which is given by

$$\bar{\rho} + i\bar{\eta} = \frac{V_{ud}V_{ub}^*}{V_{cd}V_{cb}^*}, \quad (2.15)$$

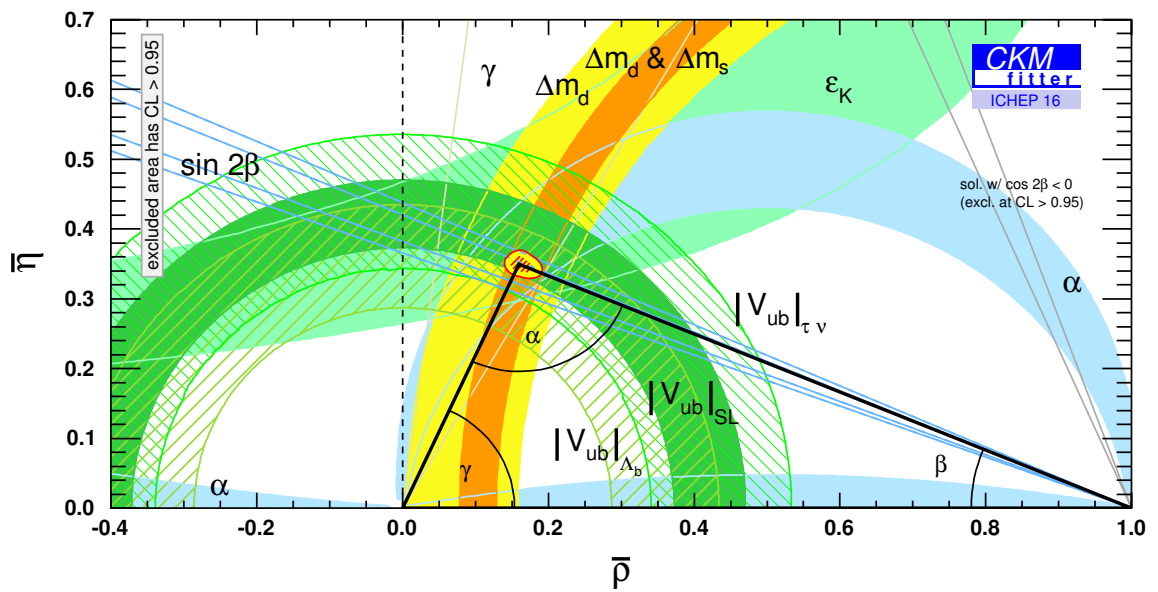
using several independent channels and approaches. Here, the notation from [25] is used with the relation

$$\rho + i\eta = \frac{\sqrt{1 - A^2\lambda^4}\bar{\rho} + i\bar{\eta}}{\sqrt{1 - \lambda^2}[1 - A^2\lambda^4\bar{\rho} + i\bar{\eta}]}. \quad (2.16)$$

In Figure 2.2 we see that a tremendous progress has been made within the last decade constraining the apex of the unitary triangle. Here, the most recent constraints are displayed compared to those in 2004.



(a)



(b)

Figure 2.2.: In (a) one of the first CKM fitter [26] results from 2004 is shown while in (b) the most recent result from 2016 is displayed.

2.3. CP Violation

A parity (P) transformation reverses the sign of the spatial coordinates. We have already seen that parity is violated in the weak interaction which distinguishes between left-handed and right-handed particles. In 1964 Cronin and Fitch [27] found that it is also violated in combination with charge-conjugation transformation (C). They observed the decays of long lived kaons K_L . If the K_L coincided with the CP eigenstate $\text{CP}|K_2\rangle = -|K_2\rangle$ it would be supposed to decay only into three pions. On the other hand its short lived partner K_S would only decay into two pions if it was identical to $|K_1\rangle$ with $\text{CP}|K_1\rangle = +|K_1\rangle$. This is also the reason for the great difference in lifetime since the phase space of the long lived kaon is much smaller. Observing the decay of the K_L they found a small amount of decays into two pions. This circumstance can be explained by a small admixture of the CP even K_1 eigenstate which is referred to as indirect CP violation. Later in the 1990s it was found that CP is also violated in the decay itself in the form of direct CP violation. Here, we find $\mathcal{A}(i \rightarrow f) \neq \mathcal{A}(\bar{i} \rightarrow \bar{f})$. The decay $\bar{i} \rightarrow \bar{f}$ is the CP conjugated decay of the initial state i into the final state f . Further reading on CP violation can be found in [25, 28–30].

In the SM the phase of the CKM matrix is the only established source of CP violation. The phases of the matrix elements

$$\begin{aligned} V_{td} &= |V_{td}|e^{-i\beta} \\ V_{ub} &= |V_{ub}|e^{-i\gamma} \end{aligned} \tag{2.17}$$

can be directly identified with the angles of the unitarity triangle. The phase from the CKM matrix is a weak phase which changes sign under CP conjugation. Strong phases on the other hand do not change sign. This is essential when it comes to the computation of CP asymmetries. The expression

$$A_{CP}^{i \rightarrow f} = \frac{\Gamma(i \rightarrow f) - \Gamma(\bar{i} \rightarrow \bar{f})}{\Gamma(i \rightarrow f) + \Gamma(\bar{i} \rightarrow \bar{f})} \tag{2.18}$$

is only non-zero when we encounter weak as well as strong phase differences. This will be relevant later in Chapter 6.

2.4. Quantum Chromodynamics

The symmetry group of QCD is $SU(3)$. This is a non-abelian group which entails some interesting properties. The quarks carry a color charge that can adopt three different colors. Thus, they transform as triplets under $SU(3)$. Since leptons are not color charged they are not subject to strong interactions. Literature giving more details on QCD can be found in [31, 32].

The local gauge transformation of the fields in QCD is

$$\psi(x) \rightarrow e^{i\theta^a(x)t^a} \psi(x), \quad (2.19)$$

where $\theta^a(x)$ are some arbitrary functions and t^a denotes the generators of the gauge group.

The QCD Lagrangian

$$\mathcal{L}_{\text{QCD}} = -\frac{1}{4} G_a^{\mu\nu} G_{\mu\nu}^a + \sum_{q=u,d,\dots} \bar{q} (i\not{D} - m_q) q. \quad (2.20)$$

is gauge invariant once we replace the partial derivative by the covariant derivative

$$D_\mu = \partial_\mu - ig_s A_\mu = \partial_\mu - ig_s t^a A_\mu^a, \quad (2.21)$$

which is expressed through the strong coupling g_s , the gluon field A_μ and most importantly the generators t^a of the symmetry group, where $a = 1, \dots, 8$. The latter follow the commutation relation

$$[t^a, t^b] \equiv if^{abc} t^c, \quad (2.22)$$

where f^{abc} are the so-called structure constants of the $SU(3)$ which can be chosen to be fully anti-symmetric in a, b and c . The gluon field strength tensor is defined by

$$G_{\mu\nu} = G_{\mu\nu}^a t^a = \frac{i}{g_s} [D_\mu, D_\nu]. \quad (2.23)$$

Thus, we find that

$$G_{\mu\nu}^a = \partial_\mu A_\nu^a - \partial_\nu A_\mu^a + g_s f^{abc} A_\mu^b A_\nu^c. \quad (2.24)$$

This is different than for abelian symmetry groups. Due to the last term we encounter terms including three or four gluon fields when we insert this into the QCD Lagrangian in Equation (2.20). Thus, gluons can couple to themselves and we find vertices with three or four gluons.

Another interesting feature of QCD is the dependence of the coupling on the renormalization scale. The running of the coupling at first order is given by

$$\alpha(\mu) = \frac{\alpha(M)}{1 + \frac{\beta_0 \alpha(M)}{2\pi} \ln\left(\frac{M}{\mu}\right)}, \quad (2.25)$$

where $\alpha \equiv \frac{g^2}{4\pi}$. Here, $\alpha(M)$ is known at a reference scale M . The β function depends on the number of active flavors and on the number of colors N_C . The latter depends

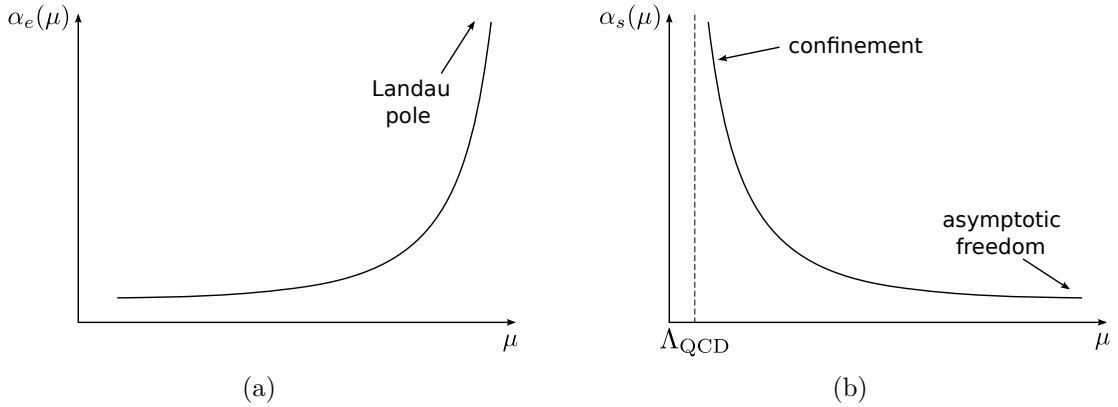


Figure 2.3.: Here, we schematically illustrate the running of the coupling in QED and QCD. (a) The electromagnetic coupling increases with the energy until it diverges (“Landau pole”). This corresponds to an increase of the coupling at small distances. (b) For the strong coupling we observe the exact opposite. For small energies and large distances the coupling increases rapidly (“quark confinement”) and for large energies it becomes very small (“asymptotic freedom”). The scale where α_s diverges and quarks hadronize is denoted as Λ_{QCD} .

on the gauge group $SU(N_C)$, where we assume $N_C = 3$. The difference between an abelian theory such as e.g. QED and the non-abelian QCD is, that in the latter case this β function is negative [33, 34]. In particular, we have

$$\beta_0^{\text{QCD}} = - \left(\frac{11}{3} N_C - \frac{2}{3} n_f \right), \quad (2.26)$$

where n_f is the number of active quark flavors, and [35]

$$\beta_0^{\text{QED}} = \frac{4}{3} \left((n_u Q_u^2 + n_d Q_d^2) N_C + n_\ell Q_\ell^2 \right), \quad (2.27)$$

where $n_{u,d}$ is the number of active up- and down-type quark flavors, n_ℓ is the number of charged lepton flavors and $Q_{u,d,\ell}$ are their respective electromagnetic charges.

As a consequence, the strong coupling decreases when the energy increases. This is referred to as asymptotic freedom which allows us to perform perturbative computations. In Figure 2.3 the difference between the running of the electromagnetic and strong coupling is displayed schematically. Here, we see that for low energies the strong coupling becomes large, rendering perturbation theory useless. In this region confinement sets in, which is responsible for the constitution of hadrons. This circumstance makes it quite complicated to compute hadronic quantities in full QCD. Therefore, we rely on effective field theories such as e.g. HQET which is described in the following chapter.

3. Heavy Quark Expansion

In many physical problems there are two or more fundamental scales involved which are disparate. In such cases we can benefit from effective theories in which we concentrate on the degrees of freedom that are relevant for the physical system at hand. In accordance with the decoupling theorem [36] we can separate the scales into a low-energy and high-energy contribution, where the latter can be computed perturbatively in QCD. Then the effective theory does not explicitly depend on the non-relevant degrees of freedom anymore. Their effects are suppressed by the inverse power of the respective scale. One of the advantages of effective theories is that computations can simplify drastically. Another benefit is the manifestation of symmetries that are not present in the full theory.

A well-known example for an effective theory is for instance classical mechanics as an effective theory of quantum mechanics ($\hbar \rightarrow 0$) and relativistic mechanics ($c \rightarrow \infty$). Quantum mechanics is also an effective theory of quantum field theory ($c \rightarrow \infty$). Other examples for effective field theories are the weak effective theory, chiral perturbation theory (ChPT) and soft-collinear effective theory (or SCET). It is commonly claimed that even the Standard Model is only an effective theory of a hitherto unknown full theory.

An effective field theory (EFT) was first used in 1933 when Fermi expressed the β decay with an effective coupling [37, 38]. We can use the Operator Product Expansion (OPE) to express the effective Hamiltonian as an expansion in a series of local operators [39]

$$\mathcal{H}_{\text{eff}} = \sum_i C_i(\mu) \mathcal{O}_i(\mu). \tag{3.1}$$

The short-distance effects are contained by the effective couplings $C_i(\mu)$, which are the so-called Wilson coefficients. They contain the physics above the renormalization scale μ . Long-distance contributions below the scale μ are enclosed in the local operators $\mathcal{O}_i(\mu)$. The Hamiltonian has mass dimension four. Therefore, higher dimensions need to be compensated by inverse powers of the large scale.

In the following section we aim to give a brief introduction to Heavy Quark Effective Theory (HQET) which is defined within the Heavy Quark Expansion (HQE). It can be used to describe processes with heavy hadrons which contain one heavy and one light quark, respectively. Hadronic interactions take place at the scale $\Lambda_{\text{QCD}} \ll m_Q$, where quarks and gluons hadronize. This allows for perturbative computations in

α_s at the scale of the heavy quark mass m_Q , which is the high-energy scale in this case.

We can roughly compare the framework of HQET to a hydrogen atom. Analogous to the atomic nucleus, or rather the proton, the heavy quark acts as a static source of color in the B meson rest frame [40]. In contradiction to the electron, the light degrees of freedom such as the light quarks and gluons are now of relativistic nature. In analogy to the energy levels in the hydrogen atom we can even perform some spectroscopy for heavy hadrons. We will take a closer look at this in Chapter 4.

This chapter is leaned on the reviews on this subject in [41–44].

3.1. Heavy Quark Limit

3.1.1. Derivation of the Effective Lagrangian

First we can derive the effective Lagrangian in the heavy quark limit, which has been used since the 1930s [45]. For this purpose we start with the Lagrangian for a heavy quark field $Q(x)$ in QCD (cf. Equation (2.20))

$$\mathcal{L}_{\text{QCD}}^Q = \bar{Q}(i\not{D} - m_Q)Q, \quad (3.2)$$

where m_Q denotes the mass of the heavy quark.

In other effective field theories, such as e.g. the weak effective theory, the degrees of freedom which are only relevant at high energies do not appear explicitly any more. In this case it is quite easy to perform the OPE. In the case of HQET the heavy quark is still present at scales below the heavy quark mass m_Q acting as a static source of color. Thus, we need to take a short detour before constructing the effective Lagrangian.

We now consider a heavy meson containing a heavy quark Q and a light quark q with momentum $p_H = m_H \cdot v$. Here, m_H is the mass of the heavy meson and v its velocity, which satisfies $v^2 = 1$. The heavy quark has almost the same momentum as the meson. We can decompose it into

$$p_Q^\mu \equiv m_Q v^\mu + k^k, \quad (3.3)$$

where k is a small residual momentum with $|k| \sim \mathcal{O}(\Lambda_{\text{QCD}}) \ll m_Q$. The heavy quark is almost on-shell and k indicates the amount of its off-shellness.

In the heavy quark limit the velocity is not a dynamical degree of freedom anymore and is now a conserved quantity [46]. We can redefine the heavy quark field extracting the static part of the momentum into a phase

$$Q(x) \equiv e^{-im_Q v \cdot x} [h_v(x) + H_v(x)], \quad (3.4)$$

where the fields

$$\begin{aligned} h_v(x) &= e^{im_Q v \cdot x} P_+ Q(x), \\ H_v(x) &= e^{im_Q v \cdot x} P_- Q(x) \end{aligned} \quad (3.5)$$

now only carry the residual momentum k .

With the projectors

$$P_{\pm} = \frac{1 \pm \not{v}}{2}$$

these fields satisfy the relations

$$\begin{aligned} P_+ h_v(x) &= h_v(x), \quad P_- H_v(x) = H_v(x), \\ P_- h_v(x) &= P_+ H_v(x) = 0. \end{aligned} \quad (3.6)$$

Inserting Equation (3.4) in Equation (3.2) and using Equation (3.6) we can now rewrite the QCD-Lagrangian for the heavy quark in terms of the fields h_v and H_v

$$\begin{aligned} \mathcal{L}_{\text{QCD}}^Q &= (\bar{h}_v + \bar{H}_v) (i\not{D} - 2m_Q P_-) (h_v + H_v) \\ &= \bar{h}_v i v \cdot D h_v - \bar{H}_v (i v \cdot D + 2m_Q) H_v + \bar{h}_v i \not{D}_{\perp} H_v + \bar{H}_v i \not{D}_{\perp} h_v, \end{aligned} \quad (3.7)$$

where D_{\perp} is defined through $D^{\mu} = D_{\perp}^{\mu} + (v \cdot D)v^{\mu}$.

Here, we see that the effective heavy quark field h_v is actually massless, whereas H_v has the twice the mass of the heavy quark $2m_Q$. The latter can be identified with the heavy degrees of freedom that we want to get rid of.

A formal derivation with path integrals can be found in [47] and we will briefly describe the procedure in the following.

We start with the generating functional related to the heavy field H_v

$$Z[J, \bar{J}] = \int \mathcal{D}H_v \mathcal{D}\bar{H}_v e^{-i \int d^4x [\bar{H}_v A H_v - \bar{J} H_v - \bar{H}_v J]}, \quad (3.8)$$

where $A = i v \cdot D + 2m_Q$, $\bar{J} = \bar{h}_v i \not{D}_{\perp}$ and $J = i \not{D}_{\perp} h_v$. Here, J and \bar{J} act as external sources. We can then rewrite the expression by completing the square

$$\bar{H}_v A H_v + \bar{J} H_v + \bar{H}_v J = (\bar{H}_v - \bar{J} A^{-1}) A (H_v - A^{-1} J) - \bar{J} A^{-1} J$$

and shifting the field H_v and \bar{H}_v . Then the Gaussian integration can be performed and we can identify the expression with the effective Lagrangian

$$\begin{aligned} Z[J, \bar{J}] &= \int \mathcal{D}H_v \mathcal{D}\bar{H}_v e^{-i \int d^4x \bar{H}_v A H_v} e^{i \int d^4x \bar{J} A^{-1} J} \\ &= \frac{\pi^{n/2}}{\sqrt{i \det(A)}} e^{i \int d^4x \bar{J} A^{-1} J} \sim e^{i \int d^4x \mathcal{L}_{\text{eff}}^{H_v}}. \end{aligned}$$

The determinant is constant and does not have an effect on the physics. Our effective Lagrangian corresponding to the heavy field H_v can be then identified with

$$\mathcal{L}_{\text{eff}}^{H_v} = \bar{J} A^{-1} J = \bar{h}_v i \not{D}_\perp \frac{1}{i v \cdot D + 2m_Q} i \not{D}_\perp h_v. \quad (3.9)$$

This term includes a derivative in the denominator which means that the Lagrangian is not local.

The same result can be obtained by replacing

$$H_v = \left(\frac{1}{i v \cdot D + 2m_Q} \right) i \not{D}_\perp h_v, \quad (3.10)$$

which can be obtained using the equations of motion from Equation (3.7). Here we can see why the fields h_v and H_v are usually referred to as the ‘‘large’’ and ‘‘small’’ component fields. The covariant derivative acting on h_v corresponds to k in momentum space which is much smaller than the quark mass m_Q . Hence, H_v is suppressed by $\frac{\Lambda_{\text{QCD}}}{2m_Q}$ compared to h_v .

We can now perform a Taylor expansion in $\left(\frac{v \cdot D}{2m_Q}\right)$. As a consequence, we achieve an expansion in local operators

$$\begin{aligned} \mathcal{L}_{\text{HQET}}^{\text{eff}} &= \bar{h}_v i v \cdot D h_v + \frac{1}{2m_Q} \sum_{n=0}^{\infty} \bar{h}_v (i \not{D}_\perp)^n \left(-\frac{v \cdot D}{2m_Q} \right)^n (i \not{D}_\perp) h_v \\ &= \bar{h}_v i v \cdot D h_v + \frac{1}{2m_Q} \bar{h}_v (i \not{D}_\perp) (i \not{D}_\perp) h_v + \mathcal{O}\left(\frac{1}{2m_Q}\right). \end{aligned} \quad (3.11)$$

The second term can be rewritten using $[D_\mu, D_\nu] = -ig_s G_{\mu\nu} = -ig_s G_{\mu\nu}^a t^a$

$$\begin{aligned} \mathcal{L}_{1/m_Q}^{\text{eff}} &= \bar{h}_v i v \cdot D h_v + \frac{1}{2m_Q} \bar{h}_v (i D_\perp)^2 h_v + \frac{1}{2m_Q} \bar{h}_v \frac{g_s}{2} \sigma^{\mu\nu} G_{\mu\nu} h_v \\ &\quad + \mathcal{O}\left(\frac{1}{2m_Q}\right), \end{aligned} \quad (3.12)$$

where $\sigma^{\mu\nu} = \frac{i}{2}[\gamma^\mu, \gamma^\nu]$. In the first term a flavor and spin symmetry manifest which are described in more detail in the next subsection. The second and third term obviously break flavor symmetry due to the mass m_Q . In addition, the third term violates spin symmetry which becomes more clear when we rewrite it

$$\frac{1}{2m_Q} \bar{h}_v \frac{g_s}{2} \sigma^{\mu\nu} G_{\mu\nu} h_v = -\frac{g_s}{m_Q} \bar{h}_v \vec{S} \cdot \vec{B} h_v = -\frac{g_s}{2m_Q} \bar{h}_v \vec{\sigma} \cdot \vec{B} h_v, \quad (3.13)$$

where $B^i = -\frac{1}{2}\epsilon^{ijk} G^{jk}$ are the components of the chromo-magnetic field and

$$S^i = \frac{1}{2} \begin{pmatrix} \sigma^i & 0 \\ 0 & \sigma^i \end{pmatrix} = \frac{1}{2} \gamma^5 \gamma_0 \gamma_i \quad (3.14)$$

now contains a heavy quark flavor and spin symmetry. In this subsection we will present them and their consequent advantages when it comes to computing processes in HQET.

Heavy Quark Flavor Symmetry

The heavy quark flavor symmetry is rather simple to see from Equation (3.17). The leading order of the Lagrangian does not depend on the mass any more. In QCD, flavor is only distinguished by the mass of the quark, though. Thus, we encounter a flavor symmetry that relates heavy quarks which move at the same velocity.

Heavy Quark Spin Symmetry

In the previous section we saw that the heavy quark spin couples to the light degrees of freedom only at order $1/m_Q$. Hence, at leading order the Lagrangian is symmetric under a heavy quark spin rotation. As a consequence, we can arrange mesons in spin-symmetry doublets with degenerate masses. At order $1/m_Q$ a hyperfine splitting is induced. This will be a major feature in Chapter 4.

3.2.1. Form Factors in Weak Decays

Normalization of States

The conventional relativistic normalization for a mesonic state M is

$$\langle M(p') | M(p) \rangle = 2E_{\vec{p}} (2\pi)^3 \delta^3(\vec{p} - \vec{p}'). \quad (3.18)$$

The normalization for a state in HQET

$$\langle M(v') | M(v) \rangle = 2v^0 \delta_{vv'} (2\pi)^3 \delta^3(\vec{k} - \vec{k}') \quad (3.19)$$

on the other hand is defined in a mass-independent way. By comparing these two normalizations we find a relation between QCD and HQET states

$$|M(p)\rangle = \sqrt{m_H} |M(v)\rangle + \mathcal{O}(1/m_Q). \quad (3.20)$$

Heavy Meson Decay Constants

The aforementioned normalization difference has also impact on the decay constants of the heavy meson. For a pseudoscalar meson P we obtain in QCD

$$\langle 0 | \bar{q} \gamma_\mu \gamma_5 Q | P(p) \rangle = i f_P p_\mu, \quad (3.21)$$

whereas in HQET we find

$$\langle 0 | \bar{q} \gamma_\mu \gamma_5 Q | P(v) \rangle = i F v_\mu, \quad (3.22)$$

with some unknown constant F . We can now compare the two definitions and find the relation

$$F = \sqrt{m_P} f_P, \quad (3.23)$$

using $p_\mu = m_P v_\mu$.

Heavy Meson Form Factors

The matrix element for two heavy mesons can be described by one single form factor in HQET. This emerges from the heavy quark spin symmetry. As already mentioned, mesons fall into spin-symmetry doublets with degenerate masses in the heavy quark limit. We can define a covariant tensor representation $\mathcal{H}(v)$ for the two states in the doublet. The wave function for our mesonic states are not known. What we do know, though, is that they transform bilinearly like a tensor under Lorentz transformation. From this we can construct the representation matrices for the members of the doublet. For the lowest lying states we find

$$\begin{aligned} H(v) &= -\gamma_5 \frac{1 - \not{v}}{2} && \text{for the pseudoscalar meson, and} \\ H^*(v, \epsilon) &= \not{\epsilon} \frac{1 - \not{v}}{2} && \text{for the vector meson,} \end{aligned} \quad (3.24)$$

where ϵ_μ is the polarization vector.

The covariant tensor representation also transforms linearly under a heavy quark spin rotation

$$\mathcal{H}(v) \rightarrow D(R)\mathcal{H}(v). \quad (3.25)$$

Here, $D(R)$ denotes the rotation matrix for the rotation of the heavy quark. We require the Dirac structure to transform as $\Gamma \rightarrow D(R)\Gamma D^{-1}(R)$ in order for the current to be invariant under heavy quark spin transformations. Thus, it only occurs as a product to which the matrix element is proportional to. Since the amplitude must be scalar we need to contract this product with some matrix $\mathcal{M}(v, v')$ ¹. This leaves us with a trace

$$\langle \mathcal{H}'(v') | \bar{h}_{v'} \Gamma h_v | \mathcal{H}(v) \rangle = \text{Tr}[\mathcal{M}(v, v') \bar{\mathcal{H}}'(v') \Gamma \mathcal{H}(v)], \quad (3.26)$$

where $\mathcal{M}(v, v')$ describes the dynamics of the light degrees of freedom. We can decompose the matrix into all possible combinations of the velocities v and v'

$$\mathcal{M}(v, v') = M_1 \mathbf{1} + M_2 \not{v} + M_3 \not{v}' + M_4 \not{v} \not{v}'. \quad (3.27)$$

The covariant representations satisfy the projection properties $P_+ \mathcal{H} = \mathcal{H}$ and $\mathcal{H} P_- = \mathcal{H}$. Hence, we find that $\mathcal{M}(v, v')$ reduces to

$$\mathcal{M}(v, v') \rightarrow M_1 - M_2 - M_3 + M_4 \equiv -\xi(\omega), \quad (3.28)$$

where $\xi(\omega)$ only depends on the combination $\omega = v \cdot v'$ due to Lorentz invariance. We can then write the matrix element as [48]

$$\langle \mathcal{H}'(v') | \bar{h}_{v'} \Gamma h_v | \mathcal{H}(v) \rangle = -\xi(\omega) \text{Tr}[\bar{\mathcal{H}}'(v') \Gamma \mathcal{H}(v)]. \quad (3.29)$$

¹We omit the renormalization scale in $\mathcal{M}(v, v', \mu)$.

Note, that this relation is independent of the heavy quark flavor and the Dirac structure Γ . The function $\xi(\omega)$ is chosen such that it coincides with the Isgur-Wise function [49,50] that emerges describing the scattering of a pseudoscalar into another pseudoscalar

$$\langle P'(v') | \bar{h}_{v'} \gamma_\mu h_v | P(v) \rangle = \xi(\omega) (v + v')_\mu. \quad (3.30)$$

The Isgur-Wise function is a non-perturbative universal object. Physically it describes the overlap of the light degrees of freedom, which results in a suppression of the form factor.

Due to normalization of the meson states we find that the Isgur-Wise form factor is normalized to

$$\xi(\omega = 1) = 1 \quad (3.31)$$

at the zero recoil point.

3.2.2. Further Features in HQET

Reparameterization Invariance

The full QCD Lagrangian is invariant under Lorentz transformation. If we truncate the $1/m_Q$ heavy quark expansion we end up with a dependence on the four-velocity v . Then, the HQET Lagrangian does not exhibit Lorentz invariance any more, since we chose v in the rest frame of the heavy meson. Nevertheless, when we take the Lagrangian to all orders in $1/m_Q$ it is independent of the four-velocity and therefore Lorentz invariant. Thus, infinitesimal changes of v should leave the Lagrangian invariant, which is called reparameterization invariance [51,52]. A shift in the four-velocity results in corresponding shifts of the fields and the covariant derivative.

$$\begin{aligned} v &\rightarrow v + \delta v, \quad v \cdot \delta v = 0, \\ h_v &\rightarrow h_v + \frac{\delta\psi}{2} \left(1 + P_- \frac{1}{2m_Q + iv \cdot D} i\not{D}\right) h_v, \\ iD &\rightarrow iD - m_Q \delta v. \end{aligned} \quad (3.32)$$

Up to higher orders the HQET Lagrangian is invariant under those shifts. This leads to a connection between coefficients of different orders in $1/m_Q$.

Luke's Theorem

Luke's theorem states that the contributions at order $1/m_Q$ of the matrix elements $\langle D^{(*)}(v') | V_\mu | B(v) \rangle$ and $\langle D^{(*)}(v') | A_\mu | B(v) \rangle$ vanish at zero recoil $v = v'$ [53]. It is true to all orders in α_s since this statement does not concern the perturbative part of the OPE [54,55]. It is a consequence of the Ademollo-Gatto theorem [56].

3.3. Renormalization

3.3.1. On-Shell Renormalization

Higher-order QCD corrections to a given process result in loop diagrams. Every loop implies an integration over the enclosed momentum which diverges in many cases. To get a handle on these divergencies we use dimensional regularization [57]. Here, we perform the loop integration in $D = 4 - 2\epsilon$ dimensions by replacing the integration measure

$$\int \frac{d^4k}{(2\pi)^4} \rightarrow \mu^{4-D} \int \frac{d^Dk}{(2\pi)^D}, \quad (3.33)$$

where μ is the renormalization scale. Then, the divergencies manifest in poles of the parameter ϵ of the dimensional regularization. Along with the poles we also encounter the term $-\gamma_E + 4\pi$, where γ_E is the Euler-Mascheroni constant. In the modified minimal subtraction scheme ($\overline{\text{MS}}$) those characteristic constants are removed by redefining the renormalization scale μ via

$$\mu \rightarrow \tilde{\mu} \equiv \mu \frac{e^{\frac{\gamma_E}{2}}}{\sqrt{4\pi}}. \quad (3.34)$$

Since QCD is a renormalizable theory we can introduce a finite number of parameters to absorb these divergencies. This can be achieved using different renormalization schemes. In this section we will introduce the on-shell renormalization scheme also described in [9, 42, 58]

We begin with the propagator of one free Dirac field ψ_0 which is given by the two-point correlation function

$$S_0(p) = \int d^4x e^{ipx} \langle 0|T \{ \psi_0(x) \bar{\psi}_0(0) \} |0\rangle = \frac{i}{\not{p} - m_0 + i0}, \quad (3.35)$$

where T is the time-ordered product and p and m_0 denote the momentum and the bare mass of the quark, respectively.

Since we are rather dealing with an interactive theory, the Green function in Equation (3.35) is actually of the form

$$S(p) = \int d^4x e^{ipx} \langle \Omega|T \{ \psi(x) \bar{\psi}(0) \} |\Omega\rangle = \frac{iR}{\not{p} - m + i0} + \begin{array}{l} \text{analytic terms} \\ \text{for } p^2 = m^2 \end{array}. \quad (3.36)$$

Here, we see that the pole of the propagator is now shifted and the residue is $R \neq 1$.

This propagator can also be visualized as a sum of the self-energy diagrams as shown in Figure 3.1, which leads to the expression

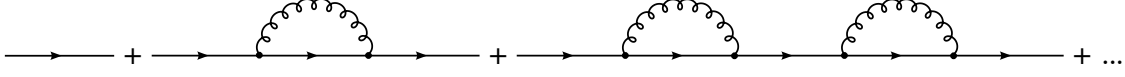


Figure 3.1.: Propagator self-energy

$$\begin{aligned}
S(p) &= \int d^4x e^{ipx} \langle \Omega | T \{ \psi(x) \bar{\psi}(0) \} | \Omega \rangle \\
&= \frac{i}{\not{p} - m_0} + \frac{i}{\not{p} - m_0} \frac{\Sigma(\not{p})}{\not{p} - m_0} + \frac{i}{\not{p} - m_0} \left(\frac{\Sigma(\not{p})}{\not{p} - m_0} \right)^2 + \dots \\
&= \frac{i}{\not{p} - m_0 - \Sigma(\not{p})}
\end{aligned} \tag{3.37}$$

where

$$\Sigma(\not{p}) = (ig_s)^2 C_F \tilde{\mu}^{2\epsilon} \int \frac{d^D k}{(2\pi)^4} \gamma_\mu \frac{i}{\not{p} - \not{k} - m + i0} \gamma^\mu \frac{i}{k^2 + i0} \tag{3.38}$$

is the quark self-energy to first non-trivial order. In the on-shell renormalization scheme the physical quark mass m is given by the position of the pole of the propagator in Equation (3.37).

For $\Sigma(\not{p})$ we can make the ansatz $\Sigma(\not{p}) = Am_0 + B\not{p} = m_0\Sigma_1(p^2) + (\not{p} - m_0)\Sigma_2(p^2)$ based on Lorentz invariance and mass dimension. Hence, we have

$$\begin{aligned}
S(p) &= \frac{i}{\not{p} - m_0} \left[1 + \Sigma(\not{p}) \frac{1}{\not{p} - m_0} + \dots \right] \\
&= \frac{i}{\not{p} - m_0} \left[1 + \Sigma_2(p^2) + (\not{p} + m_0) \frac{m_0 \Sigma_1(p^2)}{p^2 - m_0^2} + \dots \right],
\end{aligned} \tag{3.39}$$

which is divergent for $p^2 = m_0^2$. We can define the on-shell scheme renormalization constant for the mass $m_0 = Z_m^{\text{os}} m$ and replace the bare mass in the Lagrangian

$$\mathcal{L} = \bar{\psi}(iD - m_0)\psi = \bar{\psi}(iD - m)\psi + \delta m \bar{\psi}\psi, \tag{3.40}$$

which yields the counterterm $\delta m = m(1 - Z_m^{\text{os}}) = m - m_0$.

Hence, we find that Equation (3.39) now takes the form

$$S(p) = \frac{i}{\not{p} - m} \left[1 + \Sigma_2(p^2) + (\not{p} + m) \frac{m \Sigma_1(p^2) - \delta m}{p^2 - m^2} + \dots \right]. \tag{3.41}$$

In order for the Green function to be finite for $p^2 = m^2$ we can choose $\delta m = m \Sigma_1(m^2)$. This means the renormalization constant for the mass is given by $Z_m^{\text{os}} = 1 - \Sigma_1(m^2)$. We then find

$$S(p) = \frac{i}{\not{p} - m} \left[1 + \Sigma_2(p^2) + (\not{p} + m) \frac{m \Sigma_1(p^2) - m \Sigma_1(m^2)}{p^2 - m^2} + \dots \right]. \tag{3.42}$$

We can expand $\Sigma_1(p^2)$ at $p^2 = m^2$ using a Taylor expansion and find

$$\begin{aligned} S(p) &= \frac{i}{\not{p} - m} \left[1 + \Sigma_2(p^2) + m(\not{p} + m)\Sigma'_1(m^2) + \dots \right] \\ &= m\Sigma'_1(m^2) + \frac{i}{\not{p} - m} \left[1 + \Sigma_2(p^2) + 2m^2\Sigma'_1(m^2) + \dots \right] \\ &\stackrel{!}{=} \frac{iZ_\psi^{\text{os}}}{\not{p} - m} + \text{analytic terms} \\ &\quad \text{for } p^2 = m^2, \end{aligned} \quad (3.43)$$

where $\Sigma'_1(m^2) = \left. \frac{d\Sigma_1}{dp^2} \right|_{p^2=m^2}$. Here, we used that the renormalized quark field is given by

$$\psi_0 = \left(Z_\psi^{\text{os}} \right)^{1/2} \psi. \quad (3.44)$$

and hence the propagator is renormalized by

$$S(p) = Z_\psi^{\text{os}} S_{\text{os}}(p). \quad (3.45)$$

Hence, the renormalization constant for the quark field must be

$$Z_\psi^{\text{os}} = 1 + \Sigma_2(m^2) + 2m^2\Sigma'_1(m^2) + \mathcal{O}(\alpha^2), \quad (3.46)$$

which can be explicitly computed. We find

$$Z_{\text{QCD}}^{\text{os}} \equiv Z_\psi^{\text{os}} = 1 + \frac{g_s^2}{(4\pi)^2} C_F \left[\frac{3}{\epsilon} - 3 \ln \left(\frac{m^2}{\mu^2} \right) + 4 \right], \quad (3.47)$$

where $C_F = \frac{N_C^2 - 1}{2N_C}$ and N_C is the number of colors.

Analogously we can perform the same approach to the propagator in HQET

$$S(v) = \frac{1}{v \cdot k} + \left[1 + \frac{\partial \Sigma}{\partial v \cdot k} \Big|_{v \cdot k=0} + \dots \right] \quad (3.48)$$

and find for the heavy quark field h that

$$Z_{\text{HQET}}^{\text{os}} \equiv Z_h^{\text{os}} = 1 + \frac{\partial \Sigma}{\partial v \cdot k} \Big|_{v \cdot k=0} = 1. \quad (3.49)$$

For the loop calculations we make use of Appendix C.1.

3.3.2. Quark Self-Energy

We can now calculate the renormalization constant for the heavy quark field h_v in HQET. We define

$$h_v^0 = \sqrt{Z_h} h_v, \quad (3.50)$$

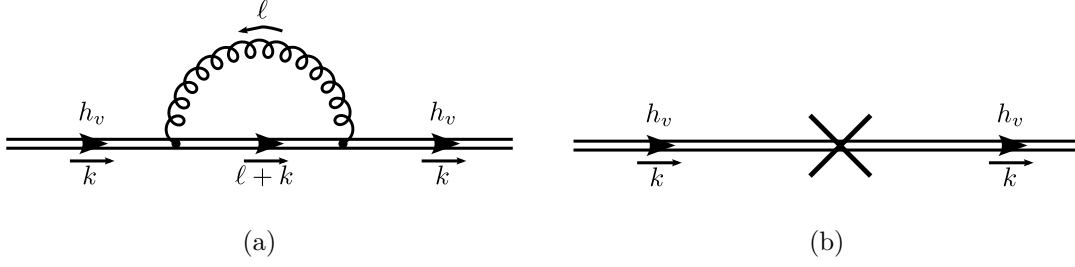


Figure 3.2.: (a) Heavy quark self-energy and (b) the corresponding counterterm.

where h_v^0 is the bare heavy quark and h_v is the renormalized field. We start with the bare HQET Lagrangian and insert Equation (3.50)

$$\begin{aligned}
\mathcal{L}_{\text{QHET}} &= i\bar{h}_v^0 v \cdot \partial h_v^0 \\
&= iZ_h \bar{h}_v v \cdot \partial h_v \\
&= i\bar{h}_v v \cdot \partial h_v + i(Z_h - 1)\bar{h}_v v \cdot \partial h_v.
\end{aligned} \tag{3.51}$$

We find the contribution of the counterterm in Figure 3.2(b) to be

$$\delta_h = iv \cdot k(Z_h - 1), \tag{3.52}$$

where k is the external residual momentum. The heavy quark self-energy is depicted in Figure 3.2(a). We find it to be

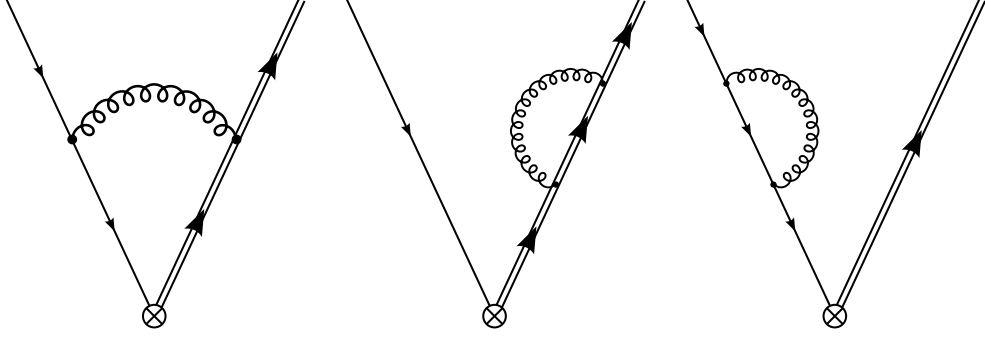
$$\begin{aligned}
&\int \frac{d^D \ell}{(2\pi)^D} (-ig_s \tilde{\mu}^\epsilon T^A) v_\alpha \frac{i}{v \cdot (\ell + k)} (-ig_s \tilde{\mu}^\epsilon T^A) v^\alpha \frac{(-i)}{\ell^2} \\
&= -g_s^2 C_F \tilde{\mu}^{2\epsilon} \int \frac{d^D \ell}{(2\pi)^D} \frac{1}{[v \cdot (\ell + k)][\ell^2]} \\
&= -i \frac{g_s^2}{8\pi^2} C_F v \cdot k \frac{1}{\epsilon}.
\end{aligned} \tag{3.53}$$

The contribution of the counterterm should cancel the divergent part of the self-energy. Thus, we find in the $\overline{\text{MS}}$ scheme

$$\begin{aligned}
&-i \frac{g_s^2}{8\pi^2} C_F v \cdot k \frac{1}{\epsilon} + iv \cdot k(Z_h - 1) \stackrel{!}{=} 0 \\
\Rightarrow Z_h^{\overline{\text{MS}}} &= 1 + \frac{g_s^2}{8\pi^2} C_F \frac{1}{\epsilon}.
\end{aligned} \tag{3.54}$$

The renormalization constant of the quark in QCD can be found analogously using the QCD Lagrangian

$$Z_q \equiv Z_\psi^{\overline{\text{MS}}} = 1 - \frac{g_s^2}{(4\pi)^2} C_F \frac{1}{\epsilon}. \tag{3.55}$$



(a) Vertex correction. (b) Heavy quark self-energy (c) Light quark self-energy

Figure 3.3.: One-loop corrections to the heavy-light composite operator.

3.3.3. Composite Operators

Perturbative Corrections

Composite operators behave differently from the individual fields that they consist of. Hence, we need another, additional, renormalization constant. The bare operator can be written as

$$\mathcal{O}_\Gamma^{(0)} = Z_\mathcal{O} \mathcal{O}_\Gamma = \bar{h}_v^{(0)} \Gamma q^{(0)} = \sqrt{Z_q Z_h} \bar{h}_v \Gamma q \quad (3.56)$$

for some arbitrary structure of Dirac matrices Γ and hence we find

$$\begin{aligned} \mathcal{O}_\Gamma &= \frac{1}{Z_\mathcal{O}} \mathcal{O}_\Gamma^{(0)} = \frac{\sqrt{Z_q Z_h}}{Z_\mathcal{O}} \bar{h}_v \Gamma q \\ &= \bar{h}_v \Gamma q + \left(\frac{\sqrt{Z_q Z_h}}{Z_\mathcal{O}} - 1 \right) \bar{h}_v \Gamma q. \end{aligned} \quad (3.57)$$

Thus, our counterterm for the composite heavy-light-operator is

$$\left(\frac{\sqrt{Z_q Z_h}}{Z_\mathcal{O}} - 1 \right) \Gamma. \quad (3.58)$$

The self-energy diagrams in 3.3(b) and (c) are taken care of by the renormalization constants Z_h and Z_q from the previous subsection. The vertex correction in Figure 3.3(a) is

$$\begin{aligned} &\int \frac{d^D \ell}{(2\pi)^D} (-ig_s T^a v_\mu) \frac{i}{v \cdot (\ell + k)} \Gamma \frac{i \ell}{\ell^2} (-ig_s T^a \gamma_\nu) \frac{-ig^{\mu\nu}}{\ell^2} \\ &= -ig_s^2 C_F \int \frac{d^D \ell}{(2\pi)^D} \frac{\ell^\psi}{[v \cdot (\ell + k)][\ell^2]^2} \Gamma. \end{aligned} \quad (3.59)$$

We can now write

$$\ell_\mu = (v \cdot \ell)v_\mu + \ell_\mu^\perp \quad (3.60)$$

and hence

$$\not{\ell} = (v \cdot \ell)\not{\psi} + \not{\ell}^\perp. \quad (3.61)$$

The only possible vector-like Lorentz structure to parameterize this is the four-velocity v , since the residual momentum k only appears as the projection $\omega = v \cdot k$. Since ℓ^\perp is perpendicular to v the corresponding integral becomes zero because of the projection $v \cdot \ell^\perp = 0$. With the other term we get

$$\begin{aligned} & -ig_s^2 C_F \int \frac{d^D \ell}{(2\pi)^D} \frac{\not{\ell} \not{\psi}}{[\ell^2]^2 v \cdot (\ell + k)} \Gamma \\ &= -ig_s^2 C_F \int \frac{d^D \ell}{(2\pi)^D} \frac{(v \cdot \ell) \not{\psi} \not{\psi}}{[\ell^2]^2 v \cdot (\ell + k)} \Gamma \\ &= -ig_s^2 C_F \int \frac{d^D \ell}{(2\pi)^D} \frac{v \cdot \ell}{[\ell^2]^2 v \cdot (\ell + k)} \Gamma \\ &= -ig_s^2 C_F \int \frac{d^D \ell}{(2\pi)^D} \frac{v \cdot (\ell + k) - v \cdot k}{[\ell^2]^2 v \cdot (\ell + k)} \Gamma \\ &= -ig_s^2 C_F \int \frac{d^D \ell}{(2\pi)^D} \left(\frac{1}{[\ell^2]^2} - \frac{\omega}{[\ell^2]^2 v \cdot (\ell + k)} \right) \Gamma. \end{aligned} \quad (3.62)$$

The first integral is zero since it is scaleless. The second can be evaluated as in [58] and yields

$$\begin{aligned} & ig_s^2 \omega C_F \int \frac{d^D \ell}{(2\pi)^D} \frac{1}{[\ell^2]^2 v \cdot (\ell + k)} \Gamma \\ &= ig_s^2 \omega C_F \left(-\frac{i}{(4\pi)^2} \frac{1}{\omega \epsilon} \right) \Gamma \\ &= \frac{g_s^2}{(4\pi)^2} C_F \frac{1}{\epsilon} \Gamma. \end{aligned} \quad (3.63)$$

Hence, we find that the sum of the counterterm and the result of the correction to the operator must be finite

$$\left(\frac{\sqrt{Z_q Z_h}}{Z_{\mathcal{O}}} - 1 \right) \Gamma + \frac{g_s^2}{(4\pi)^2 \epsilon} \Gamma \stackrel{!}{=} 0. \quad (3.64)$$

Inserting Z_h and Z_q from above, expanding in g_s and solving for $Z_{\mathcal{O}}$ yields in the $\overline{\text{MS}}$ scheme

$$Z_{\mathcal{O}}^{HQET} = 1 + \frac{3}{2} \frac{g_s^2}{(4\pi)^2} C_F \frac{1}{\epsilon}, \quad (3.65)$$

which is independent of the structure of the Γ . In QCD, this is not as easy and the currents for the different Dirac structures need to be considered separately. Since the current $\bar{q}\gamma_\mu Q$ is conserved we find in this case

$$Z_{\mathcal{O}}^{QCD} = 1. \quad (3.66)$$

Matching

We can find a connection between the heavy quark field Q in QCD and h_v in HQET through a matching procedure. Coupling the full and the effective side with renormalized fields through

$$\bar{Q}_R Q_R = C \bar{h}_{v,R} h_{v,R} \quad (3.67)$$

and with

$$\frac{1}{Z_{\text{QCD}}^{\text{os}}} \bar{Q} Q = C \frac{1}{Z_{\text{HQET}}^{\text{os}}} \bar{h}_v h_v \quad (3.68)$$

we find that $C = 1/Z_{\text{QCD}}^{\text{os}}$ and therefore

$$Q = \frac{1}{[Z_{\text{QCD}}^{\text{os}}]^{1/2}} h_v. \quad (3.69)$$

The QCD composite operator can now be related to the HQET operator. Thus, we can perform a matching calculation for the heavy-light vector current. Therefore, we compute perturbative corrections to the operator in the full and the effective theory, namely QCD and HQET, and compare the renormalized currents

$$\mathcal{O}_R^{QCD} = \sum_i C_i \mathcal{O}_{i,R}^{HQET}. \quad (3.70)$$

The quantities are much easier to calculate when they are bare, where we have $\mathcal{O}_B = Z_{\mathcal{O}} \mathcal{O}_R$. Thus we have

$$\frac{1}{Z_{\mathcal{O}}^{\text{QCD}}} \bar{q}\gamma_\mu Q = C_1 \frac{1}{Z_{1,\mathcal{O}}^{\text{HQET}}} \bar{q}\gamma_\mu h_v + C_2 \frac{1}{Z_{2,\mathcal{O}}^{\text{HQET}}} \bar{q}v_\mu h_v. \quad (3.71)$$

Since $Z_{1,\mathcal{O}}^{\text{HQET}} = Z_{2,\mathcal{O}}^{\text{HQET}} = Z_{\mathcal{O}}^{\text{HQET}}$ we find using Equation (3.69)

$$\frac{Z_{\mathcal{O}}^{\text{HQET}}}{Z_{\mathcal{O}}^{\text{QCD}} [Z_{\text{QCD}}^{\text{os}}]^{1/2}} \bar{q}\gamma_\mu h_v = C_1 \bar{q}\gamma_\mu h_v + C_2 \bar{q}v_\mu h_v. \quad (3.72)$$

The Wilson coefficients $C_{1,2}$ contain the short-distance effects. This means that they are not sensitive to the infrared properties of the amplitude. This allows us to freely choose the properties of the external states. We set the external momentum of the light quark to be zero. Further, we choose the momentum of the heavy quark to be $p = mv$. Thus, the external residual momentum is $k = 0$ which results in scaleless

one-loop integrals in HQET. Therefore, higher orders in HQET are zero and we solely need to compute diagrams in the full theory which we find to be

$$\begin{aligned} & -ig_s^2 C_F \int \frac{d^D \ell}{(2\pi)^D} \frac{\gamma_\mu \not{\ell} \gamma^\lambda (\not{p} + \not{\ell} + m) \gamma^\mu}{[(p + \ell)^2 - m^2][\ell^2]^2} \\ &= \frac{g_s^2}{(4\pi)^2} C_F 2 (v^\lambda - \gamma^\lambda). \end{aligned} \quad (3.73)$$

Since $Z_{\mathcal{O}}^{\text{QCD}} = 1$ we find that

$$\frac{Z_{\mathcal{O}}^{\text{HQET}}}{[Z_{\text{QCD}}^{\text{os}}]^{1/2}} \bar{q} \left(\gamma_\mu + 2 \frac{g_s^2 C_F}{(4\pi)^2} (\gamma_\mu - v_\mu) \right) Q = C_1 \bar{q} \gamma_\mu h_\nu + C_2 \bar{q} v_\mu h_\nu \quad (3.74)$$

$$\Rightarrow \bar{q} \left[\gamma_\mu \frac{g_s^2 C_F}{(4\pi)^2} \left(4v_\mu + \left[3 \ln \left(\frac{m^2}{\mu^2} \right) - 8 \right] \right) \right] h_\nu = C_1 \bar{q} \gamma_\mu h_\nu + C_2 \bar{q} v_\mu h_\nu \quad (3.75)$$

and as a result

$$C_1 = 1 + \frac{g_s^2(\mu)}{(4\pi)^2} C_F \left[\frac{3}{2} \ln \left(\frac{m^2}{\mu^2} \right) - 4 \right], \quad (3.76)$$

$$C_2 = 2 \frac{g_s^2(\mu)}{(4\pi)^2} C_F. \quad (3.77)$$

3.4. Matching of the Four-Quark Operator

3.4.1. Four-Quark Operator

The $\Delta B = 2$ four-quark operator in QCD is given by

$$\mathcal{O}^{\Delta B=2} = \bar{b} \gamma_\mu \frac{1}{2} (1 - \gamma_5) q \bar{b} \gamma^\mu \frac{1}{2} (1 - \gamma_5) q, \quad (3.78)$$

and the corresponding effective operators in HQET are

$$\mathcal{O}_L^{\text{eff}} = 2 \bar{h}^+ \gamma_\mu \frac{1}{2} (1 - \gamma_5) q \bar{h}^- \gamma^\mu \frac{1}{2} (1 - \gamma_5) q, \quad (3.79)$$

$$\mathcal{O}_S^{\text{eff}} = 2 \bar{h}^+ \frac{1}{2} (1 - \gamma_5) q \bar{h}^- \frac{1}{2} (1 - \gamma_5) q. \quad (3.80)$$

Here, the field \bar{h}^+ creates a heavy quark and \bar{h}^- annihilates a heavy antiquark. The four-quark operator in QCD contains two b fields which can represent both, a quark or an antiquark field. One of them eventually becomes the h^+ field and the other one the h^- field. Thus, we find an additional factor of 2 in Equations (3.79) and (3.80). The tree level Feynman diagram is displayed in Figure 3.4.

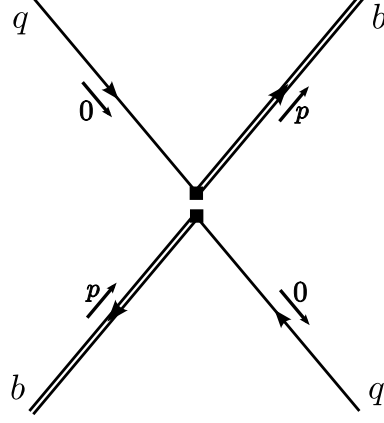


Figure 3.4.: Here, the $\Delta B = 2$ four-quark operator is depicted. The heavy quark has the momentum p and the light quark 0 . Here, h^+ denotes the heavy quark and h^- denotes the heavy anti-quark.

Computing the perturbative corrections to the QCD four-quark operator we eventually end up with two different operator structures

$$\mathcal{O}_L = \bar{b}\gamma_\mu(1 - \gamma_5)q\bar{b}\gamma^\mu(1 - \gamma_5)q, \quad (3.81)$$

$$\mathcal{O}_S = \bar{b}(1 - \gamma_5)q\bar{b}(1 - \gamma_5)q. \quad (3.82)$$

We write the partonic matrix element of an operator as

$$\langle \mathcal{O} \rangle = \langle b\bar{q} | \mathcal{O} | \bar{b}q \rangle, \quad (3.83)$$

where b , \bar{b} , q and \bar{q} are the external quark states.

For the matrix elements of the two operator structures in Equation (3.81) and (3.82) we find

$$\begin{aligned} \langle \mathcal{O}_L \rangle_0 &= \langle b\bar{q} | \bar{b}\gamma_\mu(1 - \gamma_5)q\bar{b}\gamma^\mu(1 - \gamma_5)q | \bar{b}q \rangle \\ &= 2\bar{u}_b^\alpha \gamma_\mu(1 - \gamma_5)u_q^\alpha \bar{v}_b^\beta \gamma^\mu(1 - \gamma_5)v_q^\beta - 2\bar{u}_b^\alpha \gamma_\mu(1 - \gamma_5)v_q^\alpha \bar{v}_b^\beta \gamma^\mu(1 - \gamma_5)u_q^\beta, \end{aligned} \quad (3.84)$$

where α and β are color factors, and analogously

$$\begin{aligned} \langle \mathcal{O}_S \rangle_0 &= \langle b\bar{q} | \bar{b}(1 - \gamma_5)q\bar{b}(1 - \gamma_5)q | \bar{b}q \rangle \\ &= 2\bar{u}_b^\alpha(1 - \gamma_5)u_q^\alpha \bar{v}_b^\beta(1 - \gamma_5)v_q^\beta - 2\bar{u}_b^\alpha(1 - \gamma_5)v_q^\alpha \bar{v}_b^\beta(1 - \gamma_5)u_q^\beta. \end{aligned} \quad (3.85)$$

3.4.2. Perturbative Corrections

During the calculation of the partonic matrix elements of the diagrams in Figure 3.5 we encounter matrix elements with the following color structures

$$\begin{aligned}\langle \bar{b}\gamma_\mu(1-\gamma_5)T^A q \bar{b}\gamma^\mu(1-\gamma_5)T^A q \rangle &= \frac{N_C - 1}{2N_C} \langle \mathcal{O}_L \rangle, \\ \langle \bar{b}(1-\gamma_5)T^A q \bar{b}(1-\gamma_5)T^A q \rangle &= -\frac{N_C + 1}{2N_C} \langle \mathcal{O}_S \rangle - \frac{1}{4} \langle \mathcal{O}_L \rangle,\end{aligned}$$

where we used the Fierz transformations (see Appendix A)

$$\begin{aligned}\bar{u}_1\gamma_\mu(1-\gamma_5)u_2\bar{u}_3\gamma^\mu(1-\gamma_5)u_4 \\ = -\bar{u}_1\gamma_\nu(1-\gamma_5)u_4\bar{u}_3\gamma^\nu(1-\gamma_5)u_2\end{aligned}\tag{3.86}$$

and

$$\begin{aligned}\bar{u}_1(1-\gamma_5)u_2\bar{u}_3(1-\gamma_5)u_4 \\ = \bar{u}_1(1-\gamma_5)u_4\bar{u}_3(1-\gamma_5)u_2 + \frac{1}{2}\bar{u}_1\gamma_\mu(1-\gamma_5)u_4\bar{u}_3\gamma^\mu(1-\gamma_5)u_2.\end{aligned}$$

We also encounter structures including several γ matrices which we can simplify using the following relations

$$\begin{aligned}\bar{b}\gamma_\alpha\gamma_\beta\gamma_\mu(1-\gamma_5)q\bar{b}\gamma^\alpha\gamma^\beta\gamma^\mu(1-\gamma_5)q &= 4(4-\epsilon)\mathcal{O}_L + E, \\ \bar{b}\gamma_\alpha\gamma_\beta(1-\gamma_5)q\bar{b}\gamma^\alpha\gamma^\beta(1-\gamma_5)q &= -4\mathcal{O}_L,\end{aligned}$$

where the evanescent operator E vanishes in $D = 4$ dimensions.

We can now compute the diagrams in Figure 3.5. The diagrams (a) and (b) factorize and are already known from the calculation of the heavy-light two-quark current. Their result is the same, namely

$$D_{(a)} = D_{(b)} = -2C_F \frac{\alpha_s(\mu)}{4\pi} (\langle \mathcal{O}_L \rangle_0 + \langle \mathcal{O}_S \rangle_0).$$

The diagrams (c) and (d) also yield the same result which is

$$D_{(c)} = D_{(d)} = -\frac{2N_C - 1}{2N_C} \frac{\alpha_s(\mu)}{4\pi} \langle \mathcal{O}_L \rangle_0 - \frac{N_C + 1}{N_C} \frac{\alpha_s(\mu)}{4\pi} \langle \mathcal{O}_S \rangle_0$$

and for diagram (e) we find

$$D_{(e)} = -\frac{5(N_C - 1)}{2N_C} \frac{\alpha_s(\mu)}{4\pi} \langle \mathcal{O}_L \rangle_0 - \frac{3(N_C - 1)}{N_C} \frac{\alpha_s(\mu)}{4\pi} \frac{1}{\epsilon} \langle \mathcal{O}_L \rangle_0.$$

The diagram (f) is scaleless and therefore does not contribute

$$D_{(f)} = 0.$$

The final result for the operator including radiative corrections in QCD is then

$$\langle \mathcal{O}_L \rangle = \langle \mathcal{O}_L \rangle_0 + 2D_{(a)} + 2D_{(c)} + D_{(e)}.$$

As above, the perturbative corrections vanish in HQET by choosing the external residual momentum to be zero.

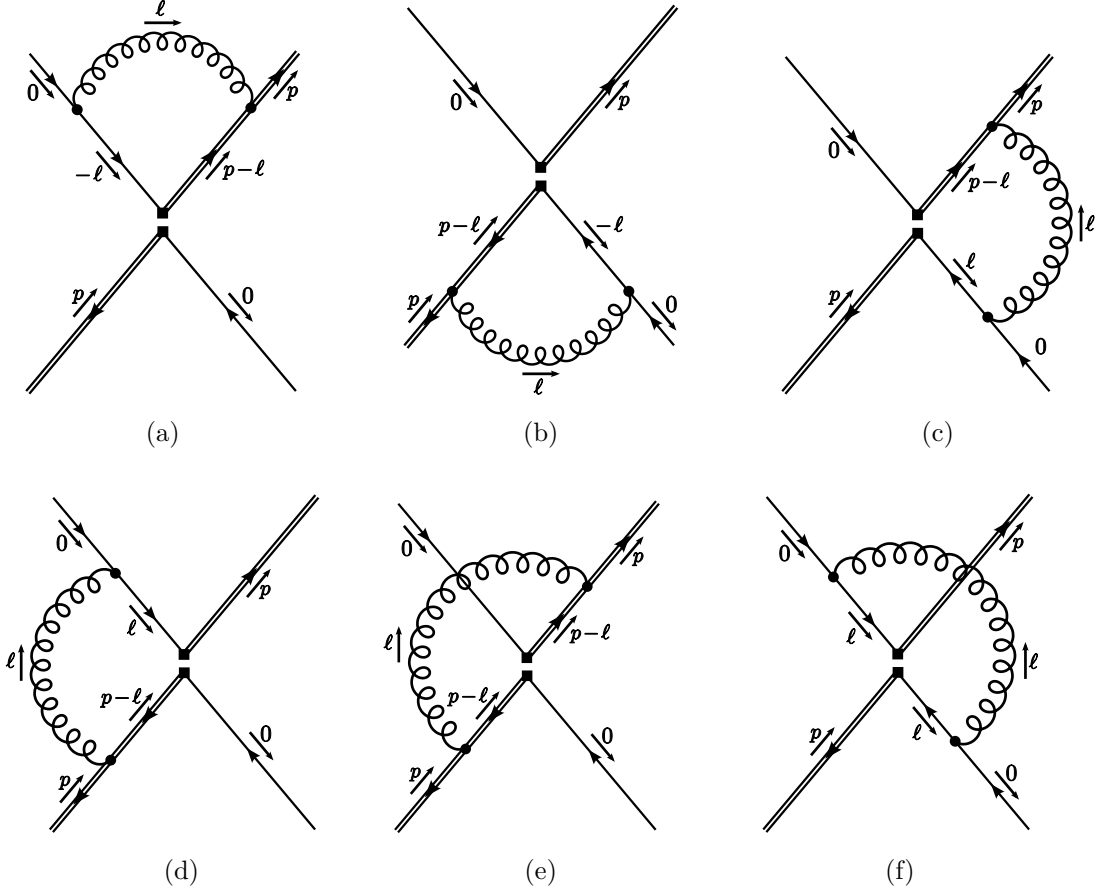


Figure 3.5.: Four-Quark Operator Loop Corrections

3.4.3. Matching

We can now perform the matching analogously to the one for the heavy-light current above

$$\langle \mathcal{O}_L^R \rangle = C_L \langle \mathcal{O}_L^{eff,R} \rangle + C_S \langle \mathcal{O}_S^{eff,R} \rangle \quad (3.87)$$

$$\Rightarrow \frac{Z_{eff}}{Z_{full} Z_{\text{QCD}}^{\text{os}}} \langle \mathcal{O}_L \rangle = C_L \langle \mathcal{O}_L^{eff} \rangle + C_S \langle \mathcal{O}_S^{eff} \rangle. \quad (3.88)$$

Here, obtain for the renormalization constants of the operators in the full and the effective theory

$$Z_{full} = 1 - \frac{\alpha_s(\mu)}{4\pi} \frac{3(N_C - 1)}{N_C} \frac{1}{\epsilon}, \quad (3.89)$$

$$Z_{eff} = 1 + 3C_F \frac{\alpha_s(\mu)}{4\pi} \frac{1}{\epsilon}. \quad (3.90)$$

We perform the matching at the scale $\mu = m_b$. This way the Wilson coefficients do not include large logarithms. As a final result we find

$$C_L(m_b) = 1 - \frac{8N_C^2 + 9N_C - 15}{2N_C} \frac{g_s^2}{(4\pi)^2} \quad (3.91)$$

$$C_S(m_b) = -2(N_C + 1) \frac{g_s^2}{(4\pi)^2}, \quad (3.92)$$

which coincides with the result in [59–61].

3.4.4. Running of the Four-Quark Operator

The dependence of the four-quark operator on the renormalization scale is known up to two loops [62] and is given by

$$\begin{aligned} \mathcal{O}^{\Delta B=2}(\mu) &= \mathcal{O}^{\Delta B=2}(\mu_0) \left(\frac{\alpha_s^{(n_f)}(\mu)}{\alpha_s^{(n_f)}(\mu_0)} \right)^{\gamma_0/(2\beta_0^{(n_f)})} \\ &\times \left[1 + \frac{\gamma_0}{2\beta_0^{(n_f)}} \left(\frac{\gamma_1}{\gamma_0} - \frac{\beta_1^{(n_f)}}{\beta_0^{(n_f)}} \right) \frac{\alpha_s^{(n_f)}(\mu) - \alpha_s^{(n_f)}(\mu_0)}{4\pi} + \mathcal{O}(\alpha_s^3) \right], \end{aligned} \quad (3.93)$$

where μ_0 is a reference scale where $\alpha(\mu_0)$ is known. Here, the anomalous dimension of the operator $\mathcal{O}^{\Delta B=2}(\mu)$ is given by

$$\gamma(\alpha_s) = \frac{d \log Z(\alpha_s(\mu))}{d \log \mu} = \gamma_0 \frac{\alpha_s}{4\pi} + \gamma_1 \left(\frac{\alpha_s}{4\pi} \right)^2 + \mathcal{O}(\alpha_s^3), \quad (3.94)$$

with

$$\gamma_0 = 6 \frac{N_c - 1}{N_c}, \quad \gamma_1 = -\frac{N_c - 1}{2N_c} \left(\frac{19}{3} N_c + 21 - \frac{57}{N_c} - \frac{4}{3} n_f \right). \quad (3.95)$$

In this case the number of flavors includes the b quark and is given by $n_f = 5$. The coefficients of the β -function are given by

$$\beta_0 = \frac{11}{3} N_c - \frac{2}{3} n_f, \quad \beta_1 = \frac{34}{3} N_c^2 - \left(\frac{13}{3} N_c - \frac{1}{N_c} \right) n_f. \quad (3.96)$$

4. D^{**} Spectroscopy and $B \rightarrow D^{**} \ell \nu$

Within the last years there has been a great experimental progress concerning semileptonic B decays at the B -factories. Several decays into excited charm mesons have been seen such as $B \rightarrow D^{**} \ell \nu$, where D^{**} denotes the first four orbital excitations of the mesonic ground states. Experimentally, only the product of the branching ratios $\mathcal{B}(B \rightarrow D^{**} \ell \nu) \times \mathcal{B}(D^{**} \rightarrow D^{(*)} \pi)$ can be extracted from data.

We consider these orbitally excited D mesons to be heavy, which means that we treat the contained c quark as a heavy quark within HQET. Then, the four states can be classified by their total angular momentum of the light degrees of freedom, in particular $j = 1/2$ and $j = 3/2$. Preceding theoretical approaches predict that the rates $\mathcal{B}(B \rightarrow D^{**} \ell \nu) \times \mathcal{B}(D^{**} \rightarrow D^{(*)} \pi)$ for the $j = 3/2$ states are significantly larger than the ones for the $j = 1/2$ states. This is in contradiction with the experimental findings, where the sums of the rates of the respective $j = 1/2$ and $j = 3/2$ states are roughly the same. In the literature this tension is referred to as the ‘1/2 vs. 3/2 puzzle’ [63].

This puzzle has been addressed by experimentalists and theorists in the past. Experimentalists have tried to resolve the issue by improving their understanding of the data and by optimizing the analyses. A theoretical approach to relief the tension was to include radially excited states as a background that may also contribute to the rate of the $j = 1/2$ states and thus enhance it [64].

The two states with total angular momentum $k = 1$ have the same quantum numbers. Those states can mix due to higher order terms in HQET that couple the light degrees of freedom to the heavy quark spin. Here, we will investigate if this mixing can ease the tension between the values extracted from theory and data. This mixing is a subleading effect in HQET but has the potential to produce a substantial effect [65]. Previous investigations claim that the mixing is too small and omit it [66] or that it is not favored by present data [67]. Other studies have determined a small mixing angle [68, 69].

We re-investigate the aspect of mixing in [70], which this chapter is based on.¹ First, we will briefly summarize the spectroscopy of heavy mesons. Then, we will investigate the mixing of the orbitally excited states and extract the mixing angle from data. We then study the effect on semileptonic decays and finally we will examine the impact of mixing on the total widths.

¹The numerical values are slightly updated compared to the ones in the paper.

4.1. Spectroscopy

Heavy mesons contain one heavy quark Q and a light quark q . In the heavy quark limit, where $m_Q \rightarrow \infty$, we encounter a heavy quark spin symmetry (see Chapter 3). This means that the heavy quark spin decouples from the light degrees of freedom (namely the light quarks and gluons) and that they are both separately conserved by strong interactions [71].

Due to this symmetry we can arrange all heavy hadrons into spin-symmetry doublets in which their masses and widths are degenerate in the heavy quark limit. They can be classified by the total angular momentum of their light degrees of freedom j , which is a conserved quantum number in the heavy quark limit. The ground states of the heavy mesons consisting of the 0^- pseudoscalar meson and the 1^- vector meson then emerge in one doublet, such as (D, D^*) or (B, B^*) .

Orbitally excited mesons in which the light degrees of freedom have an additional orbital angular momentum of $\ell = 1$, can be arranged in two doublets with $j = 1/2$ and $j = 3/2$, respectively. If we couple j to the spin of the heavy quark and consider a parity factor $(-1)^{\ell+1}$ we obtain for $j = 1/2$ a doublet with quantum numbers $(0^+, 1^+)$, and for $j = 3/2$ we obtain $(1^+, 2^+)$. Here, the total angular momentum \vec{K} is

$$\vec{K} = \vec{J} + \vec{\sigma} = \vec{L} + \vec{s} + \vec{\sigma},$$

where \vec{L} is the orbital angular momentum and \vec{J} the angular momentum of the light degrees of freedom. The spin of the light quark is denoted by \vec{s} and $\vec{\sigma}$ is the spin of the heavy quark.

For higher orbital excitations we can proceed in the same way and get doublets with the quantum numbers [71]

$$\left((\ell - 1)^{(-1)^{\ell+1}}, \ell^{(-1)^{\ell+1}} \right) \quad \text{for } j = \ell - 1/2$$

and

$$\left(\ell^{(-1)^{\ell+1}}, (\ell + 1)^{(-1)^{\ell+1}} \right) \quad \text{for } j = \ell + 1/2.$$

Possible higher orbitally excited states listed in the PDG book [72] do not give conclusive quantum numbers, though.

We are interested in the first set of four orbitally excited D mesons and use the notation

$$\begin{aligned} & \left(\begin{array}{l} |D(0^+)\rangle \\ |D(1^+)\rangle \end{array} \right) \quad \text{with } j = 1/2, \\ & \left(\begin{array}{l} |D^*(1^+)\rangle \\ |D^*(2^+)\rangle \end{array} \right) \quad \text{with } j = 3/2. \end{aligned} \tag{4.1}$$

State	Masse [MeV]	Width [MeV]	j
$D(0^+)$	2318 ± 29	267 ± 40	$1/2$
$D(1^+)$	2427 ± 40	380 ± 120	$1/2$
$D^*(1^+)$	2421.4 ± 0.6	27.4 ± 2.5	$3/2$
$D^*(2^+)$	2462.6 ± 0.15	49.0 ± 1.3	$3/2$

Table 4.1.: Averages of the existing mass and width measurements for the D^{**} states taken from the PDG [72]. We assign them to the different j according to the size of their total decay widths.

As already mentioned, in the limit $m_c \rightarrow \infty$ we have degenerate masses for the states in the respective spin symmetry doublets, which can be expressed by [41]

$$\begin{aligned} M(D(0^+)) &= M(D(1^+)) = m_c + \bar{\Lambda}_{1/2}, \\ M^*(D(1^+)) &= M(D^*(2^+)) = m_c + \bar{\Lambda}_{3/2}, \end{aligned} \quad (4.2)$$

where $\bar{\Lambda}_j$ is the binding energy of the mesons in this exact limit. From Equation (4.2) it is obvious, that the splitting between the two doublets is independent of the mass of the heavy quark. In fact, it does not even depend on the quark flavor. It is related to the excitations of the light degrees of freedom and therefore of order Λ_{QCD} .

In Table 4.1, we show the averages of the existing mass and width measurements for the D^{**} states taken from the PDG [72]. We have assigned the 1^+ states to the respective j doublets according to their total decay widths. The strong decays of the $j = 3/2$ states correspond to D wave transitions. These are suppressed by angular momentum compared to the $j = 1/2$ states which only decay through an S wave transition. Hence, we classify the $j = 1/2$ states to be broad and the $j = 3/2$ states to be narrow.

Assigning the 1^+ states to the doublets on the basis of their widths results in the mass hierarchy as shown in Figure 4.1. Here we observe a “level inversion” of the states if we disregard mixing.

4.2. Power Corrections to the HQET Hamiltonian

We now switch on power corrections. The Hamiltonian density at order $1/m$ is

$$\mathcal{H}_{1/m} = \frac{1}{2m_c} \bar{c} (iD_\perp)^2 c + \frac{g_s}{2m_c} \bar{c} (\vec{\sigma} \cdot \vec{B}) c. \quad (4.3)$$

Here, the first term is the kinetic operator and the second term is the chromomagnetic operator. The latter couples the heavy quark spin $\vec{\sigma}$ to the chromomagnetic field \vec{B} and thus to the light degrees of freedom. This eventually leads to the breaking of heavy-quark spin-symmetry. Then j is not an invariant quantity any more.

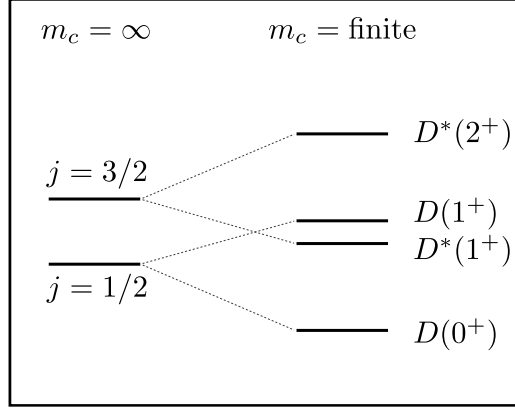


Figure 4.1.: Schematic depiction of the mass hierarchy of the orbitally excited D mesons in the heavy quark limit and for a finite mass of the c quark.

Nevertheless, we still consider j to be a conserved quantum number since its change is $1/m$ suppressed.

The first term in Equation (4.3) only affects the doublets in a spin-independent way

$$M_j = m_c + \bar{\Lambda}_j + \frac{1}{2m_c} \mu_\pi^2(j), \quad (4.4)$$

where $\mu_\pi^2(j)$ is related to the kinetic operator. We see that this contribution solely leads to a mass shift of the entire doublet and for further treatments we will simply absorb this shift into the doublet masses M_j .

The second term in Equation (4.3) is of much more interest since it is responsible for the mixing that we want to investigate. We do not know much about the dynamics of the chromomagnetic field for the D^{**} mesons. Hence, we will make some assumptions based on the fact that it is generated by the angular momentum of the light degrees of freedom, namely \vec{L} and \vec{s} , at the location of the heavy quark spin. Our conjecture is that we have two different gyro-chromomagnetic factors α' and β' for the orbital momentum and the spin of the light quark, and therefore

$$\vec{B} \sim \alpha' \vec{L} + \beta' \vec{s} = \alpha \vec{J} + \beta \vec{s}. \quad (4.5)$$

The second term we obtain using that $\vec{J} = \vec{L} + \vec{s}$ and by redefining the gyro-chromomagnetic factors.

We can now re-write the second term in Equation (4.3)

$$H_{1/m}^G = \int d^3\vec{x} \frac{g_s}{2m_c} \bar{c}(\vec{\sigma} \cdot \vec{B})c \equiv P_1(\vec{J} \cdot \vec{\sigma}) + P_2(\vec{s} \cdot \vec{\sigma}) \quad (4.6)$$

introducing operators P_1 and P_2 which only act on the radial wave functions of the light degrees of freedom. Here, the last term is eventually responsible for the mixing between our 1^+ states allowing j to change. The mixing of the two states is possible because they have the same external quantum numbers, such as the total angular momentum and parity.

We can now let our Hamiltonian

$$H = \int d^3\vec{x} (\mathcal{H}_0 + \mathcal{H}_{1/m})$$

act on the states in the spin symmetry doublets. The states $|D(0^+)\rangle$ and $|D^*(2^+)\rangle$ remain eigenstates of the Hamiltonian

$$H|D(0^+)\rangle = \left(M_{1/2} - \frac{3}{4}g + \frac{1}{4}g'\right) |D(0^+)\rangle, \quad (4.7)$$

$$H|D^*(2^+)\rangle = \left(M_{3/2} + \frac{3}{4}g + \frac{1}{4}g'\right) |D^*(2^+)\rangle, \quad (4.8)$$

where the masses $M_{1/2}$ and $M_{3/2}$ are defined in Equation (4.4). For simplicity, we assume that the constants $g \sim \langle P_1 \rangle$ and $g' \sim \langle P_2 \rangle$, which are obtained from the radial wave functions, are equal for both spin symmetry doublets.

Applying the Hamiltonian to the two 1^+ states yields that they are not eigenstates of the Hamiltonian any more when we consider $1/m$ corrections

$$H|D(1^+)\rangle = \left(M_{1/2} + \frac{1}{4}g - \frac{1}{12}g'\right) |D(1^+)\rangle + \frac{\sqrt{2}}{3}g'|D^*(1^+)\rangle, \quad (4.9)$$

$$H|D^*(1^+)\rangle = \left(M_{3/2} - \frac{5}{4}g - \frac{5}{12}g'\right) |D^*(1^+)\rangle + \frac{\sqrt{2}}{3}g'|D(1^+)\rangle. \quad (4.10)$$

We observe that the respective other 1^+ state mixes in there. All spin wave functions used to compute the impact of the Hamiltonian on the states above are given in the Appendix B.1.

4.3. Extracting the Mixing Angle

In order to compute the size of the mixing we consider the 2×2 sub matrix of the Hamiltonian

$$\mathbf{H} = \begin{pmatrix} M & a \\ a & M^* \end{pmatrix}, \quad (4.11)$$

where we define

$$M \equiv M_{1/2} + \frac{1}{4}g - \frac{1}{12}g', \quad (4.12)$$

$$M^* \equiv M_{3/2} - \frac{5}{4}g - \frac{5}{12}g', \quad (4.13)$$

$$\Delta \equiv M^* - M = M_{3/2} - M_{1/2} - \frac{3}{2}g - \frac{1}{3}g', \quad (4.14)$$

$$a \equiv \frac{\sqrt{2}}{3}g'. \quad (4.15)$$

We can diagonalize the Hamiltonian and find the physical 1^+ states which are linear combinations of the states which we defined in the heavy quark limit

$$|D_L(1^+)\rangle = \cos\theta|D(1^+)\rangle + \sin\theta|D^*(1^+)\rangle, \quad (4.16)$$

$$|D_H(1^+)\rangle = -\sin\theta|D(1^+)\rangle + \cos\theta|D^*(1^+)\rangle. \quad (4.17)$$

Here, D_L is the eigenstate with the lower and D_H is the one with the higher eigenvalue. The corresponding eigenvalues are given by

$$M_{L/H} = \frac{1}{2} \left[(M + M^*) \pm \sqrt{\Delta^2 + 4a^2} \right]. \quad (4.18)$$

In Figure 4.2, all eigenvalues of the Hamiltonian are displayed. We notice, that we always have $M_H > M_L$ which means that we actually observe a “level repulsion”, which is typical for two-state systems. We see that the splitting within each doublet is identical when we put $g' = -g$, which we regard as a benchmark point. In this case we obtain from Equation (4.5)

$$\vec{B} \sim g\vec{J} + g'\vec{s} = g(\vec{J} - \vec{s}) = g\vec{L}, \quad (4.19)$$

which would imply that the spectrum does not depend on the light quark spin anymore.

The mixing angle can be determined by (see Appendix B.2)

$$\tan 2\theta = \frac{-2a}{\Delta} = \frac{-4\sqrt{2}g'}{6(M_{3/2} - M_{1/2}) - 9g + 2g'}. \quad (4.20)$$

At a mixing angle of $|\theta| = 45^\circ$ we find maximal mixing of the two 1^+ states. A value for our mixing angle of $45^\circ \leq |\theta| \leq 90^\circ$ is beyond the crossing point of equal mixing. Then, we find that the $j = 3/2$ state now becomes the dominant contribution in the $|D_L(1^+)\rangle$ eigenstate. This way we can justify both, the “level inversion” shown in Figure 4.1 as well as the “level repulsion” observed in Figure 4.2. Looking at Equation (4.20) we see that a mixing angle of $|\theta| = 45^\circ$ corresponds to a value of $\Delta = 0$. A mixing angle beyond the crossing point results in a negative $\Delta < 0$.

The mixing angle θ is shown in Figure 4.3 as a function of g' with the constraint $g = -g'$. The horizontal line corresponds to the angle of maximum mixing and the vertical line indicates the best-fit value of g' of the fit we will discuss next.

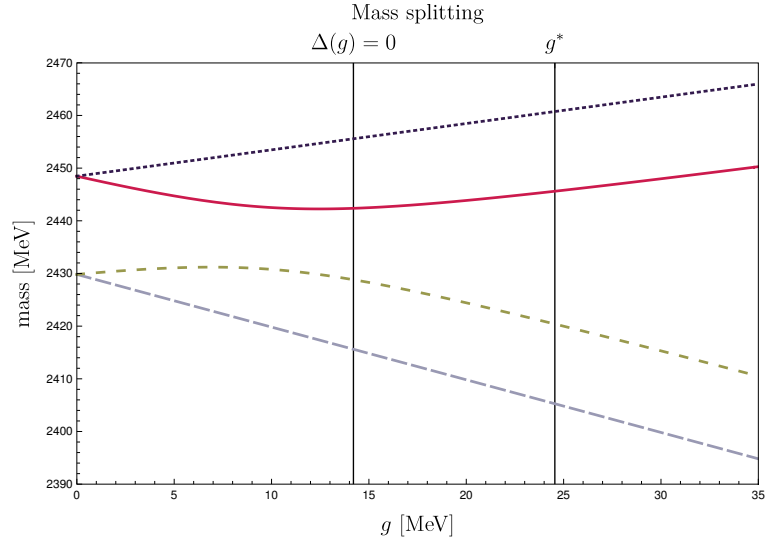


Figure 4.2.: In the heavy quark limit $m_c \rightarrow \infty$, corresponding to $g = g' = 0$, we observe that the orbitally excited states in the $j = 1/2$ and $j = 3/2$ doublet have degenerate masses. When we pass over to a finite mass m_c we find a splitting of the states within the doublets. We plot the masses of the orbitally excited states $D(0^+)$ (light-blue, long-dashed), $D_L(1^+)$ (green, short-dashed), $D_H(1^+)$ (red, solid) and $D^*(2^+)$ (dark blue, dotted) as a function of the parameter g . We fix the parameter g' by the condition $g' = -g$, where the splitting within each doublet is equal. The vertical lines indicate the best fit value g^* for g and the root of $\Delta(g, g' = -g) = 0$.

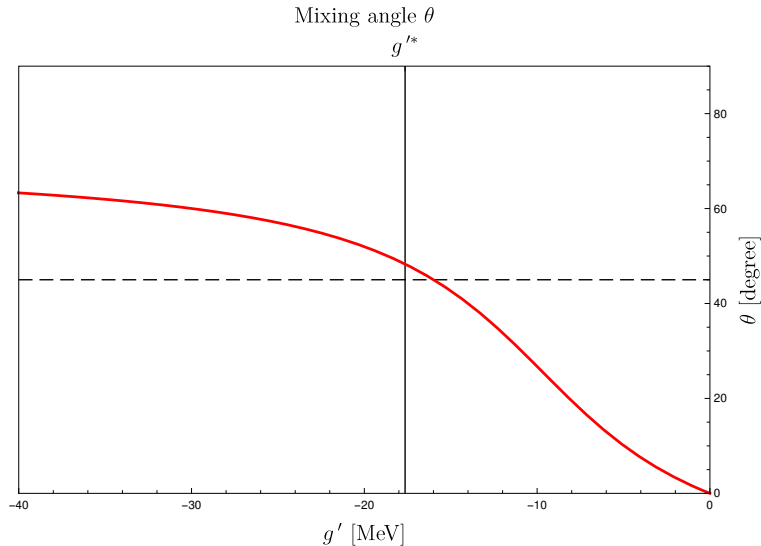


Figure 4.3.: The mixing angle θ plotted as a function of g' , where $g = -g'$. The vertical line corresponds to the best-fit point for g' . The horizontal line indicates the angle $\theta = 45^\circ$ of maximal mixing.

4.4. Fitting the Mixing Angle

Current measurements of the masses and widths of the orbitally excited D mesons do not give conclusive results. The fact that the errors on the average values published by the PDG [72] include statistical scale factors indicates that the individual measurements are not in good agreement with the averages. However, we still use these results to fit the parameters of our simple model. A more detailed description on how the fit is performed can be found in Appendix B.3.

Overall, there are four model parameters that we have to fit: $M_{1/2}$, $M_{3/2}$, g and g' . In the following, we will account for the mass hierarchy observed before by demanding $\Delta < 0$ for all fits. We also require a p-value $\geq 3\%$ to declare the fit as good.

First, we will confront our model with the PDG averages shown in Table 4.1. We observed before that we have equal splitting within our doublets when we set $g' = -g$. Here, we will use this constraint in order to reduce our model parameters to three, namely $M_{1/2}$, $M_{3/2}$ and g . With four PDG averages for the masses and three fit parameters this fit has 1 degree of freedom (d.o.f.). The fit yields the following best-fit point and parameter intervals at 68% confidence level (CL)

$$\begin{aligned} M_{1/2}^* &= (2425 \pm 2) \text{ MeV}, & M_{3/2}^* &= (2451.2 \pm 1.0) \text{ MeV}, \\ g^* &= (22.9 \pm 1.3) \text{ MeV}. \end{aligned} \tag{4.21}$$

However, computing the goodness of the fit we obtain $\chi^2 = 8.48$ which results in a p-value of 0.36% and thus we reject this fit. Nevertheless, we observe that the χ^2 is mainly driven by the 0^+ mass which corresponds to a deviation a little less than 3σ .

To study the large deviation further, we now extend our fit and use the 11 most precise individual measurements that also enter the PDG averages. Thus, we can now perform a fit including all our model parameters. We reject the fit again, since we obtain $\chi^2/\text{d.o.f.} = 35.9/7$ which corresponds to a p-value of less than 10^{-4} . However, we find that the χ^2 is mainly driven by the BaBar and Belle measurements for the 0^+ mass.

Assuming that the BaBar and Belle measurements of the 0^+ mass are inconsistent with the ZEUS measurement, we repeat our second fit without them and obtain $\chi^2/\text{d.o.f.} = 7.1/5$ with a corresponding p-value of 23%, which we consider as a good fit. For the best-fit point and the 68% CL intervals we find

$$\begin{aligned} M_{1/2}^* &= (2430 \pm 8) \text{ MeV}, & M_{3/2}^* &= (2448.5 \pm 1.2) \text{ MeV}, \\ g^* &= (24.5 \pm 1.3) \text{ MeV}, & g'^* &= (-18 \pm 6) \text{ MeV}. \end{aligned} \tag{4.22}$$

At the best-fit point the individual pull values are given by

$$\text{pull}_i \equiv \frac{M_i - M_i(M_{1/2}^*, M_{3/2}^*, g^*, g'^*)}{\sigma_i} \tag{4.23}$$

Mass [MeV]	Pull [σ]	Collaboration	Reference
$D(0^+)$			
2297±22	-5.00	BaBar	[73] ×
2308±36	-2.75	Belle	[74] ×
2407±41	0.0	FOCUS	[75]
$D_L(1^+)$			
2423.1±1.7	+1.27	ZEUS	[76]
2420.1±0.8	-1.05	BaBar	[77]
2426.0±3.2	+1.69	Belle	[78]
$D_H(1^+)$			
2427±36	-0.41	Belle	[74]
2477±56	+0.63	BaBar	[79] †
$D^*(2^+)$			
2462.5±2.7	+0.01	ZEUS	[76]
2462.2±0.8	-0.34	BaBar	[77]
2464.5±2.2	+0.92	FOCUS	[75]

Table 4.2.: Here, we display the most precise values of the masses for the various measurements of D^{**} . We also show the pull values as defined in Equation (4.23) at the best-fit point given in Equation (4.22). We omit the measurements marked with a × in the fit. The measurements marked with † lack an estimate for their systematic uncertainty. Therefore we have doubled their statistical uncertainty.

for every measurement i . They are listed in Table 4.2.

For our best-fit values in Equation (4.22) we find $g' \simeq -g < 0$ which is in accordance with equal splitting within the spin symmetry doublets. We also obtain a value of $\Delta \simeq -12$ MeV which yields a large mixing angle of

$$\theta = \left(63_{-13}^{+11}\right)^\circ$$

at 68% CL. In previous studies (e.g. in [68,69]) a mixing angle between 16° and 20° has been determined. In our case the interchange of the 1^+ states corresponds to a replacement $\theta \rightarrow 90^\circ - \theta$, though. This leads to an effective mixing of pure states of 27° , which is still larger than observed in preceding analyses.

4.5. Effects on Semileptonic Decays $B \rightarrow D^{**}\ell\nu$

Exclusive semileptonic B decays to orbitally excited charmed mesons have already been studied in [66]. They included $1/m$ corrections to the heavy quark limit but neglected the effect of mixing, which we aim to study here.

We consider both quarks that are involved in the exclusive semileptonic $b \rightarrow c$ transitions to be heavy. This means they follow the heavy quark symmetry and we can write the momenta as $p_B = M_B v$ and $p_{D^{**}} = M_{D^{**}} v'$, respectively, and we define $\omega = v \cdot v'$. The differential decay rate can be computed via

$$\frac{d^2\Gamma}{d\omega d\cos\theta^*} = \frac{V_{cb}^2 G_F^2 M_{D^{**}}^2}{256\pi^3 M_B} \sqrt{\omega^2 - 1} |\mathcal{M}|^2, \quad (4.24)$$

where θ^* is the helicity angle of the lepton, more specifically the polar angle of ℓ in the $\ell\nu$ rest frame. The matrix element can be split up into a hadronic and a leptonic part

$$|\mathcal{M}|^2 = |\langle D^{**}\ell\nu | \bar{c}\gamma_\mu(1 - \gamma_5)b \bar{\ell}\gamma^\mu(1 - \gamma_5)\nu | B \rangle|^2 = L^{\mu\nu} W_{\mu\nu}, \quad (4.25)$$

where the leptonic tensor is given by

$$\begin{aligned} L^{\mu\nu} &= \sum_{\text{spins}} \langle \ell\nu | \bar{\ell}\gamma^\mu(1 - \gamma_5)\nu | 0 \rangle \langle 0 | \bar{\nu}\gamma^\nu(1 - \gamma_5)\ell | \ell\nu \rangle \\ &= \text{Tr} \left[\not{k}' \gamma^\mu (1 - \gamma_5) \not{k} \gamma^\nu (1 - \gamma_5) \right] \\ &= 8 \left(k^\mu k'^\nu - (k \cdot k') g^{\mu\nu} + k^\nu k'^\mu - i \epsilon^{\mu\nu\alpha\beta} k_\alpha k'_\beta \right). \end{aligned} \quad (4.26)$$

Here, k denotes the momentum of the charged lepton and k' the momentum of the neutrino.

The hadronic tensor

$$W_{\mu\nu} = \langle D^{**} | \bar{c}\gamma_\mu(1 - \gamma_5)b | B \rangle \langle B | \bar{b}\gamma_\nu(1 - \gamma_5)c | D^{**} \rangle \quad (4.27)$$

can be treated in the infinite mass limit. Then, for each multiplet, we can describe the hadronic weak transition currents by a single form factor which can be generalized from the initial Isgur Wise function for the ground states

$$\langle B(v) | \bar{b}\Gamma c | D(1^+; v', \epsilon) \rangle = 2\tau_{1/2}(vv') \text{Tr} \left[\bar{B}(v) \Gamma D(1^+; v', \epsilon) \right], \quad (4.28)$$

$$\langle B(v) | \bar{b}\Gamma c | D^*(1^+; v', \epsilon) \rangle = \sqrt{3}\tau_{3/2}(vv') v^\mu \text{Tr} \left[\bar{B}(v) \Gamma D_\mu^*(1^+; v', \epsilon) \right], \quad (4.29)$$

where ϵ is the polarization of the axialvector 1^+ states. The convention we use for the Isgur Wise functions is the same as in [66] and [80]. The spin representations for the states involved can be found e.g. in [81]

$$\bar{B}(v) = \sqrt{M_B} \gamma_5 \frac{1 + \not{v}}{2}, \quad (4.30)$$

$$D(1^+; v, \epsilon) = \sqrt{M_D} \frac{1 + \not{v}}{2} \gamma_5 \not{\epsilon}, \quad (4.31)$$

$$D_\mu^*(1^+; v, \epsilon) = \sqrt{M_{D^*}} \frac{3}{2} \frac{1 + \not{v}}{2} \gamma_5 \left[\epsilon_\mu - \frac{1}{3} \not{\epsilon} (\gamma_\mu - v_\mu) \right]. \quad (4.32)$$

Model	$\tau_{1/2}(1)$	$\rho_{1/2}^2$	$\tau_{3/2}(1)$	$\rho_{3/2}^2$
GI [83]	0.22	0.83	0.54	1.50
VD [84]	0.13	0.57	0.43	1.39
CCCN [85, 86]	0.06	0.73	0.51	1.45
ISGW [87]	0.34	1.08	0.59	1.76

Table 4.3.: Fit results for the two form factors parameterized in Equation (4.34) to four different quark models as taken from [82].

For our physical states we then find

$$\begin{aligned} \langle B|\bar{b}\Gamma c|D_L\rangle &= \cos\theta\langle B|\bar{b}\Gamma c|D(1^+)\rangle + \sin\theta\langle B|\bar{b}\Gamma c|D^*(1^+)\rangle, \\ \langle B|\bar{b}\Gamma c|D_H\rangle &= -\sin\theta\langle B|\bar{b}\Gamma c|D(1^+)\rangle + \cos\theta\langle B|\bar{b}\Gamma c|D^*(1^+)\rangle, \end{aligned} \quad (4.33)$$

where they now depend on both form factors $\tau_{1/2}(\omega)$ and $\tau_{3/2}(\omega)$ as well as the mixing angle.

The usual Isgur Wise functions are normalized to unity at $\omega = 1$. This is not the case for the form factors $\tau_j(\omega)$. They can be parameterized through [82]

$$\tau_j(\omega) = \tau_j(1) \left[\frac{2}{1+\omega} \right]^{2\rho_j^2}, \quad j = 1/2 \text{ or } j = 3/2, \quad (4.34)$$

where values for $\tau_j(1)$ and ρ_j^2 are given in different quark models in Table 4.3 as taken from [82]. These quark models are most reliable near the zero recoil point $\omega_{\min} = 1$, where the momentum transfer to the lepton-neutrino pair is maximal and the excited D meson is at rest in the rest frame of the B meson. For ω_{\max} this momentum transfer is minimal. Since our kinematic region for ω is quite limited

$$1 \leq \omega \leq \frac{M_B^2 + M_{D^{**}}}{2M_B M_{D^{**}}} \simeq 1.3,$$

the parameterization in Equation (4.34) is a good approximation.

We can constrain the form factors $\tau_j(\omega)$ by sum rules [88], where we have in particular

$$\mu_\pi^2 - \mu_G^2 \geq 9\epsilon_{1/2}^2 |\tau_{1/2}(1)|^2. \quad (4.35)$$

Here, $\epsilon_{1/2}$ is the excitation energy of the $j = 1/2$ doublet compared to the doublet of the ground states. The kinetic energy and chromomagnetic moment parameters μ_π and μ_G are related to the kinetic and chromomagnetic operators in the $1/m$ Hamiltonian. It has been observed that the difference on the left-hand side is numerically small $\mu_\pi^2 - \mu_G^2 \ll \mu_\pi^2$ which leads to the Bogomolnyi-Prasad-Sommerfield limit where we obtain $\mu_\pi^2 - \mu_G^2 = 0$. This would result in $\tau_{1/2}(1) = 0$ which implies

$$\tau_{1/2}(\omega) \ll \tau_{3/2}(\omega) \quad (4.36)$$

Channel	GI	VD	CCCN	ISGW
$m_c \rightarrow \infty$				
$\mathcal{B}(B^- \rightarrow D(0^+)\ell\bar{\nu})$	$4.7 \cdot 10^{-4}$	$1.8 \cdot 10^{-4}$	$3.7 \cdot 10^{-5}$	$1.0 \cdot 10^{-3}$
$\mathcal{B}(B^- \rightarrow D(1^+)\ell\bar{\nu})$	$6.4 \cdot 10^{-4}$	$2.5 \cdot 10^{-4}$	$4.9 \cdot 10^{-5}$	$1.4 \cdot 10^{-3}$
$\mathcal{B}(B^- \rightarrow D^*(1^+)\ell\bar{\nu})$	$4.4 \cdot 10^{-3}$	$2.9 \cdot 10^{-3}$	$4.0 \cdot 10^{-3}$	$4.7 \cdot 10^{-3}$
$\mathcal{B}(B^- \rightarrow D^*(2^+)\ell\bar{\nu})$	$7.4 \cdot 10^{-3}$	$4.9 \cdot 10^{-3}$	$6.7 \cdot 10^{-3}$	$8.0 \cdot 10^{-3}$
$\mathcal{B}(B^- \rightarrow D^{**}\ell\bar{\nu})$	1.3%	0.82%	1.1%	1.5%
$\frac{\mathcal{B}(B^- \rightarrow D^*(1^+)\ell\bar{\nu})}{\mathcal{B}(B^- \rightarrow D(1^+)\ell\bar{\nu})}$	6.9	12	81	3.4
m_c finite				
$\mathcal{B}(B^- \rightarrow D_L\ell\bar{\nu})$	$3.3 \cdot 10^{-3}$	$2.3 \cdot 10^{-3}$	$3.3 \cdot 10^{-3}$	$3.5 \cdot 10^{-3}$
$\mathcal{B}(B^- \rightarrow D_H\ell\bar{\nu})$	$2.0 \cdot 10^{-3}$	$1.1 \cdot 10^{-3}$	$1.0 \cdot 10^{-3}$	$2.8 \cdot 10^{-3}$
$\frac{\mathcal{B}(B^- \rightarrow D_L\ell\bar{\nu})}{\mathcal{B}(B^- \rightarrow D_H\ell\bar{\nu})}$	1.7	2.1	3.2	1.2

Table 4.4.: Our predictions for the branching fractions within various models from Table 4.3 for the channel $B^- \rightarrow D^{**}\ell\bar{\nu}$. The first 6 rows are computed in the infinite mass limit $m_c \rightarrow \infty$, where we use the doublet masses $M_{1/2}$ and $M_{3/2}$ from our fit as input. Here, $\mathcal{B}(B^- \rightarrow D^{**}\ell\bar{\nu})$ represents the sum of the four branching fractions above. The last three rows are obtained for a finite mass m_c where mixing between the two 1^+ states is allowed. We use the PDG averages from Table 4.1 for the masses.

and indicates that decays into the 1^+ state of the $j = 1/2$ doublet are substantially suppressed in comparison to the one in the $j = 3/2$ doublet. The values obtained in the models in Table 4.3 roughly show this behavior. However, this is currently not seen by data which gives rise to the ‘ $1/2 - 3/2$ ’ puzzle in semileptonic decays.

Now, we can compute the differential decay rates for the two 1^+ eigenstates for $B \rightarrow D_{L/H}\ell\nu$. We get

$$\begin{aligned}
\frac{d\Gamma_L}{d\omega} &= \frac{G_F V_{cb}^2 M_B^5}{24\pi^3} r_L^3 (\omega - 1) \sqrt{\omega^2 - 1} \\
&\left[\sin^2 \theta (\omega + 1)^2 [2(\omega - r_L)(1 - r_L\omega) - (1 - r_L^2 - 2r_L\omega)] |\tau_{3/2}(\omega)|^2 \right. \\
&\quad + 2 \cos^2 \theta [2r_L(\omega^2 - 1) + (5\omega - 1)(1 + r_L^2 - 2r_L\omega)] |\tau_{1/2}(\omega)|^2 \\
&\quad \left. + 2\sqrt{2} \sin \theta \cos \theta (\omega + 1)^2 [(1 + r_L)^2 - 4r_L\omega] \operatorname{Re}(\tau_{1/2}(\omega)\tau_{1/2}^*(\omega)) \right]
\end{aligned} \tag{4.37}$$

and

$$\begin{aligned}
\frac{d\Gamma_H}{d\omega} = & \frac{G_F V_{cb}^2 M_B^5}{24\pi^3} r_H^3 (\omega - 1) \sqrt{\omega^2 - 1} \\
& \left[\cos^2 \theta (\omega + 1)^2 [2(\omega - r_H)(1 - r_H\omega) - (1 - r_H^2 - 2r_H\omega)] |\tau_{3/2}(\omega)|^2 \right. \\
& + 2 \sin^2 \theta [2r_H(\omega^2 - 1) + (5\omega - 1)(1 + r_H^2 - 2r_H\omega)] |\tau_{1/2}(\omega)|^2 \\
& \left. - 2\sqrt{2} \sin \theta \cos \theta (\omega + 1)^2 [(1 + r_H)^2 - 4r_H\omega] \operatorname{Re}(\tau_{1/2}(\omega)\tau_{1/2}^*(\omega)) \right],
\end{aligned} \tag{4.38}$$

where $r_{L/H}$ denotes the ratio $r_{L/H} = M_{D_{L/H}}/M_B$. We see that the differential decay rates are now dependent on both form factors $\tau_j(\omega)$ as well as the mixing angle. In the limit of no mixing $\theta = 0$ we find the result from [80].

We can now calculate the branching fractions for the semileptonic B decay into the orbitally excited D mesons via

$$\mathcal{B}(B \rightarrow D^{**}\ell\nu) = \frac{\Gamma(B \rightarrow D^{**}\ell\nu)}{\Gamma_{\text{tot}}(B)} = \tau_B \Gamma(B \rightarrow D^{**}\ell\nu), \tag{4.39}$$

where we take the result $\cos \theta \simeq 0.45$ at the best-fit point. We also use the experimental result for the lifetime of the B meson τ_B . Our predictions for the branching fractions are shown in Table 4.4. The first six rows are determined in the infinite mass limit, while we consider mixing between the two 1^+ states for a finite m_c in the last three rows. We do not consider the experimental uncertainties, which are quite large, since this is merely a qualitative study of the mixing to see if this could have the potential to solve the ‘ $1/2 - 3/2$ ’ puzzle.

In order to answer this question we need to confront our predictions with the data shown in Table 4.5. Unfortunately, at the moment we only have data on the product of the branching fractions $\mathcal{B}(B \rightarrow D^{**}\ell\nu) \times \mathcal{B}(D^{**} \rightarrow D^*\pi)$. For now, we therefore assume that the subsequent strong decays $D^{**} \rightarrow D^*\pi$ have roughly the same size and obtain

$$\frac{\mathcal{B}(B^- \rightarrow D_L(1^+)\ell\bar{\nu})}{\mathcal{B}(B^- \rightarrow D_H(1^+)\ell\bar{\nu})} \approx 2.2 \tag{4.40}$$

for the ratio of the decays into the two 1^+ states. Comparing this with our predictions in Table 4.4 we see that our estimates including the mixing (row 9) are in reasonable agreement with the measurements while we observe a deviation from our results if we neglect mixing (row 6).

Decay Mode	\mathcal{B} (%)
$\mathcal{B}(B^- \rightarrow D(0^+)\ell\bar{\nu}) \times \mathcal{B}(D(0^+) \rightarrow D^+\pi^-)$	0.29 ± 0.05
$\mathcal{B}(B^- \rightarrow D_L(1^+)\ell\bar{\nu}) \times \mathcal{B}(D_L(1^+) \rightarrow D^{*+}\pi^-)$	0.285 ± 0.018
$\mathcal{B}(B^- \rightarrow D_H(1^+)\ell\bar{\nu}) \times \mathcal{B}(D_H(1^+) \rightarrow D^{*+}\pi^-)$	0.13 ± 0.04
$\mathcal{B}(B^- \rightarrow D^*(2^+)\ell\bar{\nu}) \times \mathcal{B}(D^*(2^+) \rightarrow D^{*+}\pi^-)$	0.078 ± 0.008

Table 4.5.: HFAG averages for the products of the branching fractions for $B^- \rightarrow D^{**}\ell\bar{\nu}$ and $D^{**} \rightarrow D^{(*)+}\pi^-$ [89]. The errors are obtained by taking the squared sum of the statistical and the systematical uncertainties

4.6. Effects on the Widths of the Orbitally Excited States

Due to heavy quark spin symmetry the strong decays follow a specific pattern in the infinite mass limit [65, 71]

$$\mathcal{A}(D^*(2^+) \rightarrow D\pi) \propto \sqrt{\frac{2}{5}}a_D, \quad (4.41)$$

$$\mathcal{A}(D^*(2^+) \rightarrow D^*\pi) \propto \sqrt{\frac{3}{5}}a_D, \quad (4.42)$$

$$\mathcal{A}(D^*(1^+) \rightarrow D^*\pi) \propto a_D, \quad (4.43)$$

$$\mathcal{A}(D^*(1^+) \rightarrow D\pi) = 0, \quad (4.44)$$

$$\mathcal{A}(D(1^+) \rightarrow D^*\pi) \propto a_S, \quad (4.45)$$

$$\mathcal{A}(D(1^+) \rightarrow D\pi) = 0, \quad (4.46)$$

$$\mathcal{A}(D(0^+) \rightarrow D\pi) \propto a_S, \quad (4.47)$$

$$\mathcal{A}(D(0^+) \rightarrow D^*\pi) = 0. \quad (4.48)$$

Here, a_S and a_D are the respective amplitudes for S -wave and D -wave transitions. We assume that the total decay widths are dominated by these decay modes, i.e.

$$\Gamma_{\text{tot}}(D^{**}) = \Gamma(D^{**} \rightarrow D\pi) + \Gamma(D^{**} \rightarrow D^*\pi). \quad (4.49)$$

Since we are only interested in the qualitative picture we will ignore phase space differences in the following, well knowing that they are of the order of twenty percent. We find in the heavy quark limit that

$$\begin{aligned} \Gamma_{\text{tot}}(D^*(2^+)) &= |a_D|^2 = \Gamma_{\text{tot}}(D^*(1^+)), \\ \Gamma_{\text{tot}}(D^*(0^+)) &= |a_S|^2 = \Gamma_{\text{tot}}(D(1^+)). \end{aligned} \quad (4.50)$$

As already mentioned, we expect the states within the $j = 1/2$ spin symmetry doublet to be much broader than the members of the $j = 3/2$ one, which are suppressed by angular momentum.

Switching on the mixing we find

$$\mathcal{A}(D_L(1^+) \rightarrow D\pi) = \mathcal{A}(D_H(1^+) \rightarrow D\pi) = 0, \quad (4.51)$$

$$\mathcal{A}(D_L(1^+) \rightarrow D^*\pi) = a_S \cos \theta + a_D \sin \theta, \quad (4.52)$$

$$\mathcal{A}(D_H(1^+) \rightarrow D^*\pi) = a_D \cos \theta - a_S \sin \theta. \quad (4.53)$$

We can now compute the total decay widths. While the differential decay widths still include interference terms of the S and D amplitudes they do not appear in the total decay width anymore. This is due to the fact that the integration over the helicity angle in the $D^*\pi$ system yields zero in this case. Therefore, we obtain

$$\Gamma_{\text{tot}}(D_L) = \Gamma_L \sim \Gamma(D_L \rightarrow D^*\pi) = |a_S|^2 \cos^2 \theta + |a_D|^2 \sin^2 \theta, \quad (4.54)$$

$$\Gamma_{\text{tot}}(D_H) = \Gamma_H \sim \Gamma(D_H \rightarrow D^*\pi) = |a_D|^2 \cos^2 \theta + |a_S|^2 \sin^2 \theta. \quad (4.55)$$

We can now use the total widths of the 0^+ and 2^+ states in Table 4.1 and Equation (4.50) to extract values for $|a_S|$ and $|a_D|$. Inserting these into Equations (4.54) and (4.55) we obtain

$$\begin{aligned} \Gamma_L &\sim 92 \text{ MeV}, \\ \Gamma_H &\sim 223 \text{ MeV}. \end{aligned} \quad (4.56)$$

Again, we do not provide errors since we are only interested in the qualitative picture.

We find that the heavy 1^+ state is much broader than the light one. This coincides with the observed pattern in Table 4.1 as found by experiments.

4.7. Discussion

We have constructed a simple model for the first orbitally excited D mesons based on HQET at next-to-leading (NLO) in $1/m_Q$. Here, we made the strong assumption that the gyromagnetic factors and the radial wave functions are identical for the two doublets. At order $1/m_Q$ the two 1^+ states mix. We have investigated the effects of this mixing. In our simple model we obtain a rather large mixing angle above the point of maximal mixing which results in an interchanging role of the two states. This has quite a large influence on the semileptonic B decays to the D^{**} states as well as the total decay widths.

The main aspect of our analysis was to investigate if the observed mixing has the potential to solve, or at least ease, the ‘ $1/2 - 3/2$ ’ puzzle. We find that it indeed reduces the difference of the two rates at least for the 1^+ states.

We also examined the impact of the mixing on the total decay widths of the axial-vector states. We see that the resulting decay widths are not in contradiction to the

pattern observed in data.

The experimental results for the masses and widths are presently not in good agreement with each other and do not yield a good fit for our model. Only after removing some of the individual measurements we could obtain a fit which is sufficiently good. We are interested in data from simultaneous analyses for the masses and the widths of all orbitally excited states in the future. Hopefully, we will get more experimental insight with LHC Run II and Belle II coming up.

In order to really be able to draw some conclusions from this analysis we require more data on the masses and widths of the orbitally excited D mesons as well as on semileptonic decays. We do find that the inclusion of mixing does have the potential to ease the ‘ $1/2 - 3/2$ ’ puzzle.

5. $B - \bar{B}$ -Mixing

The mixing of quark flavors was first described by Cabbibo in 1963 [22]. This allows the mixing of neutral mesons. It was first observed in the $K-\bar{K}$ system which was predicted by Gell-Mann and Pais in 1955 [91]. The size of the observed mixing required the presence of a charm quark that was predicted by the GIM mechanism in 1970 [92]. In 1977 the b quark was discovered [93] and the mixing of neutral B mesons was first observed in 1987 by UA1 and ARGUS in the $B_d-\bar{B}_d$ system [94,95]. This discovery gave the first direct hint that the mass of the top quark was much higher than presumed at that time. Since then, analyses on oscillations in the B_d system have been published by many collaborations as ALEPH, DELPHI, L3, OPAL, BaBar, Belle, CDF, DØ and LHCb. It was not until 2006 that $B_s-\bar{B}_s$ oscillations were observed for the first time by CDF at the Tevatron [96]. A more recent result by LHCb from 2013 is shown in Figure 5.1.

Weak decays have been proven useful to gain information concerning elementary particle physics. Especially processes including heavy quarks, particularly b quarks, are experimentally and theoretically well accessible. One phenomenological application of weak decays including a heavy quark is the test of the Standard Model and the determination of its parameters. Here, the mixing of neutral B mesons helps to explore CP violation. The mass difference of the two eigenstates can be determined and gives information about the CKM matrix elements $\Delta m_s/\Delta m_d = |V_{ts}/V_{td}|$. Since Flavor Changing Neutral Currents (FCNC) are required for $B^0-\bar{B}^0$ mixing it only arises at the loop level which makes the process sensitive to New Physics beyond the Standard Model. Another interesting feature of weak hadronic interactions is that they can shed some light on strong interactions and confinement of quarks inside hadrons.

For mixing studies we have reached an era of precision measurements which calls for some effort on the theoretical side. In this chapter we will compute the non-factorizable perturbative corrections to the matrix element of the $\Delta B = 2$ operator at order α_s . In order to obtain these corrections we need to compute three-loop diagrams. With these contributions to the matrix element we end up with a complete next-to-leading order result which increases the theoretical precision.

We give a brief overview of $B^0-\bar{B}^0$ mixing and introduce the bag parameter. The latter will be determined using HQET sum rules. Here, non-factorizable contributions of the three-point correlation function need to be computed, which requires the calculation of three-loop diagrams. This chapter is based on [97].

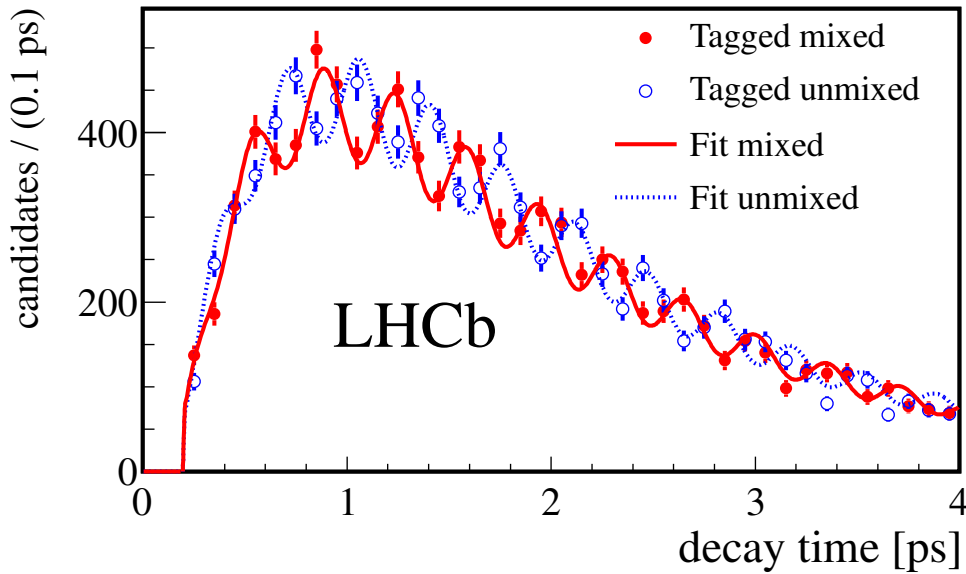


Figure 5.1.: Oscillation in the B_s^0 - \bar{B}_s^0 system as analyzed by the LHCb experiment. The plot displays the time distribution for the sum of the decay modes of $B_s^0 \rightarrow D_s^- \pi^+$. The candidates are either tagged as unmixed, where the same flavor as produced is detected (blue), or mixed with different flavors at detection and production (red). [90]

5.1. Overview

In this section we will briefly summarize the most relevant aspects of the B^0 - \bar{B}^0 mixing. A more detailed description can be found in [16, 28–30, 98–102].

The quark mixing CKM matrix has non-vanishing off-diagonal entries. This results in weak interactions mediated by W bosons which lead to flavor changes. To obtain B^0 - \bar{B}^0 mixing we need an overall flavor transition of $\Delta B = 2$ which can be mediated by Flavor Changing Neutral Currents (FCNC) only at loop level in the Standard Model. Diagrammatically, the process is depicted in Figure 5.2 as a box diagram involving two W bosons and two up-type quarks. These diagrams represent some non-local object. At this point we make use of the weak effective theory by integrating out the top quark t and the W boson. This results in two different types of diagrams depicted in Figure 5.3. The process (a) is a $\Delta B = 2$ transition which can be described by one local four-quark operator

$$\mathcal{O}^{\Delta B=2} = \bar{b} \gamma_\mu \frac{1}{2} (1 - \gamma_5) q \bar{b} \gamma^\mu \frac{1}{2} (1 - \gamma_5) q, \quad (5.1)$$

while process (b) consists of two $\Delta B = 1$ transitions.

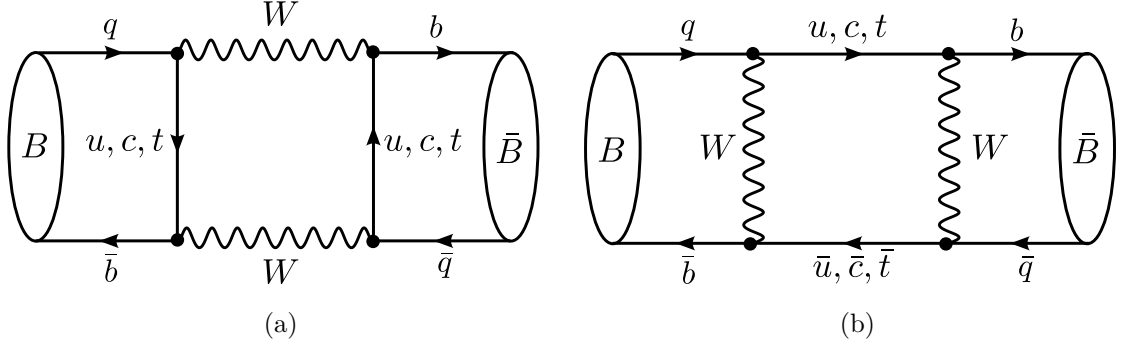


Figure 5.2.: At lowest order in the Standard Model B - \bar{B} mixing can be described by these box diagrams. The loop includes W bosons and up-type quarks.

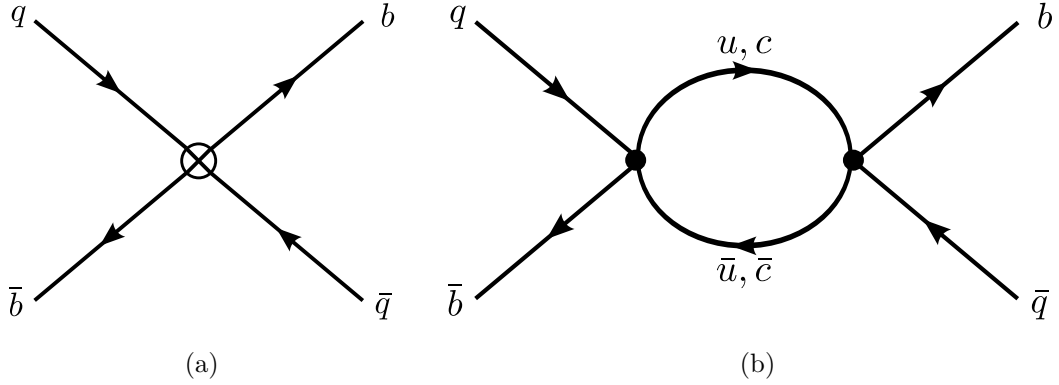


Figure 5.3.: After integrating out the heavy degrees of freedom t and W we obtain two types of diagrams. The $\Delta B = 2$ process in (a) can be described by one local four-quark operator while the process in (b) consists of two $\Delta B = 1$ transitions.

The time evolution of the oscillation in the B^0 - \bar{B}^0 system can be described by a Schrödinger equation

$$i \frac{d}{dt} \begin{pmatrix} |B_q^0(t)\rangle \\ |\bar{B}_q^0(t)\rangle \end{pmatrix} = \mathbf{H} \begin{pmatrix} |B_q^0(t)\rangle \\ |\bar{B}_q^0(t)\rangle \end{pmatrix}. \quad (5.2)$$

Here, the effective Hamilton operator \mathbf{H} consists of the Hermitian 2×2 matrices M and Γ describing the mass matrix and the decay matrix

$$\mathbf{H} = M - \frac{i}{2}\Gamma, \quad \text{where} \quad M = \begin{pmatrix} M_{11} & M_{12} \\ M_{21} & M_{22} \end{pmatrix}, \quad \Gamma = \begin{pmatrix} \Gamma_{11} & \Gamma_{12} \\ \Gamma_{21} & \Gamma_{22} \end{pmatrix}. \quad (5.3)$$

By diagonalizing \mathbf{H} we can find the physical eigenstates M_H and M_L as well as Γ_H and Γ_L . Two observables in the B^0 - \bar{B}^0 system are the mass difference and the decay

width difference. We can relate these quantities to the off-diagonal entries of the mass and decay matrix such as

$$\Delta\Gamma = \Gamma_L - \Gamma_H = 2|\Gamma_{12}| \cos \phi, \quad (5.4)$$

$$\Delta M = M_H - M_L = 2|M_{12}|, \quad (5.5)$$

where $\phi = \arg(-M_{12}/\Gamma_{12})$ is the CP phase.

The short-distance contributions, i.e. top-quark contributions, are predominant for the magnitude of ΔM . Therefore, it is dominated by $\Delta B = 2$ transitions depicted in Figure 5.3(a) while $\Delta\Gamma$ relates to the $\Delta B = 1$ transitions in Figure 5.3(b).

In the following we are only interested in the $\Delta B = 2$ transitions, namely ΔM . Thus, we need to compute the hadronic matrix element M_{12} , which can be computed using the effective weak Hamiltonian. We then find

$$M_{12} = \frac{G_F^2}{(4\pi)^2} (V_{td}^* V_{tb})^2 F(x_t) m_t^2 \eta_{\text{QCD}}(\mu) \langle \bar{B}^0 | \mathcal{O}^{\Delta B=2}(\mu) | B^0 \rangle \quad (5.6)$$

with the operator $\mathcal{O}^{\Delta B=2}$ from Equation (5.1) and the ratio $x_t = m_t^2/m_W^2$. Here, we have the so-called Fermi constant $G_F = \frac{\sqrt{2}}{8} \frac{g_2^2}{M_W^2}$ with the weak coupling g_2 and the mass of the W boson M_W . In the OPE we find a short-distance Wilson coefficient which contains the large scales that were intergrated out. Here, it can be split up into the Inami-Lim function [103]

$$F(x) = \frac{1}{4} \left[1 + \frac{9}{1-x} - \frac{6}{(1-x)^2} - \frac{6x^2}{(1-x)^3} \ln x \right] \quad (5.7)$$

which includes the electroweak loop contributions and the coefficient $\eta_{\text{QCD}}(\mu)$. The latter accounts for the short-distance QCD contributions and its μ -dependence compensates the one of the matrix element.

There are different methods to extract information on the hadronic matrix element. One way of doing this are e.g. explicit quark models like the bag model [104, 105] or naive factorization. Here, we need to rely on assumptions and cannot control the accuracy. More profound are non-perturbative methods such as lattice QCD or QCD sum rules. The former entails a numerical evaluation while in the latter method the matrix element is computed analytically.

We can write the matrix element of the local four-quark operator such that

$$\begin{aligned} \langle \bar{B}^0 | \mathcal{O}^{\Delta B=2}(\mu) | B^0 \rangle &= 2 \left(1 + \frac{1}{N_C} \right) \langle \bar{B}^0 | J_\mu | 0 \rangle \langle 0 | J^\mu | B^0 \rangle B(\mu) \\ &= 2 \left(1 + \frac{1}{N_C} \right) f_B^2 M_B^2 B(\mu), \end{aligned} \quad (5.8)$$

where $N_C = 3$ is the number of colors. Here, $\mathcal{O}^{\Delta B=2} = J_\mu J^\mu$ with $J_\mu = \bar{b}\gamma_\mu\frac{1}{2}(1-\gamma_5)q$ and

$$\langle 0|J_\mu|B(p)\rangle = \frac{i}{2}f_B p_\mu, \quad (5.9)$$

where f_B is the decay constant of the B meson.

In Equation (5.8) we encounter the so-called bag parameter $B(\mu)$ which contains the entire μ dependence of the four-quark operator. It can be seen as a measure for the deviation of the matrix element from the naive factorization prescription, which would yield $B = 1$, or rather as a parameterization of the violation of this approximation. Therefore, the bag parameter can be written as

$$B = 1 + \Delta B. \quad (5.10)$$

The bag factor is a hadronic object which requires the application of non-perturbative methods such as lattice simulations [106–111] or QCD sum rules [112–115]. Using the latter we are able to analytically distinguish between factorizable and non-factorizable contributions. Thus, we solely need to compute ΔB . Since the B meson contains a heavy quark we may use a HQET sum rule. Subleading terms of order Λ_{QCD}/m_b have already been considered in this framework [115]. The computation of perturbative contributions of order α_s are subject of this chapter. Among other things, this requires the computation of three-loop diagrams in HQET where the required master integrals have been computed in [116].

5.2. Bag Parameter

5.2.1. Matching of the Bag Parameter

In Section 3.4.3 we performed the matching calculation for the $\Delta B = 2$ four-quark operator

$$\mathcal{O}^{\Delta B=2}(m_b) = 2C_L\mathcal{O}_L^{\text{eff}}(m_b) + 2C_S\mathcal{O}_S^{\text{eff}}(m_b) \quad (5.11)$$

with the HQET operators

$$\mathcal{O}_L^{\text{eff}} = \bar{h}^+\gamma_\mu\frac{1}{2}(1-\gamma_5)q\bar{h}^-\gamma^\mu\frac{1}{2}(1-\gamma_5)q, \quad (5.12)$$

$$\mathcal{O}_S^{\text{eff}} = \bar{h}^+\frac{1}{2}(1-\gamma_5)q\bar{h}^-\frac{1}{2}(1-\gamma_5)q \quad (5.13)$$

and the Wilson coefficients

$$C_L(m_b) = 1 - \frac{8N_C^2 + 9N_C - 15}{2N_C} \frac{g_s^2}{(4\pi)^2} \quad (5.14)$$

$$C_S(m_b) = -2(N_C + 1) \frac{g_s^2}{(4\pi)^2}. \quad (5.15)$$

Analogous to the definition of the bag parameter for the operator $\mathcal{O}^{\Delta B=2}(m_b)$ we can write

$$\langle \bar{B}^0(v) | \mathcal{O}_L^{\text{eff}}(\mu) | B^0(v) \rangle = \left(1 + \frac{1}{N_C}\right) \langle \bar{B}^0(v) | J_{+\mu} | 0 \rangle \langle 0 | J_-^\mu | B^0(v) \rangle B_L^{\text{eff}}(\mu), \quad (5.16)$$

$$\langle \bar{B}^0(v) | \mathcal{O}_S^{\text{eff}}(\mu) | B^0(v) \rangle = \left(1 - \frac{1}{2N_C}\right) \langle \bar{B}^0(v) | J_+ | 0 \rangle \langle 0 | J_- | B^0(v) \rangle B_S^{\text{eff}}(\mu), \quad (5.17)$$

where

$$J_{\pm\mu} = \bar{h}^\pm \gamma_\mu \frac{1}{2} (1 - \gamma_5) d, \quad (5.18)$$

$$J_\pm = \bar{h}^\pm \frac{1}{2} (1 - \gamma_5) d. \quad (5.19)$$

We can then define

$$\langle 0 | J_{\pm\mu} | B(v) \rangle = \frac{i}{2} F(\mu) v_\mu, \quad (5.20)$$

$$\langle \bar{B}(v') | J_\pm | 0 \rangle = \frac{i}{2} F(\mu) \quad (5.21)$$

and find with Equation (3.23) that

$$\sqrt{M_B} f_B = C(\mu) F(\mu) + \mathcal{O}\left(\frac{1}{m_b}\right) \quad (5.22)$$

where [117]

$$C(m_b) = 1 - 2C_F \frac{\alpha_s(m_b)}{4\pi} + \mathcal{O}(\alpha_s^2) \quad (5.23)$$

is the coefficient for the matching of the current $\bar{b}\gamma_\mu\gamma_5 d$ onto $\bar{h}^\pm\gamma_\mu\gamma_5 d$. Thus, we find

$$F(m_b) = \frac{\sqrt{M_B}}{C(m_b)} f_B. \quad (5.24)$$

We can now take Equation (5.8) and insert Equation (5.11). Then we can use Equations (5.16) and (5.17) and replace $F(m_b)$ by Equation (5.24). This way we obtain

$$B(m_b) = \frac{C_L(m_b)}{C^2(m_b)} B_L^{\text{eff}}(m_b) - \frac{N_C - \frac{1}{2}}{N_C + 1} \frac{C_S(m_b)}{C^2(m_b)} B_S^{\text{eff}}(m_b) \quad (5.25)$$

and inserting Equations (5.14), (5.15) and (5.23) we find

$$B(m_b) = \left[1 - \frac{4N_C^2 + 9N_C - 11}{2N_C} \frac{\alpha_s^{(n_f)}(m_b)}{4\pi} \right] B_L^{\text{eff}}(m_b) + (2N_C - 1) \frac{\alpha_s^{(n_f)}(m_b)}{4\pi} B_S^{\text{eff}}(m_b) + \mathcal{O}\left(\alpha_s^2, \frac{1}{m_b}\right). \quad (5.26)$$

We are only interested in the NLO computation of the bag parameter. In particular, the non-factorizable contributions to the bag parameter, namely the deviation from unity, include α_s corrections. Thus, in Equation (5.26) we can set $B_L^{\text{eff}}(m_b) = B_S^{\text{eff}}(m_b) = 1$ in all terms that are already suppressed by α_s . We then find

$$B(m_b) = B_L^{\text{eff}}(m_b) - \frac{11}{2} \left(1 - \frac{1}{N_C}\right) \frac{\alpha_s(m_b)}{4\pi}. \quad (5.27)$$

5.2.2. Running of the Bag Parameter

The anomalous dimension of the effective currents in Equations (5.18) and (5.19) is the same (cf. Equation (3.65)) and is given by [118–120]

$$\begin{aligned} \gamma_j^{\text{eff}}(\alpha_s) = & -3C_F \frac{\alpha_s}{4\pi} + C_F \left[\frac{2}{3} \pi^2 (C_A - 4C_F) + \frac{1}{2} \left(5C_F - \frac{49}{3} C_A \right) + \frac{5}{3} n_l \right] \left(\frac{\alpha_s}{4\pi} \right)^2 \\ & + \mathcal{O}(\alpha_s^3). \end{aligned} \quad (5.28)$$

Here, the b quark is not included and $n_l = n_f - 1 = 4$ denotes the number of light flavors. We also have $C_A = N_C = 3$.

The anomalous dimension of the bag factor defined in Equation (5.16) reflects the fact that the four-quark operator can be expressed as a product of two two-quark currents

$$\begin{aligned} \gamma_1^{\text{eff}} - 2\gamma_j^{\text{eff}} = & \delta_{11} \left(\frac{\alpha_s^2}{4\pi} \right)^2 + \mathcal{O}(\alpha_s^3), \\ \delta_{11} = & \frac{N_C - 1}{3N_C} \left[2\pi^2 \left(3N_C - 2 - \frac{6}{N_C} \right) - 11N_C^2 - 15N_C - 12 + \frac{18}{N_C} + 2(N_C + 3)n_l \right] \end{aligned} \quad (5.29)$$

in naive factorization. At one loop this is scale independent which means in particular that $\gamma_1^{\text{eff}} = 2\gamma_j^{\text{eff}}$ [121, 122]. Here, γ_1^{eff} is the anomalous dimension of the four-quark operator in Equation (5.12) [123]. Then the running of the bag factor B_L^{eff} is given by

$$B_L^{\text{eff}}(\mu) = B_L^{\text{eff}}(\mu_0) \left[1 + \frac{\delta_{11}}{2\beta_0^{(n_l)}} \frac{\alpha_s^{(n_l)}(\mu) - \alpha_s^{(n_l)}(\mu_0)}{4\pi} + \mathcal{O}(\alpha_s^2) \right]. \quad (5.30)$$

In the required accuracy we can assume that $\alpha_s^{(n_f)} = \alpha_s^{(n_l)} = \alpha_s$.

The μ dependence of the bag factor in full QCD is the same as the one of the four-quark operator which is given in (3.94).

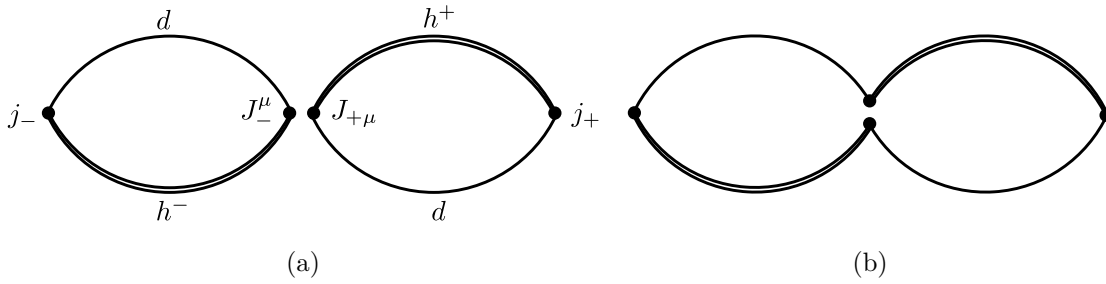


Figure 5.4.: Diagrammatic depiction of the three-point correlation function at leading order. Here, (a) shows the color-enhanced and (b) the color-suppressed contribution to the four-quark operator.

5.3. Calculation

As already mentioned, the computation of the bag parameter is quite difficult due to hadronic effects. Thus, we rely on the method of QCD sum rules. Here, we need to compute a three-point correlation function which was first introduced to study kaon mixing [124]. When it comes to the calculation of the non-factorizable NLO perturbative contributions, which are necessary to determine ΔB , we encounter three-loop diagrams. In QCD, their computation is very challenging compared to the two-point correlator [125]. Therefore, we perform the calculation in HQET where the required master integrals have been evaluated in [116]. The application of the sum rule also involves the computation of the corresponding quark-condensate contributions, which are also considered in this section.

5.3.1. Perturbative Contribution

In order to determine the hadronic matrix element in Equation (5.8) we can choose a suitable correlation function

$$K(\omega_1, \omega_1) = \int d^D x_1 d^D x_2 e^{ip_1 x_1 - ip_2 x_2} \langle 0 | T \{ j_+(x_2) \mathcal{O}_L^{\text{eff}}(0) j_-(x_1) \} | 0 \rangle \quad (5.31)$$

with the operator $\mathcal{O}_L^{\text{eff}} = J_{+\mu} J_-^\mu$ from Equation (5.12). The B meson states are interpolated by the current

$$j_\pm = \bar{d} \gamma_5 h^\pm. \quad (5.32)$$

The correlator only depends on the projections of the momenta onto the velocity of the heavy quark $\omega_{1,2} = v \cdot p_{1,2}$, which are scalar. The HQET quark and antiquark only move forward in time such that the time-ordered product only yields a result when $v \cdot x_1 < 0$ and $v \cdot x_2 > 0$. It is therefore sufficient to merely use the simple product of operators.

The leading contribution of the correlator K is shown in Figure 5.4. Here, we see that the four-quark operator results in two different structures. The diagram on the right

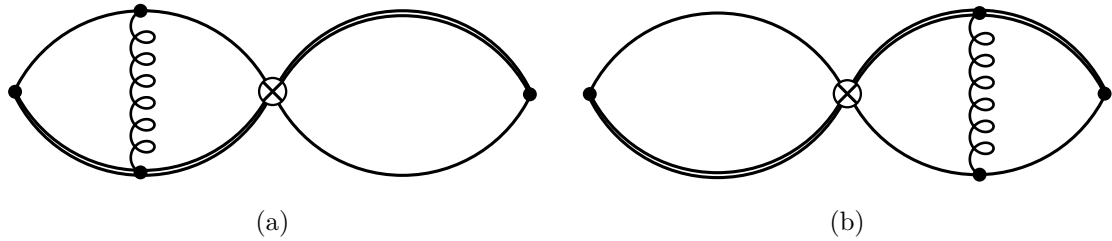


Figure 5.5.: Factorizable perturbative contributions at $\mathcal{O}(\alpha_s)$ to the correlator. The four-quark operator is denoted by \otimes and represents both, the color-enhanced and -suppressed contributions.

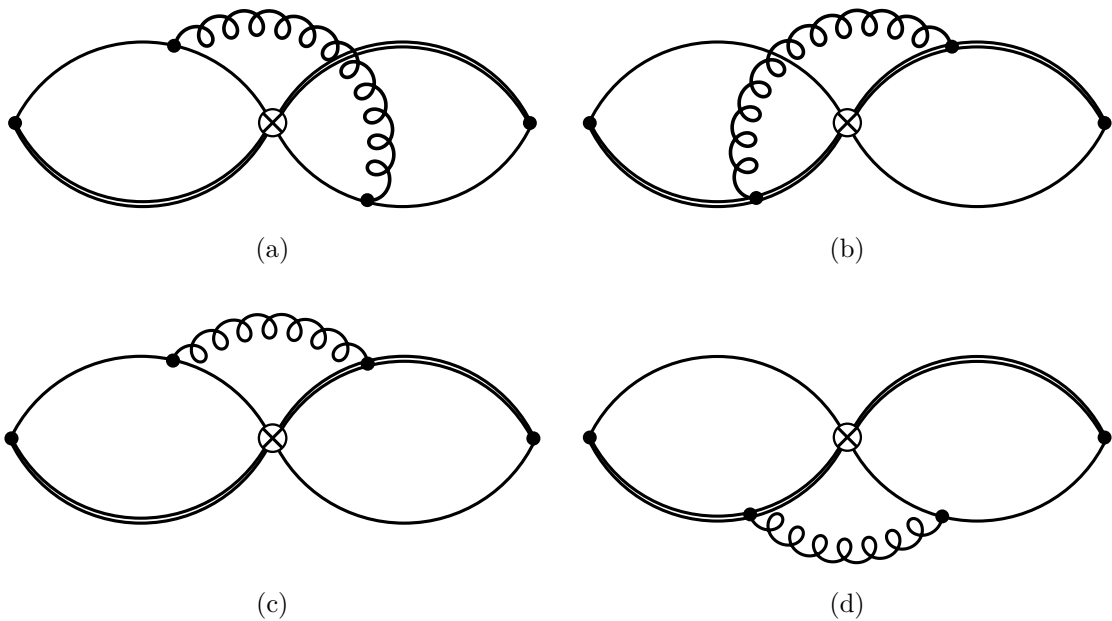


Figure 5.6.: Non-factorizable perturbative contributions at $\mathcal{O}(\alpha_s)$ to the correlator. Even though \otimes represents the color-enhanced and -suppressed contributions, the former does not contribute since it leads to traces of single generators of $SU(3)$ which vanish.

is color-suppressed compared to the left one with a factor of $(D - 2)/(2N_C)$, where $D = 4 - 2\epsilon$. Altogether, we consider the diagrams as factorizable which means that we can treat both loops separately. The same assumption applies for the diagrams in Figure 5.5, where we encounter a gluon exchange within one loop. In addition we find corrections that are not restricted to one loop as shown in Figure 5.6. These non-factorizable contributions result in three-loop diagrams.

With the separation of the two types of diagrams we find for the correlation function

$$K(\omega_1, \omega_2) = \left(1 + \frac{D - 1}{2N_C}\right) \Pi(\omega_1)\Pi(\omega_2) + \Delta K(\omega_1, \omega_2), \quad (5.33)$$

where

$$\Pi(\omega) = \frac{N_C(-2\omega)^{2-2\epsilon}}{(4\pi)^{D/2}} \left[I_1 - 2C_F \frac{g_s^2(-2\omega)^{-2\epsilon}}{(4\pi)^{D/2}} \frac{D - 2}{D - 4} \left(I_1^2 - \frac{D(2D - 5)}{D - 4} I_2 \right) \right] \quad (5.34)$$

is the correlation function for j_+ and $J_{+\mu}$ [117, 119, 126]. Further, we have the ‘sunset’ diagrams in HQET which are given by

$$I_n = \Gamma(2n + 1 - nD)\Gamma^n\left(\frac{D}{2} - 1\right). \quad (5.35)$$

The factorizable contribution yields

$$\Delta K(\omega_1, \omega_2) = N_C C_F \frac{g_s^2}{(4\pi)^{3D/2}} R(\omega_1, \omega_2), \quad (5.36)$$

where

$$\begin{aligned} R(\omega_1, \omega_2) = & -\frac{(D - 2)(3D - 7)(D^2 - 16D + 40)(\omega_1 - 2\omega_2)}{2(D - 4)(3D - 8)\omega_1(\omega_1 - \omega_2)} I_3(-2\omega_1)^{3D-5} \\ & + (\omega_1 \leftrightarrow \omega_2) \\ & + \frac{(D - 2)[(D - 4)(3D - 8)\omega_1 - (D - 2)(2D - 5)\omega_2]}{(D - 3)(D - 4)\omega_1} \\ & \times I_1 I_2(-2\omega_1)^{2D-4}(-2\omega_2)^{D-3} + (\omega_1 \leftrightarrow \omega_2) \\ & - \frac{(D - 2)[(3D - 8)(5D - 14)\omega_1 - 2(D - 4)(D^2 - 7D + 11)\omega_2]}{(D - 4)(3D - 8)(\omega_1 - \omega_2)} \\ & \times M_1(\omega_1, \omega_2) + (\omega_1 \leftrightarrow \omega_2) \\ & + \frac{(D - 2)(2D^2 - 15D + 26)}{2(D - 3)} M_2(\omega_1, \omega_2) + \frac{(D - 2)^2 \omega_1 \omega_2}{(D - 3)^2} M_2'(\omega_1, \omega_2) \\ & + \frac{4(D - 2)(D - 3)(D^2 - 16D + 40)\omega_1 \omega_2}{(D - 4)(3D - 8)} M_3(\omega_1, \omega_2) \\ & - \frac{2(D - 2)^2 \omega_1}{D - 4} M_4(\omega_1, \omega_2) + (\omega_1 \leftrightarrow \omega_2). \end{aligned} \quad (5.37)$$

Here, we used the integration-by-parts program LiteRed [127, 128] to reduce the three-loop diagrams to the master integrals shown in Appendix C.2.1. They have been computed in [116]. The master integrals can then be expanded in $\epsilon = 0$, where details can be found in [97, 116]. We obtain

$$\Delta K(\omega_1, \omega_2) = N_C C_F \frac{g_s^2}{(4\pi)^{3D/2}} [\Gamma(1+2\epsilon)\Gamma(1-\epsilon)]^3 (-2\omega_1)^{2-3\epsilon} (-2\omega_2)^{2-3\epsilon} S(x), \quad (5.38)$$

where we have

$$\begin{aligned} S(x) = & \left[\frac{1}{48}(x^2 + x^{-2}) - \frac{\pi^2}{3} + \frac{5}{4} \right] \frac{1}{3\epsilon^2} \\ & + \left[-\frac{1}{16}(x^2 - x^{-2}) \ln x + \frac{61}{288}(x^2 + x^{-2}) + x + x^{-1} - 4\zeta_3 - \frac{4}{3}\pi^2 + \frac{41}{4} \right] \frac{1}{3\epsilon} \\ & + \frac{1}{2} \left(\frac{1}{16}(x^2 + x^{-2}) + \frac{\pi^2}{3} - \frac{5}{4} \right) \ln^2 x - \left(\frac{61}{288}(x + x^{-1}) + 1 \right) (x - x^{-1}) \ln x \\ & + \frac{1}{216} \left(\pi^2 + \frac{2519}{24} \right) (x^2 + x^{-2}) - \frac{1}{3} \left(\frac{4}{9}\pi^2 - \frac{67}{4} \right) (x + x^{-1}) \\ & - \frac{1}{3} \left(16\zeta_3 + \frac{4}{45}\pi^4 + \frac{25}{6}\pi^2 - \frac{193}{4} \right) \end{aligned} \quad (5.39)$$

and $S(x) = S(x^{-1})$, where $x = \omega_2/\omega_1$. Here, $\zeta_3 = \sum_{n=1}^{\infty} \frac{1}{n^3} = 1.20206$ is the Riemann zeta function.

For $\omega_{1,2} < 0$ the correlator $K(\omega_1, \omega_2)$ is analytic and it has a cut in $\omega_{1,2}$ from 0 to $+\infty$ on which the physical states lie. Keeping $\omega_2 < 0$, the correlation function has a discontinuity

$$\rho_1(\omega_1, \omega_2) = \frac{1}{2\pi i} [K(\omega_1 + i0, \omega_2) - K(\omega_1 - i0, \omega_2)] \quad (5.40)$$

regarding the cut in ω_1 . For the discontinuity in ω_2 we find for $\omega_1 > 0$

$$\rho(\omega_1, \omega_2) = \frac{1}{2\pi i} [\rho_1(\omega_1, \omega_2 + i0) - \rho_1(\omega_1, \omega_2 - i0)]. \quad (5.41)$$

The three-point correlation function is of the form

$$K(\omega_1, \omega_2) = (-2\omega_1)^{2-3\epsilon} (-2\omega_2)^{2-3\epsilon} f(x), \quad (5.42)$$

where $f(x)$ can be derived from Equations (5.33), (5.34) and (5.38).

We can find the discontinuity by setting $\omega_{1,2} = -\nu_{1,2} e^{-i\alpha}$ with $\nu_{1,2} > 0$ and varying α from 0 to $\pi - 0$ or $-(\pi - 0)$. This way we rotate $\omega_{1,2}$ such that we approach the cut either from above or below. We first rotate ω_1 in Equation (5.40), keeping $\omega_2 < 0$, and get

$$\rho_1(\nu_1, \omega_2) = \frac{(2\nu_1)^{2-3\epsilon} (-2\omega_2)^{2-3\epsilon}}{2\pi i} \left[e^{3\pi i \epsilon} f\left(-\frac{\omega_2}{\nu_1} e^{\pi i}\right) - e^{-3\pi i \epsilon} f\left(-\frac{\omega_2}{\nu_1} e^{-\pi i}\right) \right]. \quad (5.43)$$

We repeat the procedure for Equation (5.41) and find

$$\rho(\nu_1, \nu_2) = \frac{(2\nu_1)^{2-3\epsilon}(2\nu_2)^{2-3\epsilon}}{(2\pi i)^2} \left[(e^{6\pi i\epsilon} + e^{-6\pi i\epsilon}) f(x) - f(xe^{2\pi i}) - f(xe^{-2\pi i}) \right], \quad (5.44)$$

where $x = \frac{\nu_2}{\nu_1}$. Analogous to Equation (5.33) the double spectral density is of the form

$$\rho(\omega_1, \omega_2) = \left(1 + \frac{1-\epsilon}{N_C} \right) \rho(\omega_1)\rho(\omega_2) + \Delta\rho(\omega_1, \omega_2), \quad (5.45)$$

which is a bare quantity that still includes poles. The single spectral densities are given in [117, 119, 126]

$$\rho(\omega) = \frac{N_C(2\omega)^{2-2\epsilon}}{(4\pi)^{D/2}} \frac{\Gamma(1+2\epsilon)\Gamma(1-\epsilon)}{1-2\epsilon} \times \left[1 + C_F \frac{g_s^2(2\omega)^{-2\epsilon}}{(4\pi)^{D/2}} \Gamma(1+2\epsilon)\Gamma(1-\epsilon) \left(\frac{3}{\epsilon} + \frac{4}{3}\pi^2 + 17 \right) \right], \quad (5.46)$$

whereas the non-factorizable part of the double spectral density is found to be

$$\Delta\rho(\omega_1, \omega_2) = N_C C_F \frac{g_s^2}{(4\pi)^{3D/2}} [\Gamma(1+2\epsilon)\Gamma(1-\epsilon)]^3 (2\omega_1)^{2-3\epsilon} (2\omega_2)^{2-3\epsilon} r(x), \quad (5.47)$$

where $r(x) = r(x^{-1})$. Here, the function

$$r(x) = - \left(\frac{4}{3}\pi^2 - 5 \right) \quad (5.48)$$

is independent of x

We can now renormalize the spectral density, which is finite for

$$\rho_r(\omega_1, \omega_2) = Z_L^{-1} Z_j^{-2} \rho(\omega_1, \omega_2), \quad (5.49)$$

where Z_L^{-1} is the renormalization constant for the four-quark operator $\mathcal{O}_L^{\text{eff}}$ and Z_j^{-2} is the one for the two-quark operator which is given to one loop in Equation (3.65). From the relation found in Equation (5.29) we can infer that $Z_L = Z_j^2$. Thus, we find a finite result for $\rho_r(\omega_1, \omega_2) = Z_j^{-4} \rho(\omega_1, \omega_2)$ and obtain

$$\rho_r(\omega_1, \omega_2) = \left(1 + \frac{1}{N_C} \right) \rho_r(\omega_1)\rho_r(\omega_2) + \Delta\rho_r(\omega_1, \omega_2) \quad (5.50)$$

with [117, 119, 126]

$$\rho_r(\omega) = \frac{N_C(2\omega)^2}{(4\pi)^2} \left[1 + C_F \frac{\alpha_s}{4\pi} \left(-6 \ln \left(\frac{2\omega}{\mu} \right) + \frac{4}{3}\pi^2 + 17 \right) \right] \quad (5.51)$$

and

$$\Delta\rho_r(\omega_1, \omega_2) = -N_C C_F \frac{\alpha_s}{(4\pi)^5} (2\omega_1)^2 (2\omega_2)^2 \left(\frac{4}{3}\pi^2 - 5 \right). \quad (5.52)$$

We can rewrite the expression by rearranging the leading order contribution in Equation (5.51) and inserting it. We find

$$\Delta\rho_r(\omega_1, \omega_2) = -\frac{C_F}{N_C} \frac{\alpha_s}{4\pi} \rho_r(\omega_1) \rho_r(\omega_2) \left(\frac{4}{3}\pi^2 - 5 \right), \quad (5.53)$$

which we can insert in the double spectral density and finally obtain the form

$$\begin{aligned} \Delta\rho_r(\omega_1, \omega_2) &= -\frac{1}{N_C} C_F \frac{\alpha_s}{4\pi} \rho_r(\omega_1) \rho_r(\omega_2) \left(\frac{4}{3}\pi^2 - 5 \right) \\ &= \left(1 + \frac{1}{N_C} \right) \rho_r(\omega_1) \rho_r(\omega_2) \left(1 - \frac{\alpha_s}{4\pi} \frac{N_C - 1}{2N_C} \left(\frac{4}{3}\pi^2 - 5 \right) \right). \end{aligned} \quad (5.54)$$

Here, we can directly read off the non-factorizable contribution which is already correctly normalized.

5.3.2. Quark Condensates

For the sum rule we also obtain power corrections. Here, they manifest in quark and gluon condensates. The leading contribution for our correlator K is the quark condensate and the leading order diagrams are shown in Figure 5.7. Factorizable corrections are depicted in Figure 5.8 and the non-factorizable ones in Figure 5.9. We only consider condensate contributions for the light quarks here, since the ones for the heavy quarks are strongly suppressed due to their large mass.

The diagrams in Figures 5.7 and 5.8 factorize. Thus, we can add the quark condensate contribution [129]

$$\Pi_q(\omega) = \frac{1}{2} \frac{\langle \bar{q}q \rangle}{-2\omega} \left[1 + 2C_F \frac{g_s^2 (-2\omega)^{-2\epsilon}}{(4\pi)^{D/2}} (D-1)(D-4) I_1 \right] \quad (5.55)$$

to the two-point correlator function Π in Equation (5.34).

The non-factorizable α_s corrections to the quark condensate contributions already occur at two loops as shown in Figure 5.9. They are given by

$$\Delta K_q(\omega_1, \omega_2) = C_F \frac{g_s^2 \langle \bar{q}q \rangle}{(4\pi)^D} R_q(\omega_1, \omega_2), \quad (5.56)$$

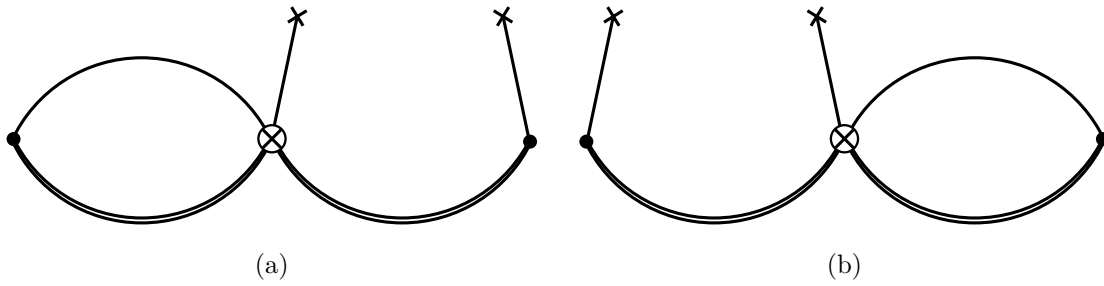


Figure 5.7.: Here, the leading contributions to the quark condensate are depicted. Again, the \otimes denotes both color-enhanced and color-suppressed contributions.

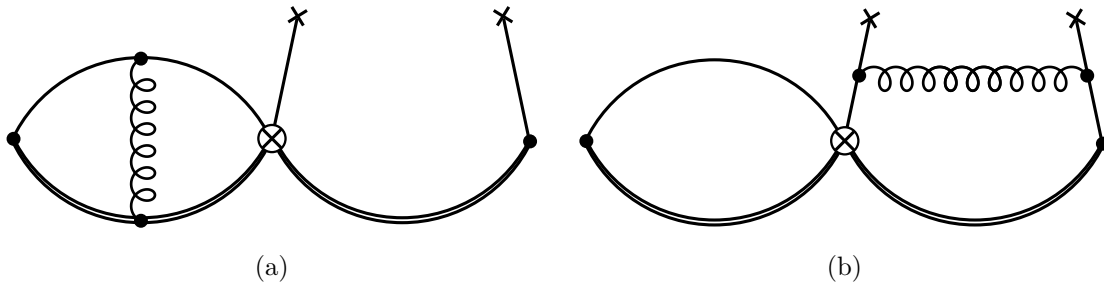


Figure 5.8.: A few of the factorizable contributions to the quark condensate. The diagrams which are symmetrically identical also contribute.

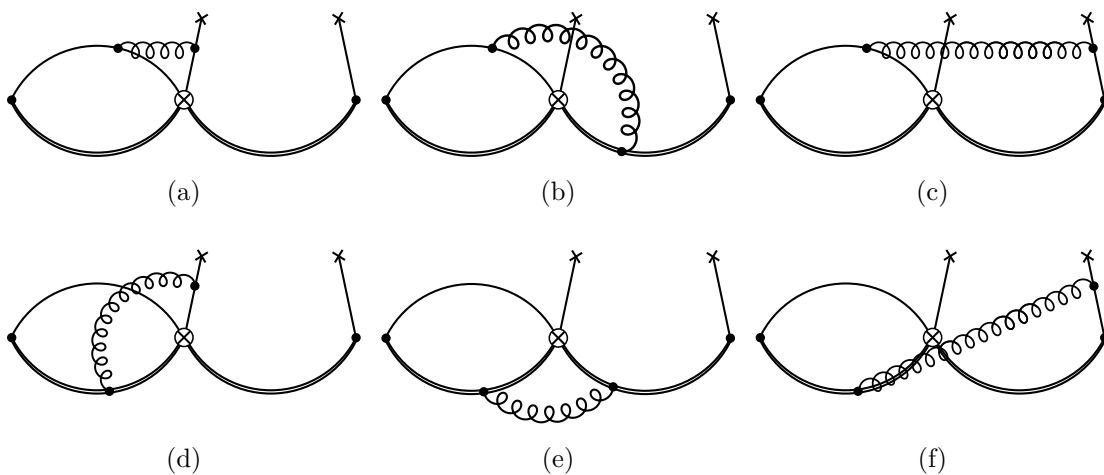


Figure 5.9.: Illustration of the non-factorizable contributions to the quark condensate. Again, also symmetrically identical diagrams exist.

where

$$\begin{aligned}
R_q = & \frac{4(\omega_1 + \omega_2) [(D-2)(D-5)(\omega_1^2 + \omega_2^2) - (D^3 - 10D^2 + 30D - 30)\omega_1\omega_2]}{(D-4)(-2\omega_1)^{5-D}(-2\omega_2)^{5-D}} I_1^2 \\
& + \frac{2D-5}{2(D-3)(D-4)(D-5)\omega_2^2(\omega_1 - \omega_2)} \\
& \times \left[(D-2)(D-5)^2\omega_1^3 + 2(D-2)(D-5)(2D-5)\omega_1^2\omega_2 \right. \\
& \quad \left. - (D-3)(D^2 - 11D + 6)\omega_1\omega_2^2 - 4(D-2)(D-3)\omega_2^3 \right] I_2(-2\omega_1)^{2D-7} \\
& + (\omega_1 \leftrightarrow \omega_2) \\
& + \frac{-(D-2)(D-5)\omega_1^3 - D\omega_1^2\omega_2 + (D-3)(D-8)\omega_1\omega_2^2 + (D-2)\omega_2^3}{4(D-4)\omega_1\omega_2^2(\omega_1 - \omega_2)} \\
& \times M(\omega_1, \omega_2) + (\omega_1 \leftrightarrow \omega_2). \tag{5.57}
\end{aligned}$$

Here, the master integral $M(\omega_1, \omega_2)$ is shown in Appendix C.2.2 and defined in the appendix of [97]. The expansion in $\epsilon = 0$ can be found to be

$$\Delta K_q(\omega_1, \omega_2) = C_F \frac{g_s^2 \langle \bar{q}q \rangle}{(4\pi)^D} [\Gamma(1+2\epsilon)\Gamma(1-\epsilon)]^2 (-2\omega_1)^{\frac{1}{2}-2\epsilon} (-2\omega_2)^{\frac{1}{2}-2\epsilon} S_q(x), \tag{5.58}$$

where

$$\begin{aligned}
S_q(x) = & -\frac{7}{16} \frac{x^{1/2} + x^{-1/2}}{\epsilon^2} \\
& + \left[\frac{7}{2} (x^{1/2} - x^{-1/2}) \ln x + (x^{1/2} + x^{-1/2})(x + x^{-1} - 3) \frac{\pi^2}{3} \right. \\
& \quad \left. - \frac{1}{4} (x^{1/2} + x^{-1/2})(5x + 5x^{-1} + 14) \right] \frac{1}{4\epsilon} \\
& + (x^{1/2} + x^{-1/2})(x + x^{-1} - 3) \\
& \quad \times [3\text{Li}_3(1-x) + 3\text{Li}_3(1-x^{-1}) - 2L(x) \ln x - 2\zeta_3] \\
& + (x^{1/2} - x^{-1/2})(x + x^{-1})L(x) + \frac{1}{8} (x^{1/2} + x^{-1/2})(2x + 2x^{-1} - 7) \ln^2 x \\
& + (x^{1/2} + x^{-1/2})(10x + 10x^{-1} - 27) \frac{\pi^2}{24} \\
& + \frac{1}{8} (x^{1/2} - x^{-1/2})(5x + 5x^{-1} + 32) \ln x \\
& - \frac{1}{4} (x^{1/2} + x^{-1/2})(9x + 9x^{-1} + 11), \tag{5.59}
\end{aligned}$$

which is also symmetric in $S_q(x) = S_q(x^{-1})$. The special function $L(x)$ is given by

$$L(x) = -L(x^{-1}) = \text{Li}_2(1-x) + \frac{1}{4} \ln^2 x, \tag{5.60}$$

where the dilogarithm is defined as

$$\text{Li}_2(x) = - \int_0^x dt \frac{\ln(1-t)}{t}. \quad (5.61)$$

The polylogarithms also fulfil the recursive relation

$$\text{Li}_n(x) = \int_0^x dt \frac{\text{Li}_{n-1}(t)}{t}, \quad n > 2 \quad (5.62)$$

and with this the Riemann zeta function from above can also be written as

$$\zeta_n = \text{Li}_n(1), \quad n \geq 2. \quad (5.63)$$

Further details and relations can be found in [97].

As before for the double spectral density $\rho(\omega_1, \omega_2)$, we can determine the double discontinuity for $R_q(\omega_1, \omega_2)$

$$\begin{aligned} \text{disc}R_q(\omega_1, \omega_2) &= 2 \left[\left(\frac{\pi^2}{3} - \frac{5}{4} \right) \omega_2^2 \delta(\omega_1) \right. \\ &\quad \left. - (\omega_2 + \omega_1) \left(\frac{\omega_2}{\omega_1} + \frac{\omega_1}{\omega_2} - 3 \right) \ln \left(1 - \frac{\omega_1}{\omega_2} \right) \right] \theta(\omega_2 - \omega_1) \\ &\quad + (\omega_2 \leftrightarrow \omega_1). \end{aligned} \quad (5.64)$$

Therefore, the non-factorizable contribution to the quark condensate part of the spectral density is

$$\begin{aligned} \Delta\rho_q(\omega_1, \omega_2) &= C_F \frac{\alpha_s \langle \bar{q}q \rangle}{4\pi} \frac{2}{16\pi^2} \left\{ \left[\left(\frac{\pi^2}{3} - \frac{5}{4} \right) \omega_2^2 \delta(\omega_1) \right. \right. \\ &\quad \left. \left. - (\omega_2 + \omega_1) \left(\frac{\omega_2}{\omega_1} + \frac{\omega_1}{\omega_2} - 3 \right) \ln \left(1 - \frac{\omega_1}{\omega_2} \right) \right] \theta(\omega_2 - \omega_1) \right. \\ &\quad \left. + (\omega_2 \leftrightarrow \omega_1) \right\}. \end{aligned} \quad (5.65)$$

5.3.3. Sum Rule

In the previous subsections we have computed the OPE representation of the correlation function which we can determine perturbatively. It does not reflect the physical picture, though, since the quarks only appear in bound states. Thus, we also need to introduce the hadronic representation of the correlator. Here, we insert a complete set of mesonic states with quantum numbers that are compatible with the interpolating current. The lightest state is stable in QCD, while higher states decay strongly and form a continuum described by the spectral function ρ_{cont} . The hadronic double spectral density is then given by

$$\begin{aligned} \rho_H(\omega_1, \omega_2) &= \langle 0 | j_+ | \bar{B} \rangle \langle \bar{B} | \mathcal{O}_L^{\text{eff}} | B \rangle \langle B | j_- | 0 \rangle \delta(\omega_1 - \bar{\Lambda}) \delta(\omega_2 - \bar{\Lambda}) + \rho_{\text{cont}}(\omega_1, \omega_2) \\ &= F^2 \langle \bar{B} | \mathcal{O}_L^{\text{eff}} | B \rangle \delta(\omega_1 - \bar{\Lambda}) \delta(\omega_2 - \bar{\Lambda}) + \rho_{\text{cont}}(\omega_1, \omega_2), \end{aligned} \quad (5.66)$$

where we used that $\langle 0|j_+|\bar{B}\rangle = iF$ and F is given in Equation (5.24). Here, $\bar{\Lambda} = M_B - m_b$ is the residual energy of the B meson. The hadronic spectral density now includes the matrix element which we are interested in. We can now use Equations (5.16) and (5.20) and find

$$\begin{aligned} \langle \bar{B}(v)|\mathcal{O}_L^{\text{eff}}(\mu)|B(v)\rangle &= \left(1 + \frac{1}{N_C}\right) \frac{1}{4} F^2(\mu) B_L^{\text{eff}}(\mu) \\ &= \left(1 + \frac{1}{N_C}\right) \frac{1}{4} F^2(\mu) \left(1 + \Delta B_L^{\text{eff}}(\mu)\right). \end{aligned} \quad (5.67)$$

The spectral density for the continuum states is not known. However, it can be equated to the perturbative OPE result by the assumption of quark hadron duality. We find that

$$\rho_{\text{cont}}(\omega_1, \omega_2) = \rho_r(\omega_1, \omega_2) [1 - \theta(\omega_c - \omega_1)\theta(\omega_c - \omega_2)], \quad (5.68)$$

where ω_c is the threshold for the continuum.

We can get a first estimate for the size of ΔB_L^{eff} by using the finite energy sum rule (FESR). Here, we only consider the square in the ω_1 - ω_2 plane up to the continuum threshold $0 < \omega_{1,2} < \omega_c$ and equate the integrals over the perturbative and hadronic spectra. The square of the decay constant F can be related to the spectral density for the two-point correlator by a sum rule. Inserting this into Equation (5.67) and using Equation (5.52) the integrals cancel and we find the expression

$$\Delta B_L^{\text{eff}} = -\frac{N_C - 1}{2N_C} \left(\frac{4}{3}\pi^2 - 5\right) \frac{\alpha_s^{(n_l)}(\mu)}{4\pi} \approx -2.72 \frac{\alpha_s^{(n_l)}(\mu)}{4\pi}. \quad (5.69)$$

A more profound way is to consider the complete energy range $0 < \omega_{1,2} < \infty$, where we also include the continuum states. In this case a Borel transformation is applied for QCD sum rules to suppress higher-energy states. In HQET the control of power corrections can be achieved by using Eukledian times $\tau_{1,2}$ with $\tau = it$. Here, $1/\tau_{1,2}$ are the Borel parameters for the double Borel transformation in $\omega_{1,2}$. We then find the renormalized perturbative correlator to be

$$K_r(\tau_1, \tau_2) = \int_0^\infty d\omega_1 d\omega_2 e^{-\omega_1\tau_1 - \omega_2\tau_2} \rho_r(\omega_1, \omega_2) + \begin{array}{c} \text{vacuum} \\ \text{condensates} \end{array}. \quad (5.70)$$

Analogously we obtain for the hadronic representation

$$K_H(\tau_1, \tau_2) = \int_0^\infty d\omega_1 d\omega_2 e^{-\omega_1\tau_1 - \omega_2\tau_2} \rho_H(\omega_1, \omega_2) \quad (5.71)$$

with the spectral density from Equation (5.66). We then equate the two representations and find

$$\begin{aligned} F^2(\mu) \langle \bar{B}^0(v)|\mathcal{O}_L^{\text{eff}}(\mu)|B^0(v)\rangle e^{-\bar{\Lambda}(\tau_1 + \tau_2)} &= \int_0^{\omega_c} d\omega_1 \int_0^{\omega_c} d\omega_2 e^{-\omega_1\tau_1 - \omega_2\tau_2} \rho_r(\omega_1, \omega_2) \\ &+ \begin{array}{c} \text{vacuum} \\ \text{condensates} \end{array}, \end{aligned} \quad (5.72)$$

where we used the semilocal quark hadron duality (cf. Equation (5.68)).

We infer the continuum threshold ω_c from the two-point sum rule [117, 119, 126]

$$\frac{1}{2}F^2(\mu)e^{-\bar{\Lambda}\tau} = \int_0^{\omega_c} d\omega e^{-\omega\tau} \rho_r(\omega) + \text{vacuum condensates} . \quad (5.73)$$

Then, we can divide Equation (5.72) by the product of two copies of Equation (5.73). This yields the bag parameter

$$\begin{aligned} B_L^{\text{eff}} &= 1 - \frac{N_C - 1}{2N_C} \left(\frac{4}{3}\pi^2 - 5 \right) \frac{\alpha_s^{(n_l)}(\mu)}{4\pi} + \text{vacuum condensates} \\ &\approx 1 - 2.72 \frac{\alpha_s^{(n_l)}(\mu)}{4\pi} + \text{vacuum condensates} , \end{aligned} \quad (5.74)$$

which coincides with Equation (5.69). Here, the same continuum threshold is assumed for the two- and three-point correlator such that the bag parameter is independent of ω_c . The result is valid at a low renormalization scale or $\mu \sim \omega_c$.

The result in Equation (5.74) is the HQET result. We can now use the matching relation from Equation (5.27) and obtain the QCD result

$$\begin{aligned} \Delta B &= -\frac{N_C - 1}{2N_C} \left[11 \frac{\alpha_s(m_b)}{4\pi} + \left(\frac{4}{3}\pi^2 - 5 \right) \frac{\alpha_s(\mu)}{4\pi} \right] \\ &\approx -(3.67 + 2.72) \frac{\alpha_s}{4\pi} . \end{aligned} \quad (5.75)$$

Note, that α_s is given at two different scales which appear in the matching and the sum rule procedure, respectively. We are free to choose the scale involved in the sum rule calculation near ω_c with $\mu > \omega_c$. However, in the following numerical analysis $\mu = m_b$ is used. The difference is of order $\alpha_s(m_b)^2 \ln(m_b/\omega_c)$ and we account for it in the uncertainty.

Now that we have computed the perturbative contribution to the bag parameter we can take care of the power corrections such as the quark condensate contribution. Using FESR (at $\tau = 0$) we find for the spectral density given in Equation (5.65)

$$\int_0^{\omega_c} d\omega_1 d\omega_2 \Delta\rho_q(\omega_1, \omega_2) = C_F \frac{\alpha_s \langle \bar{q}q \rangle}{4\pi} \frac{2}{3} \frac{\omega_c^3}{(4\pi)^2} \left(\pi^2 - \frac{149}{18} \right) . \quad (5.76)$$

The FESR for the two-point correlator yields

$$m_B f_B^2 = 2F^2 = N_C \frac{\omega_c^3}{3\pi^2} - \langle \bar{q}q \rangle . \quad (5.77)$$

We can then insert the term with the lowest lying state in Equation (5.66) as well as Equation (5.67) into Equation (5.76). Using Equation (5.77) we finally obtain

$$\Delta B_L^{\text{eff}}|_q = \frac{N_C - 1}{N_C} \frac{\langle \bar{q}q \rangle}{m_B f_B^2} \frac{\alpha_s}{4\pi} \left[1 + \frac{\langle \bar{q}q \rangle}{m_B f_B^2} \right] \left(\pi^2 - \frac{149}{18} \right). \quad (5.78)$$

With typical numerical values of

$$\langle \bar{q}q \rangle = -(0.25 \text{ GeV})^3, \quad m_B = 5.3 \text{ GeV}, \quad f_B = 200 \text{ MeV}$$

we find that

$$\frac{\langle \bar{q}q \rangle}{m_B f_B^2} \approx -0.07.$$

Thus, we neglect the contribution of the quark condensate in the squared brackets in Equation (5.78) and find

$$\Delta B_L^{\text{eff}}|_q = -0.08 \frac{\alpha_s(m_b)}{4\pi}. \quad (5.79)$$

We use rough values for the phenomenological parameters and therefore generously estimate an uncertainty for the result

$$\Delta B_L^{\text{eff}}|_q = -(0.10 \pm 0.05) \frac{\alpha_s(m_b)}{4\pi}. \quad (5.80)$$

The power corrections have already been studied in [115] as an extension and update to [112]. The former provides a value for the contribution of the gluon as well as the mixed quark-gluon condensate extracted from FESRs

$$\Delta B_L^{\text{eff}}|_{\text{cond}} = -\frac{3\pi^2}{64} \left(\frac{1}{\omega_c^4} \langle \frac{\alpha_s}{\pi} GG \rangle - \frac{1}{\omega_c^5} \langle \bar{q}Gq \rangle \right) \approx -0.008. \quad (5.81)$$

Here, the standard numerical values for $\langle \frac{\alpha_s}{\pi} GG \rangle$ [130] and $\langle \bar{q}Gq \rangle$ [131,132] were used. A proper sum rule analysis in HQET yields

$$\Delta B_L^{\text{eff}}|_{\text{cond}} = -0.006 \pm 0.005, \quad (5.82)$$

which is actually the result for a B_s meson. We will use it as an estimate for the B_d meson.

In addition to the perturbative corrections also non-factorizable $1/m_b$ power corrections can emerge. However, they only arise at order α_s/m_b and are one order of magnitude smaller than the other corrections considered here. Therefore, we account for them in the uncertainties.

5.4. Result

In this section we now gather the results of the calculations outlined above. We have found the perturbative contribution via a sum rule and performed a matching onto QCD. Taking into account the running in Equation (5.30) for Equation (5.75) and evaluating it at $\mu = m_b$ as mentioned above, we find that the perturbative contribution to the violation of factorization is given by

$$\Delta B_{\text{pert}} \approx - \left(\frac{4}{9} \pi^2 + 2 \right) \frac{\alpha_s(m_b)}{4\pi}. \quad (5.83)$$

The difference of order $\alpha_s(m_b)^2 \ln(m_b/\omega_c)$ to the computation at $\mu \approx \omega_c$ as well as higher order terms are absorbed into the uncertainty, which we estimate with

$$\Delta B_{\text{pert}} = -6.4 \frac{\alpha_s(m_b)}{4\pi} \pm \left(X \frac{\alpha_s(m_b)}{4\pi} \right) \frac{\alpha_s(m_b)}{4\pi}. \quad (5.84)$$

Here, we generously choose the factor X to be as large as $X = 20$ and $\alpha_s(m_b) = 0.20 \pm 0.02$. Thus, we obtain

$$\Delta B_{\text{pert}} = -(6.4 \pm 0.3) \frac{\alpha_s(m_b)}{4\pi}. \quad (5.85)$$

Then, the bag parameter in Equation (5.85) yields

$$\Delta B_{\text{pert}} = -0.10 \pm 0.02 \pm 0.03, \quad (5.86)$$

where we assume a systematic error of 30%.

Next, we can determine the contribution of the non-perturbative power corrections, namely the condensates. With Equation (5.80) we obtain for the quark condensate contribution

$$\Delta B_q = -(0.10 \pm 0.05) \frac{\alpha_s(m_b)}{4\pi} = -0.002 \pm 0.001. \quad (5.87)$$

The remaining condensate contribution taken from [115] was already mentioned earlier in Equation (5.82). We repeat it here for completeness

$$\Delta B_{\text{non-pert}} = -0.006 \pm 0.005.$$

This leaves us with a total violation of factorization of

$$\Delta B = -0.11 \pm 0.04, \quad (5.88)$$

where the errors were added in quadrature.

In particular, lattice results are given in terms of the renormalization group invariant (RGI) parameter $\hat{B} = \hat{Z}B(m_b)$, where [111]

$$\hat{Z} = \alpha_s(m_b)^{-\frac{\gamma_0}{2\beta_0}} \left(1 + \frac{\alpha_s(m_b)}{4\pi} \left(\frac{\beta_1\gamma_0 - \beta_0\gamma_1}{2\beta_0^2} \right) \right). \quad (5.89)$$

With Equations (3.95) and (3.96) and

$$\gamma_0 = 4, \quad \gamma_1 = -7 + \frac{4}{9}n_f, \quad n_f = 5$$

as well as $\alpha_s(m_b) = 0.2$ we find a numerical value of

$$\hat{Z} = 1.51. \quad (5.90)$$

For our result

$$B = 1 + \Delta B = 1 - (0.11 \pm 0.04) \quad (5.91)$$

we can then explicitly compute the renormalization group invariant bag parameter

$$\hat{B}_{\text{RGI}} = 1.34 \pm 0.06. \quad (5.92)$$

A recent lattice result [111] is

$$\hat{B}_{\text{latt}} = 1.38(12)(6)$$

and in a recent review [110] an average of

$$\hat{B}_{\text{latt}} = 1.26(9)$$

was given for $n_f = 2 + 1$ flavors. We see, that our result agrees within the uncertainties. In fact, we even obtain a smaller uncertainty as the current lattice estimates which is due to our capability to distinguish between factorizable and non-factorizable contributions.

Here, we have computed the result for $B_d - \bar{B}_d$ mixing. For the consideration of B_s mesons $SU(3)$ breaking effects need to be taken into account due to the mass m_s of the strange quark. From experience this effect can be quite large. However, the factorizable contributions to the bag parameter still yield unity as for the $B_d - \bar{B}_d$ system. Therefore, the difference only emerges at NLO and is quite small. An estimate for the ratio of the two bag parameters is given by $B_{B_s}/B_{B_d} = 1 \pm 0.02$ [133].

5.5. Discussion

In this chapter non-factorizable contributions to the bag parameter for $B_d^0 - \bar{B}_d^0$ mixing was computed via HQET sum rules. For α_s corrections to the correlation

function this required the computation of three-loop-diagrams. Together with the non-perturbative condensate contributions we computed the violation of naive factorization which is quite small. As a final result we obtained a complete NLO result

$$\Delta B = B - 1 = -(0.11 \pm 0.04) \quad (5.93)$$

for the B_d meson bag parameter.

The uncertainty for ΔB mainly stems from the scale $\mu \sim m_b$ that we used rather than ω_c as well as higher orders in α_s and the value for $\alpha_s(m_b)$. These uncertainties have been generously estimated within the numerical discussion. Other uncertainties due to e.g. systematics of the sum rule computation or matching procedures at NNLO were estimated on the basis of experiences with similar analyses (e.g. [117, 126]). An analysis of uncertainties within sum rules has also been performed in [115, 134].

The uncertainty for our obtained value of ΔB is quite high which is typical for sum rule computations. However, this uncertainty is solely related to the deviation of the bag parameter from unity. Together with the factorizable contribution of the bag factor, which is unity and free of errors, we obtain a result for the complete bag parameter

$$\hat{B}_{\text{RGI}} = 1.34 \pm 0.06, \quad (5.94)$$

which is very precise. Our advantage is that we are able to identify the contributing diagrams of the correlation function that factorize. They merely result in a bag parameter which is unity and therefore do not need to be computed. This ability to analytically distinguish between factorizable and non-factorizable contributions allows us to compete with the lattice results.

6. CP Violation in Three-Body Decays

In the past decades non-leptonic two-body decays have been studied extensively. Especially the framework of QCD factorization (QCDF), which has been developed by Beneke, Buchalla, Neubert and Sachrajda (BBNS) in 1999 [135, 136], has proven to render quite promising results. However, hadronic multi-body decays actually make up a significant part of the branching fraction of non-leptonic B mesons. Unlike two-body decays, they do not have fixed kinematics but populate a Dalitz plot and therefore contain more information. Thus, they are quite interesting to study, but also more difficult to treat theoretically.

Non-leptonic multi-body decays are also quite attractive when it comes to investigate CP violation. It has been studied by LHCb, BaBar and Belle [137–142] within the past years and we hope to get even more information from LHC Run 2 and Belle II. Especially three-body decays such as $B \rightarrow KKK$, $B \rightarrow KK\pi$, $B \rightarrow K\pi\pi$ and $B \rightarrow \pi\pi\pi$ were analyzed. Even though the integrated CP asymmetries have been found to be quite small, huge local CP asymmetries in some kinematic regions were found. We especially expect a rich structure of CP violation in the decay $B \rightarrow \pi\pi\pi$ as found by LHCb and shown in Figure 6.1.

In this chapter we will concentrate specifically on the decay $B^- \rightarrow \pi^- \pi^+ \pi^-$. There have been some attempts modeling hadronic three-body decays in the past such as the Isobar model [143, 144] and the K-matrix formalism [145, 146]. More recently there have been some studies based on Flavor Symmetries [147, 148], perturbative QCD (pQCD) [149] or QCDF [150]. We will use the latter formalism to develop a more profound data-driven model based on QCDF and study CP violation.

First, we will give a short introduction to QCDF in two-body decays. We then give a short description of the generalization to three-body decays and recapitulate the findings of [150]. Next, the non-perturbative quantities that we need to compute the amplitude are introduced. After showing the results for our amplitude we evaluate it by fitting and comparing it to data by the LHCb Collaboration. Finally, we will compute the CP asymmetry within our model and include a charm resonance model to investigate the possible impact of subleading effects. This chapter is based on [151].

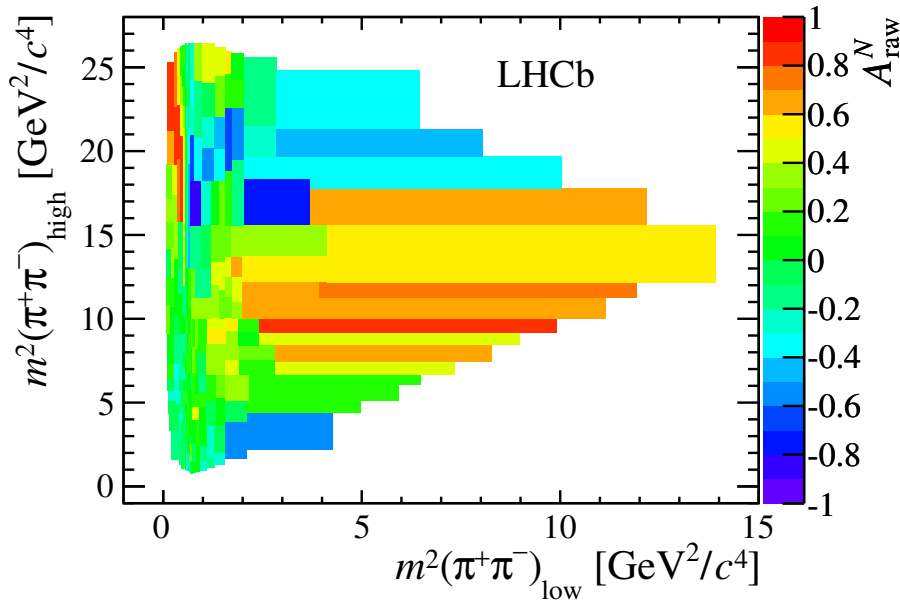


Figure 6.1.: Large local CP asymmetries in $B^- \rightarrow \pi^- \pi^+ \pi^-$ as measured by the LHCb Collaboration [137].

6.1. QCD Factorization

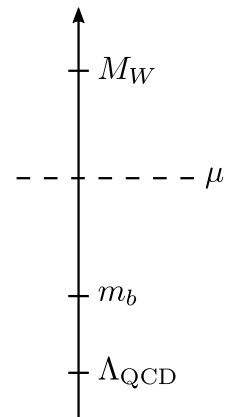
6.1.1. Two-Body Decays

Non-leptonic decays are quite difficult to deal with theoretically. Due to the all-hadronic final state non-trivial QCD dynamics are involved. BBNS address this problem in [135, 136] for two-body decays and offer a solution in terms of QCD factorization. We will briefly describe this framework.

We will start from a B meson decaying into two light mesons M_1 and M_2 , which means that we have a weak decay of a heavy meson. In this case, three fundamental scales $M_W \gg m_b \gg \Lambda_{\text{QCD}}$ are involved. The weak interaction scale M_W , the mass of the heavy quark m_b as well as the QCD scale Λ_{QCD} , where quarks hadronize. Nowadays, the primal weak decay has been studied intensively and can be computed using weak effective field theory [152]. Here we integrate out the heavy degrees of freedom which are much larger than the mass of the b quark. This results in a separation of the decay amplitude

$$\mathcal{A}(B \rightarrow M_1 M_2) = \frac{G_F}{\sqrt{2}} \sum_i \lambda_i C_i(\mu) \langle M_1 M_2 | \mathcal{O}_i | B \rangle(\mu) \quad (6.1)$$

into a high-energy contribution C_i , which comprises effects above the renormalization scale μ , and the low-energy effects, which are described by the effective local



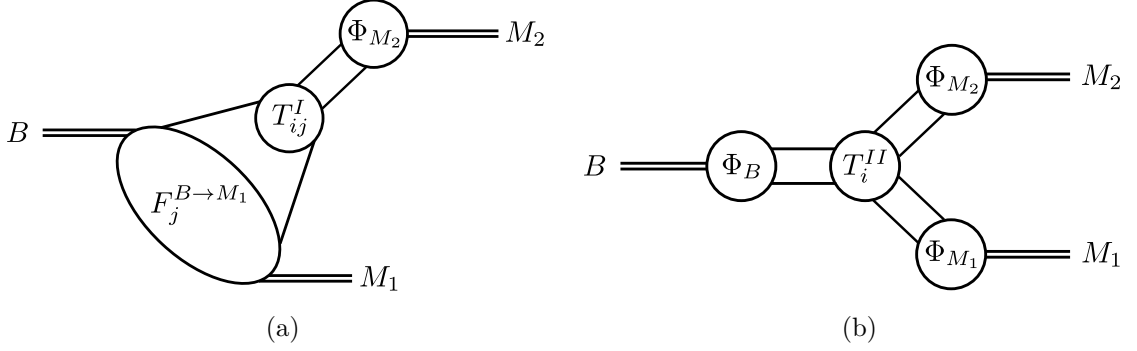


Figure 6.2.: Schematical depiction of the factorization formula in Equation (6.2). Here, (a) corresponds to the first term and (b) to the last term.

four-quark operators \mathcal{O}_i . The latter are non-perturbative objects, while the Wilson coefficients C_i can be computed perturbatively. The λ_i denote CKM factors.

As a first step we reduced the task at hand to the computation of the hadronic matrix elements of the effective local four-quark operator. In the heavy quark limit, BBNS [135, 136] find that the matrix element can be factorized into short-distance contributions, namely the hard scattering kernel, and long-distance quantities like form factors and light-cone distribution amplitudes (LCDAs). The latter they utilized similar to the factorization of exclusive processes at large momentum transfer in QCD as first proposed in [153, 154]. Thus, the hadronic matrix element can be boiled down to even simpler non-perturbative objects, which are universal and known.

For the weak effective operators \mathcal{O}_i we find the transition matrix element up to power corrections of order Λ_{QCD}/m_b to be

$$\begin{aligned} \langle M_1 M_2 | \mathcal{O}_i | B \rangle &= \sum_j F_j^{B \rightarrow M_1}(m_2^2) \int_0^1 du T_{ij}^I(u) \Phi_{M_2}(u) + (M_1 \leftrightarrow M_2) \\ &+ \int_0^1 d\xi du dv T_i^{II}(\xi, u, v) \Phi_B(\xi) \Phi_{M_1}(u) \Phi_{M_2}(v). \end{aligned} \quad (6.2)$$

Here, the amplitude is expressed through convolutions of the hard scattering functions T^I and T^{II} , which are process-dependent and perturbatively calculable at the scale m_b , and LCDAs Φ_X of the meson X . The latter are of non-perturbative nature as well as $F_j^{B \rightarrow M_{1,2}}$, which denotes the form factor for the process $B \rightarrow M_{1,2}$. Both are universal objects and can be determined from semileptonic decays using lattice QCD or sum rules. The momentum fractions of the constituents of the mesons in the LCDAs are denoted by ξ , u and v . The masses of the light mesons $M_{1,2}$ are finite in the heavy quark limit and of order Λ_{QCD} . A schematical picture of the factorization formula is shown in Figure 6.2.

The third term in Equation (6.2) describes hard interactions with the spectator

quark, which do not arise at leading order in α_s . Annihilation topologies are also power suppressed by Λ_{QCD}/m_b .

At leading order in α_s and leading power in Λ_{QCD}/m_b we find that QCDF reproduces naive factorization. This is consistent with the fact that the hard scattering kernel is independent of the momentum fraction u at leading order. Thus, the convolution integral at the local limit merely gives us a meson decay constant and the matrix element factorized into this and a form factor.

6.1.2. Three-Body Decays

We will now apply the QCDF approach to three-body decays and use the formalism which was set up in [150]. In the following, we will concentrate on charmless decays and focus on the process of $B^- \rightarrow \pi^- \pi^+ \pi^-$. The external momenta are defined as

$$B^-(p_B) \rightarrow \pi^-(k_1) \pi^+(k_2) \pi^-(k_3), \quad (6.3)$$

where momentum conservation $p_B = k_1 + k_2 + k_3$ holds. We consider the pions to be massless which leaves us with

$$p_B^2 = m_B^2, \quad k_i^2 = 0, \quad s_{ij} \equiv \frac{(k_i + k_j)^2}{m_B^2} = \frac{2k_i \cdot k_j}{m_B^2} \quad (i \neq j). \quad (6.4)$$

Here, we defined the invariant mass s_{ij} for the pion pairs, respectively, which are normalized to the square of the B meson mass m_B^2 . Due to momentum conservation our kinematic variables satisfy

$$s_{12} + s_{13} + s_{23} = 1, \quad \text{with} \quad 0 \leq s_{ij} \leq 1. \quad (6.5)$$

As a consequence of this kinematic constraint we end up with two independent invariant masses. Another restriction that we encounter is the fact that there are two identical particles involved. Therefore, we choose $E_1^{\text{CM}} < E_3^{\text{CM}}$, where $E_{1,3}^{\text{CM}}$ is the center-of-mass energy of the respective π^- in the B meson restframe. Considering our normalized invariant masses from above this results in $s_{12} < s_{23}$ and we redefine $s_{12} \equiv s_{+-}^{\text{low}}$, $s_{23} \equiv s_{+-}^{\text{high}}$ and $s_{13} \equiv s_{--}$.

The partial decay rate for the three-body decay is given by [16]

$$d\Gamma = \frac{1}{(2\pi)^3} \frac{m_B}{32} |\mathcal{A}(s_{+-}^{\text{low}}, s_{+-}^{\text{high}})|^2 ds_{+-}^{\text{low}} ds_{+-}^{\text{high}}, \quad (6.6)$$

where \mathcal{A} is the transition amplitude, which we will determine later. The partial decay rate $d\Gamma/ds_{+-}^{\text{low}} ds_{+-}^{\text{high}}$ can be displayed as a Dalitz distribution as shown in Figure 6.3 and explained in more detail in Appendix D.1. For the case of $B^- \rightarrow \pi^- \pi^+ \pi^-$ we obtain a symmetric Dalitz plot in s_{+-}^{low} and s_{+-}^{high} which is cut in half due to the identical π^- . The Dalitz plot can be divided into three regions [150] with different kinematic configurations. The respective regions correspond to the center, edges and corners of the Dalitz plot.

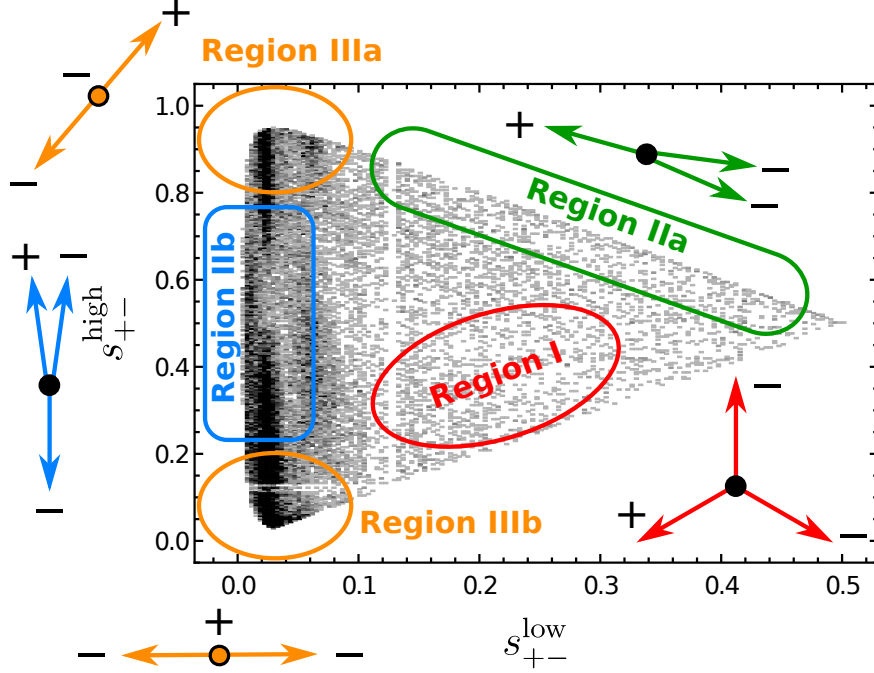


Figure 6.3.: In the Dalitz plot we can distinguish three regions with different kinematic configurations. The central region I, the collinear regions IIa, IIb and the soft regions IIIa, IIIb with different kinematic configurations, respectively.

- I. Central Region:** All three pions distribute uniformly in space and their invariant masses are roughly the same and of order m_B :

$$s_{--} \sim s_{+-}^{\text{low}} \sim s_{+-}^{\text{high}} \sim 1/3. \quad (6.7)$$

- II. Collinear Region:** Two pions move collinear and recoil against the third pion. The collinear pions generate a small invariant mass while the other two are large:

$$\text{IIa} : s_{--} \sim 0, \quad s_{+-}^{\text{low}} \sim s_{+-}^{\text{high}} \sim 1/2 \quad (6.8)$$

$$\text{IIb} : s_{+-}^{\text{low}} \sim 0, \quad s_{--} \sim s_{+-}^{\text{high}} \sim 1/2. \quad (6.9)$$

- III. Soft Region:** One pion is soft and the other two pions move back-to-back with large energy. Here, two invariant masses are small and one is large:

$$\text{IIIa} : s_{--} \sim s_{+-}^{\text{low}} \sim 0, \quad s_{+-}^{\text{high}} \sim 1, \quad (6.10)$$

$$\text{IIIb} : s_{+-}^{\text{low}} \sim s_{+-}^{\text{high}} \sim 0, \quad s_{--} \sim 1. \quad (6.11)$$

These various regions require different QCDF approaches of which two are given for the central and the collinear region in [150]. In the following, we will focus on the

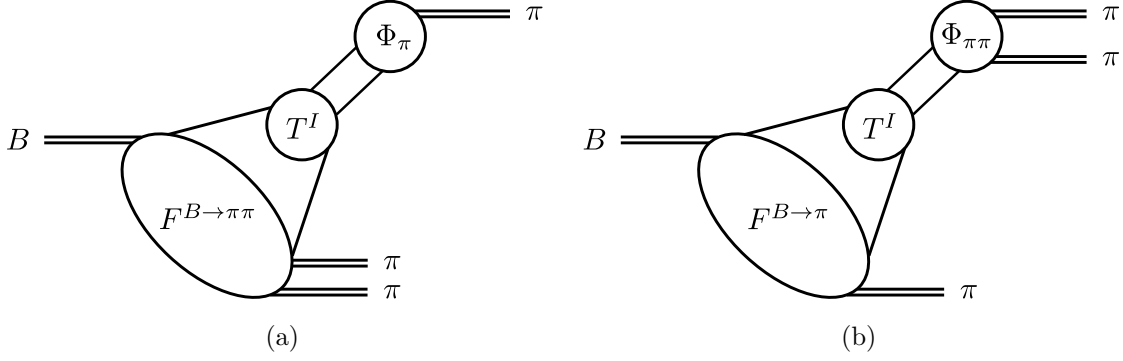


Figure 6.4.: Schematic depiction of the factorization formula in Equation (6.12). Here, (a) corresponds to the first term and (b) to the second term.

edges of the Dalitz plot, which are described by the QCDF approach for $s_{+-}^{\text{low}} \ll 1$. We favor this collinear region since the interesting resonances emerge there. The central region, on the other hand, is rather empty. This is in accordance with quasi-two-body decays and implies that in this case our three-body decay resembles a two-body decay but with different final states. We can use the same effective Hamiltonian as for the two-body decay and adjust the QCDF approach such that we replace one of the final state mesons by a system of two mesons. Now, we can set up the QCDF formula for the three-body decay amplitude in the heavy quark limit

$$\langle \pi\pi\pi | \mathcal{O} | B \rangle_{s_{+-} \ll 1} = T_1^I \otimes F^{B \rightarrow \pi\pi} \otimes \Phi_\pi + T_2^I \otimes F^{B \rightarrow \pi} \otimes \Phi_{\pi\pi}, \quad (6.12)$$

where \otimes represents a convolution. Here, $T_{1,2}^I$ denote the hard scattering kernels and \mathcal{O} is the operator in the weak effective Hamiltonian. We also have the LCDA for the pion and the form factor for the $B \rightarrow \pi$ transition. In the formula we see that there is the necessity to introduce new non-perturbative quantities such as the 2π -LCDA, which were first introduced by [155–157], and the $B \rightarrow \pi\pi$ form factor, which has been examined in [158]. In the formula, we omit the term with the spectator interaction since it vanishes at leading order. Schematically, this factorization formula is depicted in Figure 6.4.

We will only consider the transition amplitude at leading order. Then the hard scattering kernel is independent of the momentum fraction of the constituent quarks. This means that the convolution integrals are trivial and we eventually only have to deal with decay constants and form factors since we only have local operators at hand. Practically, this means that we only need to cope with naive factorization (see also [159])

$$\begin{aligned} \langle \pi^-(k_1)\pi^+(k_2)\pi^-(k_3) | j_1 \otimes j_2 | B^-(p_B) \rangle &= \langle \pi^-(k_1)\pi^+(k_2) | j_1 | B^- \rangle \langle \pi^-(k_3) | j_2 | 0 \rangle \\ &+ \langle \pi^-(k_3) | j_1 | B^- \rangle \langle \pi^-(k_1)\pi^+(k_2) | j_2 | 0 \rangle. \end{aligned} \quad (6.13)$$

6.2. QCD-factorized Effective Hamiltonian

As already mentioned, we will use the same effective Hamiltonian as for the $B \rightarrow \pi\pi$ decay. We will merely end up with different final states for which we will introduce new non-perturbative input later. Hence, we can simply take the effective Hamiltonian from [135] which we derive in Appendix D.2

$$\mathcal{H}_{\text{eff}} = \frac{G_F}{\sqrt{2}} (\lambda_u T_u + \lambda_c T_c), \quad (6.14)$$

where

$$\begin{aligned} T_u = & a_1^u \left[(\bar{u}b)_{V-A} \otimes (\bar{d}u)_{V-A} \right] + a_2^u \left[(\bar{d}b)_{V-A} \otimes (\bar{u}u)_{V-A} \right] \\ & + a_3 \sum_q \left[(\bar{d}b)_{V-A} \otimes (\bar{q}q)_{V-A} \right] + a_4^u \sum_q \left[(\bar{q}b)_{V-A} \otimes (\bar{d}q)_{V-A} \right] \\ & + a_5 \sum_q \left[(\bar{d}b)_{V-A} \otimes (\bar{q}q)_{V+A} \right] - 2a_6^u \sum_q \left[(\bar{q}b)_{S-P} \otimes (\bar{d}q)_{S+P} \right] \end{aligned}$$

and

$$\begin{aligned} T_c = & a_3 \sum_q \left[(\bar{d}b)_{V-A} \otimes (\bar{q}q)_{V-A} \right] + a_4^c \sum_q \left[(\bar{q}b)_{V-A} \otimes (\bar{d}q)_{V-A} \right] \\ & + a_5 \sum_q \left[(\bar{d}b)_{V-A} \otimes (\bar{q}q)_{V+A} \right] - 2a_6^c \sum_q \left[(\bar{q}b)_{S-P} \otimes (\bar{d}q)_{S+P} \right]. \end{aligned}$$

Here, $q = u, c$ and $\lambda_q = V_{qd}^* V_{qb}$. Further, our currents are abbreviated by $(\bar{u}b)_{V\pm A} = \bar{u}\gamma_\mu(1 \pm \gamma_5)b$ as well as $(\bar{u}b)_{S\pm P} = \bar{u}(1 \pm \gamma_5)b$. The Hamiltonian is obtained by applying the QCD factorization formula to the weak effective Hamiltonian in [152]. The coefficients a_i are combinations of the Wilson coefficients C_i [152]. For $B \rightarrow \pi\pi\pi$ we find at tree level $a_1^c = a_2^c = 0$, since no c quarks are involved, as well as $a_4^u = a_4^c$. We have

$$a_{1,2,4} = C_{1,2,4} + \frac{C_{2,1,3}}{N_C}, \quad (6.15)$$

where $N_C = 3$ is the number of colors. We will later see that the operators multiplied by $a_{3,5,6}$ will not contribute at leading order and leading twist¹. Note, that the definition of C_1 and C_2 differs from the one in [152], where 1 and 2 reversed. The values for the Wilson coefficients at $\mu = m_b$ can be taken from [160].

6.3. Non-Perturbative Input

We now need to introduce several non-perturbative quantities to finally obtain the amplitude for our decay $B^- \rightarrow \pi^- \pi^+ \pi^-$. In the following, we will define the particular decay constants and form factors needed in the further course of this calculation.

¹Twist is the difference between the canonical dimension of the matrix element and its spin. Here, the fields u and d each have dimension 3/2 and the operator $\bar{u}\gamma_\mu\gamma_5 d$ has spin 1.

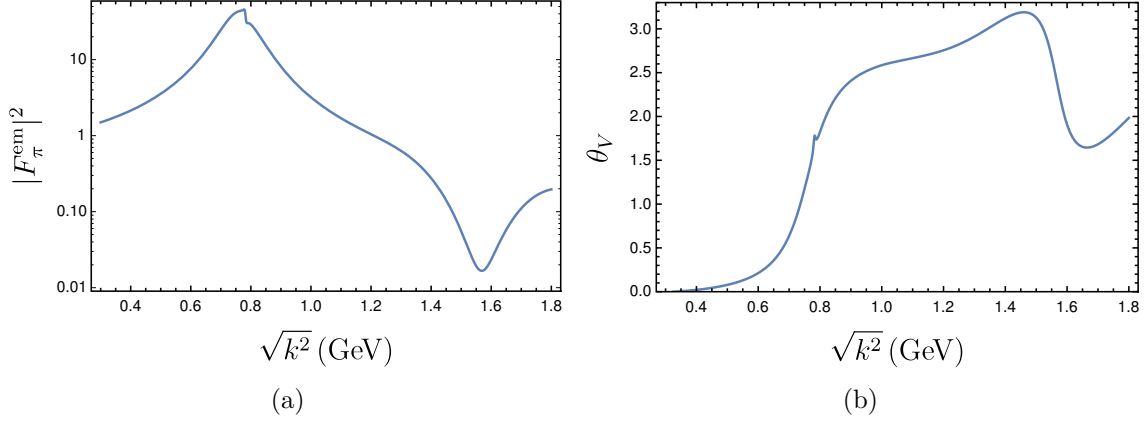


Figure 6.5.: Time-like pion vector form factor $F_\pi^{\text{em}} = |F_\pi^{\text{em}}|e^{i\theta_V}$.

6.3.1. Pion Decay Constant and Pion Form Factor

The pion decay constant is well known and defined as

$$\langle \pi^-(k_3) | (\bar{d}u)_{V-A} | 0 \rangle = i f_\pi k_{3\mu}, \quad (6.16)$$

where $f_\pi \approx 130$ MeV [16].

The time-like vector form factor in the two-pion channel is defined as

$$\begin{aligned} \langle \pi^-(k_1) \pi^+(k_2) | (\bar{u}u)_{V-A} | 0 \rangle &= -\langle \pi^-(k_1) \pi^+(k_2) | (\bar{d}d)_{V-A} | 0 \rangle \\ &= (k_1 - k_2)_\mu F_\pi^{\text{em}} = \bar{k}_\mu F_\pi^{\text{em}} \end{aligned} \quad (6.17)$$

and can be directly obtained from τ decays and from e^+e^- -annihilation. Unfortunately, there is no suitable experimental data on the phase available. Hence, we are obliged to use a parameterization as in [161] (see also [162]), which is fitted to the results of the BaBar Collaboration for $e^+e^- \rightarrow \pi^+\pi^-(\gamma)$ [163]. In addition, we include $\rho - \omega$ mixing to take into account isospin violation by adjusting the leading term of the pion vector form factor such that [164]

$$F_{\pi,\rho}^{\text{em}} \rightarrow F_{\pi,\rho}^{\text{em}} \left(1 + \frac{\Theta_{\rho\omega}}{3m_\rho^2} \frac{s}{s - m_\omega^2 + im_\omega\Gamma_\omega} \right). \quad (6.18)$$

This modification results in the small kink close to the mass of the ρ meson at about 0.78 GeV seen in Figure 6.5.

In the course of introducing the $B \rightarrow \pi\pi$ form factor we will later also require the associated scalar form factor. It is defined as [165]

$$\langle \pi^-(k_1) \pi^+(k_2) | m_u \bar{u}u + m_d \bar{d}d | 0 \rangle = m_\pi^2 F_\pi^S(k^2), \quad (6.19)$$

such that it vanishes in the chiral limit for massless quarks. This form factor can be extracted using chiral perturbation theory and we will use the results from [165],

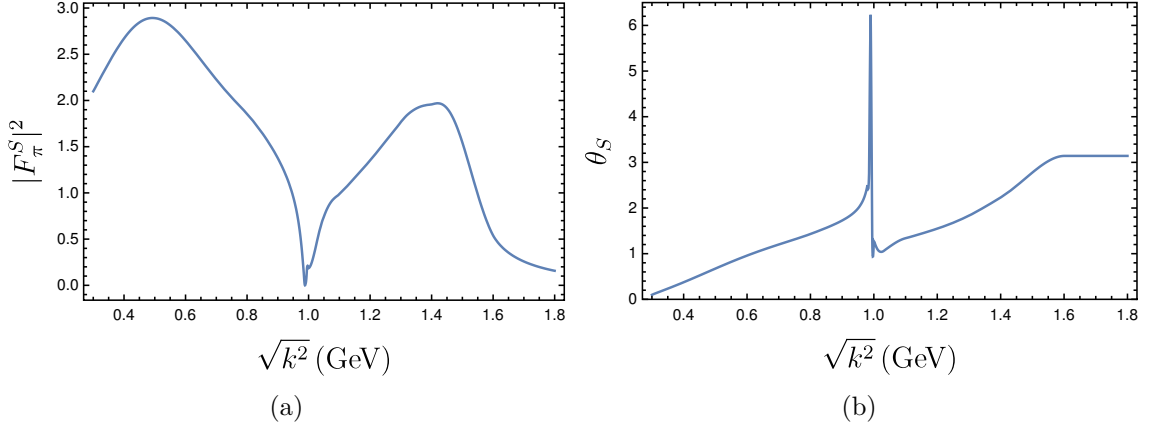


Figure 6.6.: Time-like pion scalar form factor $F_\pi^S = |F_\pi^S|e^{i\theta_S}$.

which are valid up to $k^2 \simeq 3 \text{ GeV}^2$. For higher k^2 we used an interpolation. Similar studies have been performed in [166]. In Figure 6.6 we see that it does not exhibit the usual Breit-Wigner shape of a resonance.

6.3.2. $B \rightarrow \pi$ Form Factors

The $B \rightarrow \pi$ form factor is well known and defined as [167]

$$\langle \pi^-(k_3) | \bar{d} \gamma^\mu b | B^-(p_B) \rangle = f_+(q^2) \left[p_B^\mu + k_3^\mu - \frac{m_B^2 - m_\pi^2}{k^2} k^\mu \right] + f_0(q^2) \frac{m_B^2 - m_\pi^2}{k^2} k^\mu, \quad (6.20)$$

where $k = p_B - k_3 = k_1 + k_2$. We find that we eventually only need the contraction of Equation (6.20) with Equation (6.17) and thus with the momentum $\bar{k} = k_1 - k_2$. This means that we only need

$$\langle \pi^-(k_3) | \bar{d} (\not{k}_1 - \not{k}_2) b | B^-(p_B) \rangle = 2k_3 \cdot \bar{k} f_+(q^2), \quad (6.21)$$

since $k \cdot \bar{k} = 0$. As a consequence, we only need the form factor $f_+(q^2)$ for which we use the result in [168].

6.3.3. $B \rightarrow \pi\pi$ Form Factors

Following [158] (using the phase convention of [169, 170]), the hadronic matrix element of the $B \rightarrow \pi\pi$ decay can be parameterized by four independent form factors, one vector form factor F_\perp and three axial-vector form factors F_t , F_0 and F_\parallel

$$i \langle \pi^-(k_1) \pi^+(k_2) | \bar{u} \gamma^\mu (1 - \gamma_5) b | B^-(p_B) \rangle = i F_\perp \bar{k}_{3(\perp)}^\mu + F_t \frac{k_3^\mu}{\sqrt{k_3^2}} + F_0 k_{(0)}^\mu + F_\parallel k_{(\parallel)}^\mu \quad (6.22)$$

with the orthogonal basis k_3 , $k_{(0)}$, $\bar{k}_{(\parallel)}$ and $\bar{k}_{3(\perp)}$, which spans the Minkowski space. Here, k_3 is the momentum of the unpaired pion with $k_3^2 = m_\pi^2$ and the basis vectors satisfy $k_3 \cdot k_{(0)} = k_3 \cdot \bar{k}_{(\parallel)} = k_3 \cdot \bar{k}_{3(\perp)} = 0$.

For the calculation of our transition amplitude we merely need the contraction of Equation (6.22) with Equation (6.16) and therefore simply the contraction with the momentum of the unpaired pion k_3 . This yields

$$\langle \pi^-(k_1)\pi^+(k_2) | \bar{u} k_3 \gamma_5 b | B^-(p_B) \rangle = iF_t \frac{k_3^2}{\sqrt{k_3^2}} = iF_t \frac{m_\pi^2}{\sqrt{m_\pi^2}} = im_\pi F_t(k^2, k_3 \cdot \bar{k}), \quad (6.23)$$

where $k = k_1 + k_2$ and $\bar{k} = k_1 - k_2$. Hence, we find that only the time-like form factor F_t is relevant. In the case at hand, the two pions can have isospin $I = 0$ or $I = 1$ such that we can decompose F_t into an isoscalar and isovector part

$$F_t = F_t^{I=0} + F_t^{I=1} \quad (6.24)$$

as shown in Appendix D.3.1. Our next challenge will be to find an expression for F_t .

Time Like Isovector $B \rightarrow \pi\pi$ Form Factors

We will first start with the isovector form factor $F_t^{I=1}$ since much more is known about it. Isovector contributions to the $B \rightarrow \pi\pi$ form factor have been investigated using light-cone sum rules (LCSR) [169–171]. However, similar studies have not been done for $F_t^{I=0}$. Here, we will take advantage of the fact that the isovector contribution is dominated by the resonance of the ρ meson [170]. For now, we will assume that the $B \rightarrow \pi\pi$ decay solely proceeds via a ρ resonance. We therefore insert an intermediate ρ state

$$\begin{aligned} & \langle \pi^-(k_1)\pi^+(k_2) | \bar{u} \gamma^\mu (1 - \gamma_5) b | B^-(p_B) \rangle \\ &= \sum_\epsilon \langle \pi^-(k_1)\pi^+(k_2) | \rho^0(k, \epsilon) \rangle \mathcal{B}_\rho(k) \langle \rho^0(k, \epsilon) | \bar{u} \gamma^\mu (1 - \gamma_5) b | B^-(p_B) \rangle, \end{aligned} \quad (6.25)$$

where ϵ is the polarization vector for the ρ resonance with momentum k . The Breit-Wigner

$$\mathcal{B}_P(k) = \frac{1}{k^2 - m_P^2 + i\sqrt{k^2}\Gamma_P} \quad (6.26)$$

accounts for the propagation of the intermediate state. Here, Γ_P is the total decay width of the particle P .

The $B \rightarrow \rho$ form factors have been studied in [170] and can be written as

$$\begin{aligned} \sqrt{2}\langle\rho^0(k, \epsilon)|\bar{u}\gamma_\mu(1-\gamma_5)b|B^-(p_B)\rangle &= \epsilon_{\mu\alpha\beta\gamma}\epsilon^{*\alpha}q^\beta k^\gamma \frac{2V^{B\rho}(q^2)}{m_B+m_\rho} \\ &\quad - i\epsilon_\mu^*(m_B+m_\rho)A_1^{B\rho}(q^2) \\ &\quad + i(2k+q)_\mu(\epsilon^*\cdot q)\frac{A_2^{B\rho}(q^2)}{m_B+m_\rho} \\ &\quad + iq_\mu(\epsilon^*\cdot q)\frac{2m_\rho}{q^2}\left(A_3^{B\rho}(q^2)-A_0^{B\rho}(q^2)\right), \end{aligned} \quad (6.27)$$

where $2m_\rho A_3^{B\rho}(q^2) = (m_B+m_\rho)A_1^{B\rho}(q^2) - (m_B-m_\rho)A_2^{B\rho}(q^2)$. Since ρ^0 represents a superposition $\rho^0 \sim (\bar{d}d - \bar{u}u)/\sqrt{2}$ we get the extra factor of $\sqrt{2}$ compared to the form factor for a charged ρ .

We find, that merely one form factor for the axial vector current is relevant when contracting with the momentum q

$$\langle\rho^0(k, \epsilon)|\bar{u}\not{q}\gamma_5b|B^-(p_B)\rangle = \frac{i}{\sqrt{2}}(\epsilon^*\cdot q)2m_\rho A_0(q^2), \quad (6.28)$$

where $q = p_B - k = k_3$ is the momentum transfer.

The $\rho \rightarrow \pi\pi$ transition matrix element can be parameterized using a strong coupling $g_{\rho\pi\pi}$

$$\langle\pi^-(k_1)\pi^+(k_2)|\rho^0(k, \epsilon)\rangle = g_{\rho\pi\pi}(k_1-k_2)^\mu\epsilon_\mu = g_{\rho\pi\pi}\bar{k}^\mu\epsilon_\mu. \quad (6.29)$$

Inserting Equations (6.28) and (6.29) into Equation (6.25) and contracting the result with $q = k_3$ yields

$$\begin{aligned} \langle\pi^-(k_1)\pi^+(k_2)|\bar{u}\not{k}_3\gamma_5b|B^-(p_B)\rangle &= \sum_\epsilon g_{\rho\pi\pi}\epsilon\cdot\bar{k}\mathcal{B}_\rho(k)\frac{i}{\sqrt{2}}(\epsilon^*\cdot k_3)2m_\rho A_0(m_\pi^2) \\ &= -g_{\rho\pi\pi}\mathcal{B}_\rho(k)\frac{2im_\rho}{\sqrt{2}}A_0(m_\pi^2)k_3\cdot\bar{k} \\ &= im_\pi F_t^{I=1}, \end{aligned} \quad (6.30)$$

where we used the polarization sum

$$\sum_\epsilon \epsilon_\mu\epsilon_\nu^* = -g_{\mu\nu} + \frac{k_\mu k_\nu}{k^2}. \quad (6.31)$$

We can now replace the simple Breit-Wigner shape, which describes our ρ resonance, by applying the same approximation to the matrix element for the time-like pion form factor

$$\begin{aligned} \langle\pi^-(k_1)\pi^+(k_2)|\bar{u}\gamma_\mu(1-\gamma_5)b|0\rangle &= (k_1-k_2)_\mu F_\pi^{\text{em}}(k^2) \\ &= \sum_\epsilon \langle\pi^-(k_1)\pi^+(k_2)|\rho^0(k, \epsilon)\rangle\mathcal{B}_\rho(k)\langle\rho^0(k, \epsilon)|\bar{u}\gamma_\mu(1-\gamma_5)b|0\rangle. \end{aligned} \quad (6.32)$$

For the decay constant of the ρ resonance we find that

$$\langle \rho^0(k, \epsilon) | \bar{u} \gamma_\mu (1 - \gamma_5) b | 0 \rangle = \frac{1}{\sqrt{2}} f_\rho m_\rho \epsilon_\mu^*. \quad (6.33)$$

Then, we can contract again with k_3 and find with Equations (6.33) and (6.29), using the polarization sum, that

$$\begin{aligned} \langle \pi^-(k_1) \pi^+(k_2) | \bar{u} \not{k}_3 (1 - \gamma_5) b | 0 \rangle &= k_3 \cdot \bar{k} F_\pi^{\text{em}}(k^2) \\ &= \sum_\epsilon \langle \pi^-(k_1) \pi^+(k_2) | \rho^0(k, \epsilon) \rangle \mathcal{B}_\rho(k) \langle \rho^0(k, \epsilon) | \bar{u} \not{k}_3 (1 - \gamma_5) b | 0 \rangle \\ &= -g_{\rho\pi\pi} \mathcal{B}_\rho(k) \frac{1}{\sqrt{2}} f_\rho m_\rho k_3 \cdot \bar{k}. \end{aligned} \quad (6.34)$$

We can now solve this for

$$g_{\rho\pi\pi} \mathcal{B}_\rho(k) = -\frac{\sqrt{2} F_\pi^{\text{em}}(k^2)}{f_\rho m_\rho}, \quad (6.35)$$

which allows us to replace the Breit-Wigner shape in (6.30). We can then extract a data-driven expression for

$$F_t^{I=1} = 2k_3 \cdot \bar{k} \frac{F_\pi^{\text{em}}(k^2)}{f_\rho m_\pi} A_0(m_\pi^2), \quad (6.36)$$

where $f_\rho = 0.209 \text{ GeV}$ [172] and $A_0(m_\pi^2) \simeq A_0(0) = 0.36$ [173] (following up [174]).

Time Like Isoscalar $B \rightarrow \pi\pi$ Form Factors

For the scalar resonance we use an analogous method. We now assume that the scalar contribution to the $B \rightarrow \pi\pi$ form factor predominantly enters via the process $B \rightarrow S^0 \rightarrow \pi\pi$, where S_0 is a light scalar resonance. We can now treat S_0 in the same manner as the ρ resonance above. Thus, we can write

$$\begin{aligned} \langle \pi^-(k_1) \pi^+(k_2) | \bar{u} \gamma_\mu (1 - \gamma_5) b | B^-(p_B) \rangle \\ = \langle \pi^-(k_1) \pi^+(k_2) | S^0 \rangle \mathcal{B}_S(k) \langle S^0 | \bar{u} \gamma_\mu (1 - \gamma_5) b | B^-(p_B) \rangle. \end{aligned} \quad (6.37)$$

The $B \rightarrow S_0$ form factor is defined in [175]

$$\begin{aligned} \langle S^0(k) | \bar{u} \gamma_\mu (1 - \gamma_5) b | B^-(p_B) \rangle &= -i \left[\left((p_B + k)_\mu - \frac{m_B^2 - m_S^2}{q^2} q_\mu \right) F_1^{BS}(q^2) \right. \\ &\quad \left. + \frac{m_B^2 - m_S^2}{q^2} q_\mu F_0^{BS}(q^2) \right]. \end{aligned}$$

Here, again, we will later only need the contraction with $q = k_3$. Hence, we find that only the following form factor is needed

$$\langle S^0(k) | \bar{u} \gamma_\mu (1 - \gamma_5) b | B^-(p_B) \rangle = -i(m_B^2 - m_S^2) F_0^{BS}(q^2).$$

Analogous to above we parameterize the $S^0 \rightarrow \pi\pi$ transition matrix element via a coupling $g_{S\pi\pi}$

$$\langle \pi^-(k_1)\pi^+(k_2)|S^0\rangle = g_{S\pi\pi}m_S. \quad (6.38)$$

We now find

$$\begin{aligned} \langle \pi^-(k_1)\pi^+(k_2)|\bar{u}k_3\gamma_5b|B^-\rangle &= \langle \pi^-(k_1)\pi^+(k_2)|S^0\rangle\mathcal{B}_S(k)\langle S^0|\bar{u}k_3\gamma_5b|B^-\rangle \\ &= -ig_{S\pi\pi}\mathcal{B}_S(k)m_S(m_B^2 - m_S^2)F_0^{BS} \\ &= im_\pi F_t^{I=0}. \end{aligned}$$

Then, we can replace the product of the coupling and the Breit-Wigner $g_{S\pi\pi}\mathcal{B}_S(k)$ using the time-like scalar pion form factor from Equation (6.19) and applying the same procedure as above defining

$$\langle S^0(k)|\bar{q}q|0\rangle = f_S m_S. \quad (6.39)$$

We then find

$$\begin{aligned} \langle \pi^-(k_1)\pi^+(k_2)|m_u\bar{u}u + m_d\bar{d}d|B^-(p_B)\rangle &= m_\pi^2 F_\pi^S \\ &= \langle \pi^-(k_1)\pi^+(k_2)|S^0(k)\rangle\mathcal{B}_S(k)\langle S^0(k)|m_u\bar{u}u + m_d\bar{d}d|B^-(p_B)\rangle \\ &= g_{S\pi\pi}m_S\mathcal{B}_S(k) \left[m_u\langle S^0(k)|\bar{u}u|B^-\rangle + m_d\langle S^0(k)|\bar{d}d|B^-(p_B)\rangle \right] \\ &= g_{S\pi\pi}m_S\mathcal{B}_S(k)(m_u + m_d)f_S m_S. \end{aligned}$$

Hence, we can now replace

$$g_{S\pi\pi}\mathcal{B}_S(k) = \frac{m_\pi^2 F_\pi^S}{(m_u + m_d)f_S m_S^2} \quad (6.40)$$

in Equation (6.39) and find

$$F_t^0 = -\frac{m_\pi(m_B^2 - m_S^2)}{m_S(m_u + m_d)} \frac{F_0^{BS}}{f_S} F_\pi^S. \quad (6.41)$$

Not much is known about the scalar matrix elements. In particular, we do not have information on the size of the form factor F_0^{BS} and the decay constant f_S . We do not even know which scalar is dominant at low energies. Thus, we will model the time-like isoscalar form factor via

$$F_t^0 = \frac{m_B^2}{f_\pi m_\pi} \beta e^{i\phi} F_\pi^S(k^2), \quad (6.42)$$

where β and the strong phase ϕ are constant model parameters. The factor $m_B^2/f_\pi m_\pi$ is chosen arbitrary to fit nicely into our final expression of our $B \rightarrow \pi\pi\pi$ amplitude. Due to the lack of any other data on the isoscalar form factor we will later fit β and ϕ to the data.

6.4. Calculation of the Amplitude

Now we can compute the amplitude at leading order in α_s , leading power in Λ_{QCD}/m_b and leading twist. A detailed calculation of the individual matrix elements in naive factorization can be found in Appendix D.4. Using that

$$2k_3 \cdot \bar{k} = m_B^2(1 - s_{+-}^{\text{low}} - 2s_{+-}^{\text{high}}), \quad (6.43)$$

we find the following expression for the transition amplitude

$$\begin{aligned} \mathcal{A}(s_{+-}^{\text{low}}, s_{+-}^{\text{high}}) = & \frac{G_F}{\sqrt{2}} \left\{ [\lambda_u(a_2 - a_4^u) - \lambda_c a_4^c] m_B^2(1 - s_{+-}^{\text{low}} - 2s_{+-}^{\text{high}}) f_+(s_{+-}^{\text{low}}) F_\pi^{\text{em}}(s_{+-}^{\text{low}}) \right. \\ & \left. + [\lambda_u(a_1 + a_4^u) + \lambda_c a_4^c] f_\pi m_\pi F_t(s_{+-}^{\text{low}}, s_{+-}^{\text{high}}) \right\}. \end{aligned} \quad (6.44)$$

Here, $F_t(s_{+-}^{\text{low}}, s_{+-}^{\text{high}}) = F_t^{I=1}(s_{+-}^{\text{low}}, s_{+-}^{\text{high}}) + F_t^{I=0}(s_{+-}^{\text{low}})$.

The LHCb Collaboration [137] presents their measurements in terms of the helicity angle, which is defined as (see Appendix D.5)

$$k_3 \cdot \bar{k} = \frac{\beta_\pi}{2} \sqrt{\lambda} \cos \theta_\pi, \quad (6.45)$$

where θ_π is the polar angle of the paired π^- in the dipion rest frame. This coincides with the definition of the LHCb Collaboration, where they define the angle between the momentum of the unpaired and the paired pion with the same charge in the dipion rest frame. Here, $\beta_\pi = (k^2 - m_\pi^2)/k^2$ and $\lambda = \lambda(m_B^2, m_\pi^2, k^2)$ is the Källén function with $\lambda(a, b, c) = a^2 + b^2 + c^2 - 2(ab + bc + ac)$. Hence, for massless pions we find

$$2k_3 \cdot \bar{k} = m_B^2(1 - s_{+-}^{\text{low}}) \cos \theta_\pi. \quad (6.46)$$

We do not have access to the efficiency- and background-corrected full Dalitz distribution from the LHCb Collaboration. Therefore, we will use their projections of the number of B^- and B^+ signal events in bins of the variable $m_{12} = \sqrt{m_B^2 s_{+-}^{\text{low}}}$ [137]. They distinguish between projections for $\cos \theta_\pi > 0$ and $\cos \theta_\pi < 0$. Using Equations (6.43) and (6.46) we find that in our notation $\cos \theta_\pi > 0$ corresponds to $s_{+-}^{\text{high}} < \frac{1-s_{+-}^{\text{low}}}{2}$. In Figure 6.7, the LHCb results for the projections are displayed for $B^- \rightarrow \pi^- \pi^+ \pi^-$ in bins of 0.05 GeV.

Using this piece of data we can now fit our free model parameters β and ϕ . We calculate the decay rate for each bin in our model in order to use it for a χ^2 minimization. Therefore, we perform an integration over s_{+-}^{high} for the two cases $\cos \theta_\pi > 0$ and $\cos \theta_\pi < 0$. We then need to integrate over s_{+-}^{low} for each bin of 0.05 GeV, where we approximate the integration by a Riemann sum. The obtained values can now be used to fit to the data. Since we do not know the time of measurement, we will also

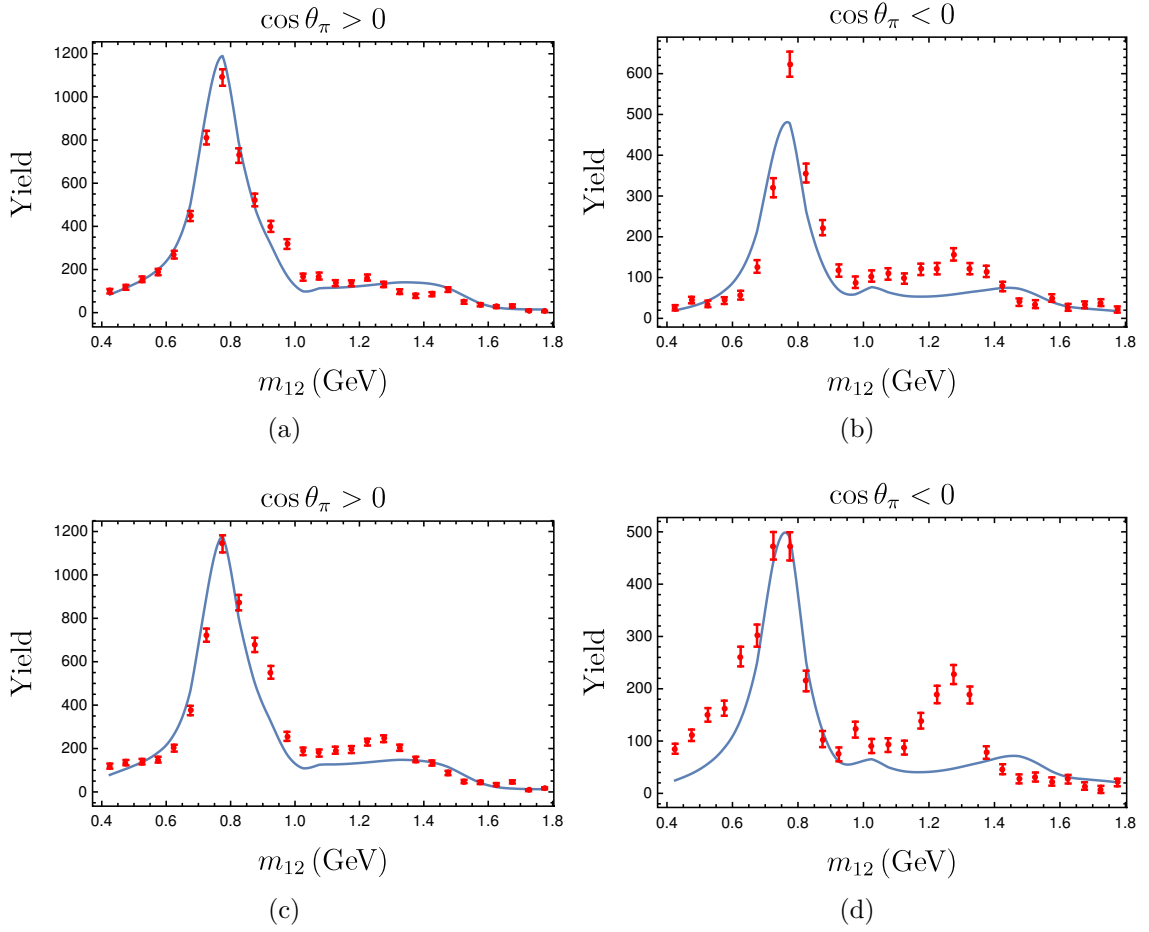


Figure 6.7.: The projections for (a),(b) B^+ and (c),(d) B^- decays with $\cos \theta > 0$ and $\cos \theta < 0$ as a function of $m_{12} = \sqrt{m_B^2 s_{+-}^{\text{low}}}$. The blue line represents the best fit for our model. The red data points are the results from the LHCb Collaboration [137].

include a fit parameter to take care of the normalization. We obtain the following best fit parameters

$$\beta = 0.18 \quad \text{and} \quad \phi = 18^\circ. \quad (6.47)$$

Since the value for χ^2 is fairly large we do not give any errors. In Figure 6.7, we show our yield predictions for our best fit result in Equation (6.47) compared to the LHCb data.

6.5. CP Violation

We are now prepared to investigate CP violation within our model. The CP asymmetry is defined as

$$A_{\text{CP}}(s_{+-}^{\text{low}}, s_{+-}^{\text{high}}) = \frac{|\mathcal{A}(s_{+-}^{\text{low}}, s_{+-}^{\text{high}})|^2 - |\bar{\mathcal{A}}(s_{+-}^{\text{low}}, s_{+-}^{\text{high}})|^2}{|\mathcal{A}(s_{+-}^{\text{low}}, s_{+-}^{\text{high}})|^2 + |\bar{\mathcal{A}}(s_{+-}^{\text{low}}, s_{+-}^{\text{high}})|^2}, \quad (6.48)$$

where $\bar{\mathcal{A}}$ is the CP conjugated of the amplitude \mathcal{A} , which means that all weak phases are conjugated. In order to obtain a value for A_{CP} that is non-zero we require a strong as well as a weak phase difference. The latter stems from the CKM matrix elements and the corresponding weak phase γ of the Unitarity Triangle. Here, $\lambda_u = V_{ub}V_{ud}^* = |V_{ub}V_{ud}^*|e^{-i\gamma}$ and $\lambda_c = V_{cb}V_{cd}^* = |V_{cb}V_{cd}^*|$ is real. We use the Wolfenstein parameterization and the values given in [176]. The pion decay constant f_π and $B \rightarrow \pi$ form factor f_+ are real. At leading order the coefficients a_i are real. Beyond leading order they do have perturbative strong phases [172] which we will not consider here. Including these $\mathcal{O}(\alpha_s)$ effects would require a great effort to compute the convolution of the hard scattering kernel with the two-pion distribution amplitude [155–157].

In Figure 6.1, we see large local CP asymmetries. These can only be induced by kinematic-dependent strong phases. In the previous sections we observed that the time-like pion form factor F_π and the time-like $B \rightarrow \pi\pi$ form factor F_t contain non-perturbative strong phases θ_S and θ_V , which are actually depending on the kinematics

$$F_\pi^S(s_{+-}^{\text{low}}) = |F_\pi^S(s_{+-}^{\text{low}})|e^{i\theta_S(s_{+-}^{\text{low}})}, \quad F_\pi^{\text{em}}(s_{+-}^{\text{low}}) = |F_\pi^{\text{em}}(s_{+-}^{\text{low}})|e^{i\theta_V(s_{+-}^{\text{low}})}. \quad (6.49)$$

Only the product $k_3 \cdot \bar{k}$ contains the variable s_{+-}^{high} which we replace by $\cos \theta_\pi$ using Equation (6.46). We can now compute the CP asymmetry in terms of s_{+-}^{low} and $\cos \theta_\pi$ which is proportional to

$$A_{\text{CP}}(s_{+-}^{\text{low}}, \cos \theta_\pi) \sim \beta \sin \gamma \sin(\theta_S + \phi - \theta_V) \cos \theta_\pi |F_\pi^S(s_{+-}^{\text{low}})| |F_\pi^{\text{em}}(s_{+-}^{\text{low}})| g(s_{+-}^{\text{low}}), \quad (6.50)$$

where

$$g(s_{+-}^{\text{low}}) = -2G_F^2(a_1 + a_2)a_4^c m_B^4 (1 - s_{+-}^{\text{low}}) |\lambda_u| |\lambda_c| f_+(s_{+-}^{\text{low}}) \quad (6.51)$$

is real.

In Equation (6.50), we observe that in fact only the interference of terms including the pion vector form factor F_π^{em} and the isoscalar $B \rightarrow \pi\pi$ form factor $F_t^{I=0}$ contribute to the CP asymmetry. This is due to the fact that $F_t^{I=1}$ has the same strong phase as F_π^{em} such that their interference leads to a vanishing CP asymmetry.

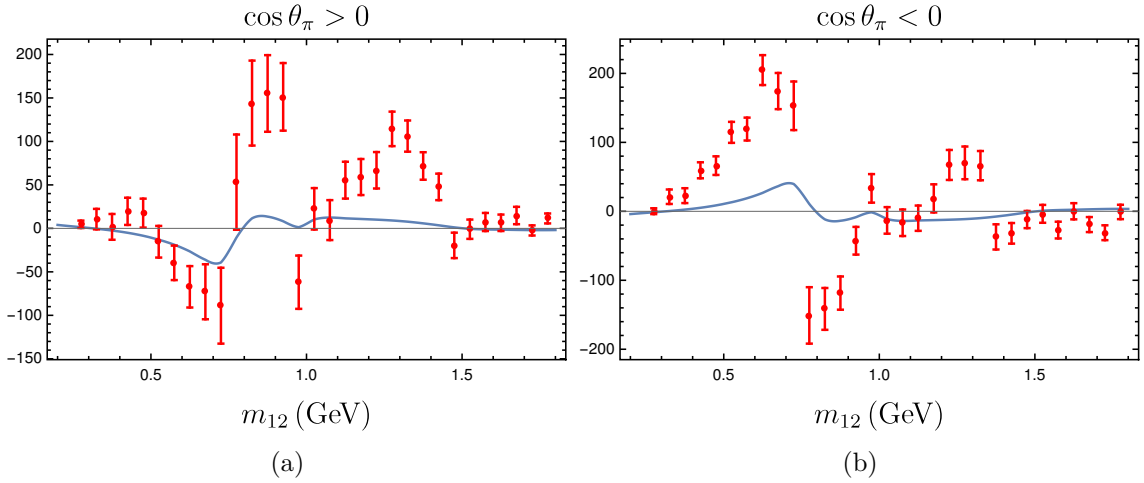


Figure 6.8.: The difference between the B^- and the B^+ yield for $\cos \theta > 0$ and $\cos \theta < 0$ as a function of m_{12} . Again, the blue line denotes our model's best fit while the red points represent LHCb data points [137].

The LHCb Collaboration also provides plots for the difference $B^- - B^+$ of the projected yield for $\cos \theta_\pi > 0$ and $\cos \theta_\pi < 0$, which is a measure for the CP asymmetry. We display our fit results in Figure 6.8 together with those that were measured. We observe that up to 1.1 GeV our result roughly reproduces the shape of the LHCb data even though the outcome of our model is much smaller. Further, we observe that the second part of our plot does not show the same behavior. This can be explained by the fact that we solely examine a scalar-vector wave interference which is proportional to $\cos \theta_\pi$. This always gives a sign switch for $\cos \theta_\pi > 0$ compared to $\cos \theta_\pi < 0$.

6.6. Charm Resonance Model

Our model is based on the conjecture that our three-body decay is dominated by resonances in the $\pi^- \pi^+$ system. This effect is only predominant at the edges of the phase space. As a matter of fact, we see in Figure 6.9(a) that most of the events can be found in that region. In Figure 6.1, we see that large local CP asymmetries were measured at high s_{+-}^{low} . We presume that this effect might emerge due to subleading effects. In Equation (6.14) we already distinguished between the amplitudes T_u and T_c , where the latter is sensitive to charm-quarks and can thus be influenced by charmed penguins. This might have the potential to create large CP asymmetries in the region around the charm threshold of $2m_c$. In order to get a qualitative picture of this effect we modify our model by adding a Breit-Wigner, which describes a propagating resonance with mass $2m_c$, to T_c

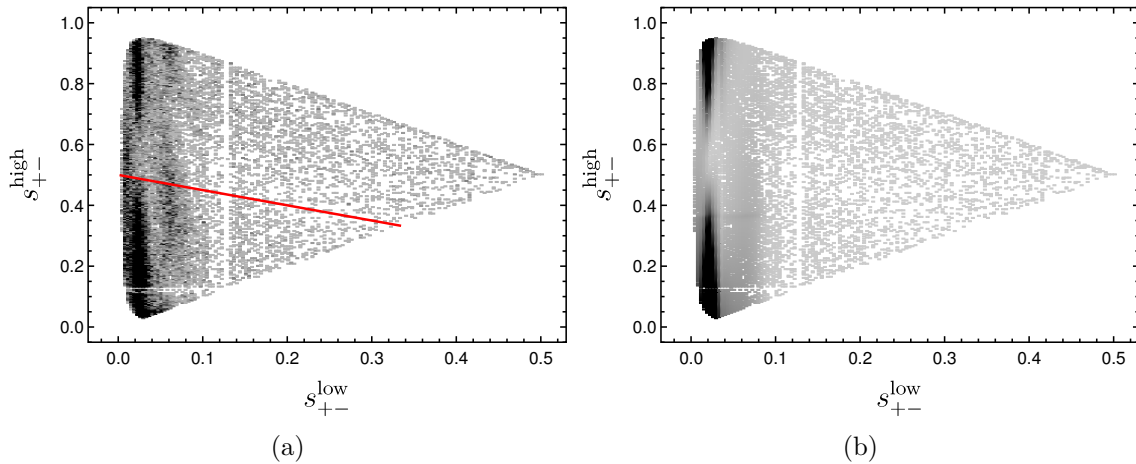


Figure 6.9.: (a) Measured Dalitz distribution with logarithmic intensity for $B^- \rightarrow \pi^- \pi^+ \pi^-$ by the LHCb Collaboration [137]. The red line denotes the $\cos \theta_\pi = 0$ line, where the region below the red line is equivalent to $\cos \theta_\pi > 0$. (b) corresponding Dalitz distribution in our model including the charm resonance.

$$\begin{aligned}
 T_u &= T_u^{(0)} \\
 T_c &= T_c^{(0)} + g \frac{4m_c^2}{m_{12}^2 - 4m_c^2 + im_c\Gamma},
 \end{aligned} \tag{6.52}$$

where the leading order amplitude given by the term proportional to λ_q in Equation (6.44) is denoted by $T_q^{(0)}$. Here, g is a coupling constant that we use to tune the strength of this subleading effect. We set it to $g = 0.02$ and assume $m_c = 1.6$ GeV as well as $\Gamma = 0.15$ GeV.

Including the charm loop leads to the Dalitz distribution with logarithmic intensity as shown in Figure 6.9(b). Here, we see that the Dalitz plot is still dominated by the ρ resonance, as it is the case for the data, and the effect of the charm penguin is not noticeable at this level of precision. This cannot be said about the resulting local CP asymmetry distribution which is displayed in Figure 6.10(b). Here, we observe significant local CP asymmetries in the region of the charm threshold.

The LHCb data is given in specific bins that all include the same number of events resulting in different bin sizes. In order to plot our results in the same bins we computed a value for the CP asymmetry for every bin by integrating the numerator and denominator of the CP violation given in Equation (6.48) separately within the boundaries of each bin. The result is shown in Figure 6.10(c). Here, we expanded our model up to higher values for s_{+-}^{low} . Note, that we use a different scale for the legend of our plot compared to the one by the LHCb Collaboration in Figure 6.10(a). Regarding our method to obtain the CP distribution in the binned plot it seems very difficult to obtain such a large CP violation in one bin as the LHCb Collaboration does.

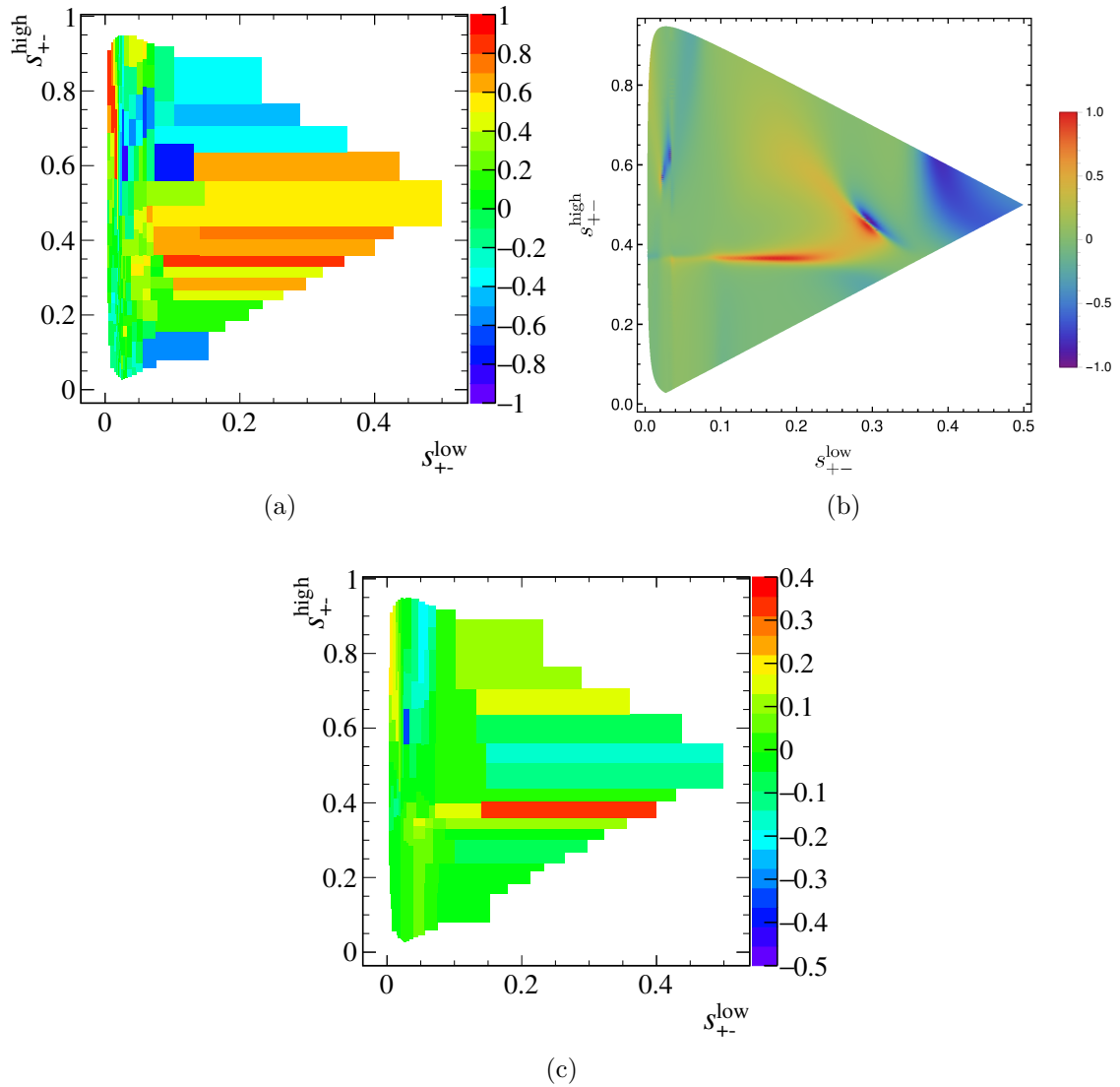


Figure 6.10.: (a) The CP asymmetry distribution as measured by the LHCb Collaboration [137], (b) the results of our model including the charm penguin and (c) the same result shown in a binned plot.

6.7. Discussion

We studied CP violation in charmless three-body B decays, in particular for $B^- \rightarrow \pi^- \pi^+ \pi^-$, using a data-driven model which is based on QCD factorization [151]. Due to the non-trivial kinematics and the resulting phase space distributions, three-body decays have the potential to give away much more information than two-body decays. Unfortunately, their theoretical treatment is also more difficult due to the occurring hadronic matrix elements. In order to get a hold on these, we used a ‘partial factorization’ as proposed in [150] to describe the edges of the Dalitz plot. Here, non-perturbative input is required such as generalized form factors, which we introduced. We came up with a model for the transition amplitude which depends on the parameter β and a strong phase ϕ . We then computed the CP asymmetry which is mostly driven by the non-perturbative strong phases of the scalar and vector time-like pion form factors. Finally, we included a charm resonance model to investigate the effect of subleading contributions.

We have seen that our simple model is able to reproduce some of the features that can be observed in the experimental results by the LHCb Collaboration [137]. In the following, we will discuss some of the challenges that need to be addressed in the future to improve our model.

At this point, we were interested to see if the QCDF framework at hand offers the possibility to qualitatively generate some of the features seen in the Dalitz distribution and local CP asymmetry as observed by experiments. Therefore, we simply investigated the process at leading order, where naive factorization applies. To include higher orders we would additionally need to introduce two-pion light-cone distribution amplitudes. The hard scattering kernels which are involved in the QCDF approach are already known from studies with two-body decays up to next-to-next-to-leading order (NNLO). The convolutions with the aforementioned 2π LCDAs still need to be computed, though.

Currently, we use a rather crude model to describe our $B \rightarrow \pi\pi$ form factors in terms of the time-like pion form factors. In the past, there were already attempts to address this problem using light-cone sum rules with pion distribution amplitudes [169,171] and B meson distribution amplitudes [170]. From this we know that $F_t^{I=1}$ is related to F_π^{em} . For $F_t^{I=0}$ the relation to F_π^S is much less certain. Since not much is known about this we are forced to introduce some model parameters. In the future, futher LCSR studies on this matter might help avoiding the modeling that we applied above.

We have observed that the CP violation is primarily driven by the interference of F_π^{em} and F_π^S , more specific by their phases. Therefore, it is of great importance to gain more precise information on those. At the moment, we got access to accurate measurements up to $k^2 \sim 3.5 \text{ GeV}^2$ for $|F_\pi^{\text{em}}|$. Not much is known about the phase

on experimental side, though, which forces us to fall back on another model. The pion scalar form factor F_π^S is much less studied. To improve the situation in the future we need more data on these form factors.

The data on $B \rightarrow \pi\pi\pi$ and especially on the CP asymmetries is not yet very precise. Right now, we only have access to data projections for small momenta. In the future it would be beneficial to have at least some information on the projections for higher momenta. Since information about the s_{+-}^{high} variable is lost performing that projection it would be preferable to gain access to the full information on the Dalitz and CP distributions. Further, we do not have access to the full efficiency- and background-corrected Dalitz distribution which makes it difficult to compare our results with the ones from the LHCb Collaboration.

At the moment, our results for the difference between the B^- and B^+ yield do not show the same behavior as the LHCb results at $\sim 1.3 \text{ GeV}$, where we observe a sign flip whereas they do not. We only have a scalar-vector interference which is proportional to $\cos\theta_\pi$ and therefore obviously switches sign when comparing regions with $\cos\theta_\pi > 0$ and $\cos\theta_\pi < 0$. The absence of a sign-change could be explained by the interference of pure scalar contributions.

Our model is a first step towards describing three-body decays using a data-driven approach. In order to improve our model we will need to include higher orders in the future. Obtaining both $B \rightarrow \pi\pi$ form factors from LCSR would also enhance the quality of our model. Furthermore, it will be beneficial to gain more data on the time-like form factor as well as on the Dalitz and CP distribution. Altogether, this will reduce the model-dependence of our approach.

7. Summary and Conclusion

Within the last decades, a tremendous progress has been made in high energy physics. With the discovery of the Higgs boson, all particles which the Standard Model predicted have been verified by experiments. Nevertheless, there are still many open questions to be answered in the future. Some of them are related to tensions between theory and experiment, which concern the quark and lepton flavor sector. Here, especially B mesons open up a rich field for flavor studies. Their large mass and long lifetime make them easy to access experimentally, which led to the construction of the big B factories. On theory side, the large mass of the b quark allows the application of Heavy Quark Effective Theory (HQET). We have shown three applications of HQET in this thesis.

One advantage of HQET is the emergence of a heavy flavor and spin symmetry. The latter leads to the formation of spin-symmetry doublets. Particularly, for the orbitally excited D mesons two doublets with the total angular momentum of the light degrees of freedom of $j = 1/2$ and $j = 3/2$ are obtained. Contributions of the HQET Lagrangian at order $1/m$ allowed us to investigate the mixing of the two meson states with the same total angular momentum of 1^+ . We developed a model to extract the mixing angle and fitted the model parameters to data on the masses of the orbitally excited states. The main goal was to investigate if the mixing can resolve the ‘ $1/2$ vs. $3/2$ puzzle’. Here, the observed semileptonic B decay rate into the orbitally excited D meson states with $j = 1/2$ is roughly equal to the one into states with $j = 3/2$. The latter are predicted to be much more dominant, though. With our model we obtained an effective mixing angle of 27° and observed that this indeed eases the tension between experiment and theory. Nevertheless, our model aimed for a rather qualitative picture and the current experimental situation is not very conclusive. For the future, a simultaneous analysis for the masses and the widths of the orbitally excited states would be interesting and we are hoping for more precise data on this matter.

Another benefit of HQET is the tremendous simplification of loop calculations. During the computation of the $\Delta B = 2$ matrix element for B - \bar{B} mixing the bag parameter arises. It is a measure for the deviation from the naive factorization. We computed the non-factorizable $\mathcal{O}(\alpha_s)$ corrections to the bag parameter, which required the evaluation of tree-loop diagrams. This calculation was performed in HQET. The bag parameter was then extracted from sum rules. Due to the fact that our result was computed analytically we were able to distinguish between factorizable and non-factorizable contributions to the bag parameter. The former are

predominant and yield unity. Thus, they did not need to be computed and we only had to determine the deviation from factorization, which is rather small. This way, we were able to determine the result for the complete bag parameter with high accuracy. Therefore, we are able to compete with the results obtained by lattice QCD. With $\hat{B} = 1.34 \pm 0.06$, our result is in good agreement with the lattice result $\hat{B}_{\text{latt}} = 1.38(12)(6)$.

When it comes to flavor physics the violation of CP symmetry is an interesting field to study. In the last years there was much experimental progress concerning CP violation in three-body decays. Those decays are quite interesting since, in contrary to two-body decays, their kinematics are not fixed. This allows us to study local CP asymmetries, which can be displayed in Dalitz plots. For the decay $B \rightarrow \pi\pi\pi$, large local CP asymmetries have been found. We made a first preliminary study of this decay in a new data-driven and QCD based approach. Therefore, we used a QCD factorization framework for three-body decays which was recently established. Here, we needed to introduce new non-perturbative input quantities such as generalized form factors and at higher orders also the two-pion light-cone distribution amplitude. In order to obtain a non-zero CP asymmetry, we used the weak CKM phase and strong phases coming from the time-like $B \rightarrow \pi\pi$ form factors. The latter can be related to the time-like pion form factor which is known quite well. Nonetheless, there are some parts of our theory that needed to be modeled, especially the isoscalar contribution, since not much is known about it. The model parameters were fit to data that is provided by the LHCb Collaboration. We were able to reproduce some of the rough features of the patterns of local CP asymmetries observed by experiments. However, we used a rather crude model. For future studies, we can use sum rules to connect the $B \rightarrow \pi\pi$ form factor and the pion form factor, which would yield a more profound model. Further, more experimental data on this subject would be useful, especially on scalar resonances. We also only considered leading order here. Subleading effects will also be important for future considerations. This can also be seen in our naive model for a charm penguin contribution.

Despite the tremendous progress in high energy physics especially flavor physics remains a very interesting field to study. With Belle II coming up and LHC experiments collecting more and more data, a enormous amount of measurements will be available. This will enable us to gain an even better insight into many decay channels and processes. Especially the flavor sector, where most of the deviations from theory are observed, requires a better understanding in the future. Here, B physics will continue to play a major role to resolve these tensions.

Appendix

A. Fierz Transformations

Here, we calculate some Fierz transformations. For the Dirac matrices we use the basis

$$\Gamma = \{\mathbb{1}, \gamma_\mu, \gamma_5, i\gamma_\mu\gamma_5, \sigma_{\mu\nu}\}. \quad (\text{A.0.1})$$

We can decompose a matrix M into this basis using $\text{Tr}[\Gamma^A\Gamma^B] = 4\delta^{AB}$ such that

$$\begin{aligned} M &= \sum_A M_A \Gamma^A \quad | \cdot \Gamma^B \\ \Rightarrow M\Gamma^B &= \sum_A M_A \Gamma^A \Gamma^B \quad | \text{Tr} \\ \Rightarrow \text{Tr}[M\Gamma^B] &= \sum_A \text{Tr}[M_A \Gamma^A \Gamma^B] = \sum_A M_A \text{Tr}[\Gamma^A \Gamma^B] = 4 \sum_A M_A \delta^{AB} = 4M_B \\ \Rightarrow M_B &= \frac{1}{4} \text{Tr}[M\Gamma^B] \\ \Rightarrow M &= \sum_A M_A \Gamma^A = \frac{1}{4} \sum_A \text{Tr}[M\Gamma^A] \Gamma^A \end{aligned} \quad (\text{A.0.2})$$

and with

$$\begin{aligned} M &= \frac{1}{4} \sum_A \text{Tr}[M\Gamma^A] \Gamma^A = \frac{1}{4} \sum_A M_{lk} \Gamma_{kl}^A \Gamma^A \\ \Rightarrow M_{ij} &= \frac{1}{4} \sum_A M_{lk} \Gamma_{kl}^A \Gamma_{ij}^A \\ \Rightarrow M_{lk} \delta_{il} \delta_{kj} &= \frac{1}{4} \sum_A M_{lk} \Gamma_{kl}^A \Gamma_{ij}^A \\ \Rightarrow \delta_{il} \delta_{kj} &= \frac{1}{4} \sum_A \Gamma_{kl}^A \Gamma_{ij}^A \end{aligned} \quad (\text{A.0.3})$$

we find for fermion fields that

$$\begin{aligned} \psi_{1,i} \bar{\psi}_{2,j} &= \psi_{1,i} \bar{\psi}_{2,k} \delta_{il} \delta_{jk} = \psi_{1,i} \bar{\psi}_{2,k} \frac{1}{4} \Gamma_{kl}^A \Gamma_{ij}^A = -\bar{\psi}_{2,k} \psi_{1,i} \frac{1}{4} \Gamma_{kl}^A \Gamma_{ij}^A \\ &= -\frac{1}{4} \Gamma_{ij}^A (\bar{\psi}_2 \Gamma^A \psi_1). \end{aligned} \quad (\text{A.0.4})$$

Hence, we have

$$\begin{aligned}
\bar{\psi}_1 \Gamma^A \psi_2 \bar{\psi}_3 \Gamma^B \psi_4 &= \Gamma_{ij}^A \Gamma_{kl}^B \bar{\psi}_{1,i} \psi_{2,j} \bar{\psi}_{3,k} \psi_{4,l} = \Gamma_{ij}^A \Gamma_{kl}^B \bar{\psi}_{1,i} \underbrace{\psi_{2,j} \bar{\psi}_{3,k}}_{= -\frac{1}{4} \Gamma_{jk}^C (\bar{\psi}_3 \Gamma^C \psi_2)} \psi_{4,l} \\
&= -\frac{1}{4} \Gamma_{ij}^A \Gamma_{kl}^B \bar{\psi}_{1,i} \Gamma_{jk}^C (\bar{\psi}_3 \Gamma^C \psi_2) \psi_{4,l} \\
&= -\frac{1}{4} \sum_C \bar{\psi}_1 \Gamma^A \Gamma^C \Gamma^B \psi_4 \bar{\psi}_3 \Gamma^C \psi_2
\end{aligned} \tag{A.0.5}$$

or in the case of spinors

$$\bar{u}_1 \Gamma^A u_2 \bar{u}_3 \Gamma^B u_4 = \frac{1}{4} \sum_C \bar{u}_1 \Gamma^A \Gamma^C \Gamma^B u_4 \bar{u}_3 \Gamma^C u_2.$$

We can then find a couple of Fierz identities such as

$$\begin{aligned}
&\bar{u}_1 \gamma_\mu (1 - \gamma_5) u_2 \bar{u}_3 \gamma^\mu (1 - \gamma_5) u_4 \\
&= -\bar{u}_1 \gamma_\mu (1 - \gamma_5) u_4 \bar{u}_3 \gamma^\mu (1 - \gamma_5) u_2
\end{aligned} \tag{A.0.6}$$

and

$$\begin{aligned}
&\bar{u}_1 (1 - \gamma_5) u_2 \bar{u}_3 (1 - \gamma_5) u_4 \\
&= \bar{u}_1 (1 - \gamma_5) u_4 \bar{u}_3 (1 - \gamma_5) u_2 + \frac{1}{2} \bar{u}_1 \gamma_\mu (1 - \gamma_5) u_4 \bar{u}_3 \gamma^\mu (1 - \gamma_5) u_2
\end{aligned} \tag{A.0.7}$$

or

$$\begin{aligned}
&\bar{\psi}_1 \gamma_\mu (1 - \gamma_5) \psi_2 \bar{\psi}_3 \gamma^\mu (1 - \gamma_5) \psi_4 \\
&= -\frac{1}{4} \bar{\psi}_1 \gamma_\mu (1 - \gamma_5) \gamma_\nu \gamma^\mu (1 - \gamma_5) \psi_4 \bar{\psi}_3 \gamma^\nu \psi_2 \\
&\quad + \frac{1}{4} \bar{\psi}_1 \gamma_\mu (1 - \gamma_5) \gamma_\nu \gamma_5 \gamma^\mu (1 - \gamma_5) \psi_4 \bar{\psi}_3 \gamma^\nu \gamma_5 \psi_2 \\
&= \bar{\psi}_1 \gamma_\mu (1 - \gamma_5) \psi_4 \bar{\psi}_3 \gamma^\mu (1 - \gamma_5) \psi_2
\end{aligned} \tag{A.0.8}$$

as well as

$$\begin{aligned}
&\bar{\psi}_1 \gamma_\mu (1 - \gamma_5) \psi_2 \bar{\psi}_3 \gamma^\mu (1 + \gamma_5) \psi_4 \\
&= -\frac{1}{4} \bar{\psi}_1 \gamma_\mu (1 - \gamma_5) \gamma^\mu (1 + \gamma_5) \psi_4 \bar{\psi}_3 \psi_2 \\
&\quad - \frac{1}{4} \bar{\psi}_1 \gamma_\mu (1 - \gamma_5) \gamma_5 \gamma^\mu (1 + \gamma_5) \psi_4 \bar{\psi}_3 \gamma_5 \psi_2 \\
&= -2 \bar{\psi}_1 (1 + \gamma_5) \psi_4 \bar{\psi}_3 (1 - \gamma_5) \psi_2.
\end{aligned} \tag{A.0.9}$$

B. Details on D^{**} Spectroscopy and $B \rightarrow D^{**} \ell \nu$

B.1. Spin Wave Functions

Here, we give the explicit coupling of the angular momentum $L = 1$ and the light quark spin $s = 1/2$. With the table for the Clebsch-Gordan coefficients we find that the spin wave functions for $j = 1/2$ are

$$\begin{aligned} |j = 1/2, +1/2\rangle &= \sqrt{\frac{2}{3}}|+1\rangle| - 1/2\rangle_l - \sqrt{\frac{1}{3}}|0\rangle| + 1/2\rangle_l \\ |j = 1/2, -1/2\rangle &= \sqrt{\frac{1}{3}}|0\rangle| - 1/2\rangle_l - \sqrt{\frac{2}{3}}| - 1\rangle| + 1/2\rangle_l \end{aligned} \quad (\text{B.1.1})$$

and for $j = 3/2$

$$\begin{aligned} |j = 3/2, +3/2\rangle &= |+1\rangle| + 1/2\rangle_l \\ |j = 3/2, +1/2\rangle &= \sqrt{\frac{1}{3}}|+1\rangle| - 1/2\rangle_l + \sqrt{\frac{2}{3}}|0\rangle| + 1/2\rangle_l \\ |j = 3/2, -1/2\rangle &= \sqrt{\frac{2}{3}}|0\rangle| - 1/2\rangle_l + \sqrt{\frac{1}{3}}| - 1\rangle| + 1/2\rangle_l \\ |j = 3/2, -3/2\rangle &= | - 1\rangle| - 1/2\rangle_l, \end{aligned} \quad (\text{B.1.2})$$

where $|\cdot\rangle_l$ denotes the spin of the light quark. The first ket vector is for the angular momentum. In order to obtain the spin wave functions for the D^{**} mesons we need to combine these states with the spin of the heavy quark. We get

$$|D(0^+), M = 0\rangle = \sqrt{\frac{1}{2}}(|j_{\text{light}} = 1/2, 1/2\rangle| - 1/2\rangle_H - |j_{\text{light}} = 1/2, -1/2\rangle|1/2\rangle_H) \quad (\text{B.1.3})$$

and

$$\begin{aligned} |D(1^+), M = 1\rangle &= |j = 1/2, 1/2\rangle|1/2\rangle_H \\ |D(1^+), M = 0\rangle &= \sqrt{\frac{1}{2}}(|j = 1/2, 1/2\rangle| - 1/2\rangle_H + |j = 1/2, -1/2\rangle|1/2\rangle_H) \\ |D(1^+), M = -1\rangle &= |j = 1/2, -1/2\rangle| - 1/2\rangle_H \end{aligned} \quad (\text{B.1.4})$$

as well as

$$\begin{aligned}
|D^*(1^+), M = 1\rangle &= \sqrt{\frac{3}{4}}|j = 3/2, 3/2\rangle|-1/2\rangle_H - \sqrt{\frac{1}{4}}|j = 3/2, 1/2\rangle|1/2\rangle_H \\
|D^*(1^+), M = 0\rangle &= \sqrt{\frac{1}{2}}(|j = 3/2, 1/2\rangle|-1/2\rangle_H - |j = 3/2, -1/2\rangle|1/2\rangle_H) \\
|D^*(1^+), M = -1\rangle &= \sqrt{\frac{1}{4}}|j = 3/2, -1/2\rangle|-1/2\rangle_H - \sqrt{\frac{3}{4}}|j = 3/2, -3/2\rangle|1/2\rangle_H
\end{aligned} \tag{B.1.5}$$

and

$$\begin{aligned}
|D^*(2^+), M = 2\rangle &= |j_{\text{light}} = 3/2, 3/2\rangle|1/2\rangle_H \\
|D^*(2^+), M = 1\rangle &= \sqrt{\frac{1}{4}}|j_{\text{light}} = 3/2, 3/2\rangle|-1/2\rangle_H + \sqrt{\frac{3}{4}}|j_{\text{light}} = 3/2, 1/2\rangle|1/2\rangle_H \\
|D^*(2^+), M = 0\rangle &= \sqrt{\frac{1}{2}}(|j_{\text{light}} = 3/2, 1/2\rangle|-1/2\rangle_H + |j_{\text{light}} = 3/2, -1/2\rangle|1/2\rangle_H) \\
|D^*(2^+), M = -1\rangle &= \sqrt{\frac{3}{4}}|j_{\text{light}} = 3/2, -1/2\rangle|-1/2\rangle_H + \sqrt{\frac{1}{4}}|j_{\text{light}} = 3/2, -3/2\rangle|1/2\rangle_H \\
|D^*(2^+), M = -2\rangle &= |j_{\text{light}} = 3/2, -3/2\rangle|-1/2\rangle_H,
\end{aligned} \tag{B.1.6}$$

where $|\cdot\rangle_H$ denotes the spin of the heavy quark. We can then combine these with Equations (B.1.1) and (B.1.2).

The coupling of the angular momentum with the heavy quark spin can be computed using

$$(\vec{J} \cdot \vec{\sigma}) = \frac{1}{2} (\vec{K}^2 - \vec{J}^2 - \vec{\sigma}^2) \tag{B.1.7}$$

and the spin-spin coupling using

$$(\vec{s} \cdot \vec{\sigma}) = \frac{1}{2} (s_+ \sigma_- + s_- \sigma_+) + s_3 \sigma_3. \tag{B.1.8}$$

The operators act on the states in the following manner

$$\begin{aligned}
\vec{J}^2 |j, m\rangle &= j(j+1) |j, m\rangle, \\
J_z |j, m\rangle &= m |j, m\rangle, \\
J_{\pm} |j, m\rangle &= \sqrt{j(j+1) - m(m \pm 1)} |j, m \pm 1\rangle.
\end{aligned} \tag{B.1.9}$$

This yields the result

$$(\vec{s} \cdot \vec{\sigma}) |D(1^+)\rangle = -\frac{1}{12} |D(1^+)\rangle + \frac{\sqrt{2}}{3} |D^*(1^+)\rangle \tag{B.1.10}$$

$$(\vec{s} \cdot \vec{\sigma}) |D^*(1^+)\rangle = -\frac{5}{12} |D^*(1^+)\rangle + \frac{\sqrt{2}}{3} |D(1^+)\rangle \tag{B.1.11}$$

for any M.

B.2. Mixing of the 1^+ States

For the Hamiltonian we have

$$\mathbf{H} = \begin{pmatrix} M & a \\ a & M^* \end{pmatrix} = \begin{pmatrix} M & a \\ a & M + \Delta \end{pmatrix} \quad (\text{B.2.1})$$

with

$$\begin{aligned} M &\equiv M(D(1^+)) + \frac{1}{4}g - \frac{1}{12}g', \\ M^* &\equiv M(D^*(1^+)) - \frac{5}{4}g - \frac{5}{12}g', \\ \Delta &\equiv M(D^*(1^+)) - M(D(1^+)) - \frac{3}{2}g - \frac{1}{3}g', \\ a &\equiv \frac{\sqrt{2}}{3}g'. \end{aligned}$$

We find a heavy and a light eigenvalue for this Hamiltonian

$$M_{H/L} = \frac{1}{2} \left[(M + M^*) \pm \sqrt{\Delta^2 + 4a^2} \right] \quad (\text{B.2.2})$$

The Hamiltonian can be rewritten

$$\begin{aligned} \mathbf{H} &= \begin{pmatrix} M(D(1^+)) & a \\ a^* & M(D^*(1^+)) \end{pmatrix} \\ &= \begin{pmatrix} \langle D(1^+) | \mathcal{H}_{1/m} | D(1^+) \rangle & \langle D(1^+) | \mathcal{H}_{1/m} | D^*(1^+) \rangle \\ \langle D^*(1^+) | \mathcal{H}_{1/m} | D(1^+) \rangle & \langle D^*(1^+) | \mathcal{H}_{1/m} | D^*(1^+) \rangle \end{pmatrix} \\ &= \begin{pmatrix} \langle D(1^+) | \\ \langle D^*(1^+) | \end{pmatrix} \mathcal{H}_{1/m} \begin{pmatrix} |D(1^+)\rangle \\ |D^*(1^+)\rangle \end{pmatrix}^T \end{pmatrix} \quad (\text{B.2.3}) \end{aligned}$$

and diagonalized with the orthogonal transformation matrix S

$$\mathbf{H}_{\text{diag}} = S^{-1} \mathbf{H} S = S^T \mathbf{H} S.$$

So in the diagonal basis we have

$$\mathbf{H}_{\text{diag}} = S^T \mathbf{H} S = S^T \begin{pmatrix} \langle D(1^+) | \\ \langle D^*(1^+) | \end{pmatrix} \mathcal{H}_{1/m} \begin{pmatrix} |D(1^+)\rangle \\ |D^*(1^+)\rangle \end{pmatrix}^T S \quad (\text{B.2.4})$$

$$= \begin{pmatrix} \langle D_L | \\ \langle D_H | \end{pmatrix} \mathcal{H}_{1/m} \begin{pmatrix} |D_L\rangle \\ |D_H\rangle \end{pmatrix}^T, \quad (\text{B.2.5})$$

where in the last step we redefined the states

$$\begin{pmatrix} |D(1^+)\rangle \\ |D^*(1^+)\rangle \end{pmatrix}^T S = \begin{pmatrix} |D_L\rangle \\ |D_H\rangle \end{pmatrix}^T \Rightarrow \begin{pmatrix} |D_L\rangle \\ |D_H\rangle \end{pmatrix} = S^T \begin{pmatrix} |D(1^+)\rangle \\ |D^*(1^+)\rangle \end{pmatrix}. \quad (\text{B.2.6})$$

We want S to be a rotation matrix

$$S = \begin{pmatrix} \cos(\theta) & -\sin(\theta) \\ \sin(\theta) & \cos(\theta) \end{pmatrix}.$$

Then, we have

$$\begin{pmatrix} |D_L\rangle \\ |D_H\rangle \end{pmatrix} = S^T \begin{pmatrix} |D(1^+)\rangle \\ |D^*(1^+)\rangle \end{pmatrix} = \begin{pmatrix} \cos(\theta) & \sin(\theta) \\ -\sin(\theta) & \cos(\theta) \end{pmatrix} \begin{pmatrix} |D(1^+)\rangle \\ |D^*(1^+)\rangle \end{pmatrix} \quad (\text{B.2.7})$$

and we find that the physical states $|D_H\rangle$ and $|D_L\rangle$ are given by

$$|D_L(1^+)\rangle = \cos(\theta)|D(1^+)\rangle + \sin(\theta)|D^*(1^+)\rangle, \quad (\text{B.2.8})$$

$$|D_H(1^+)\rangle = -\sin(\theta)|D(1^+)\rangle + \cos(\theta)|D^*(1^+)\rangle. \quad (\text{B.2.9})$$

We then get

$$\begin{aligned} \mathbf{H}_{\text{diag}} &= S^T \mathbf{H} S = \begin{pmatrix} \cos(\theta) & \sin(\theta) \\ -\sin(\theta) & \cos(\theta) \end{pmatrix} \begin{pmatrix} M & a \\ a & M + \Delta \end{pmatrix} \begin{pmatrix} \cos(\theta) & -\sin(\theta) \\ \sin(\theta) & \cos(\theta) \end{pmatrix} \\ &= \begin{pmatrix} M \cos^2 \theta + M^* \sin^2 \theta + 2a \sin \theta \cos \theta & (M^* - M) \sin \theta \cos \theta + a(\cos^2 \theta - \sin^2 \theta) \\ (M^* - M) \sin \theta \cos \theta + a(\cos^2 \theta - \sin^2 \theta) & M \sin^2 \theta + M^* \cos^2 \theta - 2a \sin \theta \cos \theta \end{pmatrix}, \end{aligned} \quad (\text{B.2.10})$$

where the off-diagonal entries must be zero since it is a diagonal matrix. Hence, we find with $M^* - M = \Delta$

$$\Delta \sin \theta \cos \theta + a(\cos^2 \theta - \sin^2 \theta) \stackrel{!}{=} 0, \quad (\text{B.2.11})$$

$$\Delta \sin \theta \cos \theta \stackrel{!}{=} a(\sin^2 \theta - \cos^2 \theta), \quad (\text{B.2.12})$$

and with the addition theorem

$$\sin(x \pm y) = \sin x \cos y \pm \cos x \sin y, \quad (\text{B.2.13})$$

$$\cos(x \pm y) = \cos x \cos y \mp \sin x \sin y \quad (\text{B.2.14})$$

we find that

$$\sin(2\theta) = 2 \sin \theta \cos \theta, \quad (\text{B.2.15})$$

$$\cos(2\theta) = \cos^2 \theta - \sin^2 \theta, \quad (\text{B.2.16})$$

and therefore

$$\frac{1}{2} \Delta \sin 2\theta \stackrel{!}{=} -a \cos 2\theta, \quad (\text{B.2.17})$$

$$\tan 2\theta \stackrel{!}{=} -\frac{2a}{\Delta} = -\frac{2a}{M - M^*}. \quad (\text{B.2.18})$$

B.3. Details On The Fit

A likelihood is the probability density for the data given a hypothesis or a model. It is not a probability density function (PDF), which means that the sum of all likelihoods generally is not unity. Here, we have a likelihood expressed through the observables M_0, M_L, M_H, M_2 , which are modelled via the parameters $\vec{\Theta} = M_{1/2}, M_{3/2}, g, g'$.

The likelihoods for the individual masses will be multiplied. We therefore take the log-likelihood, so that the product emerges as a sum

$$\begin{aligned} \ln \mathcal{L} = & \ln P(M_0^E, \sigma_{M_0}^E; M_0(M_{1/2}, M_{3/2}, g, g')) \\ & + \ln P(M_L^E, \sigma_{M_L}^E; M_L(M_{1/2}, M_{3/2}, g, g')) \\ & + \ln P(M_H^E, \sigma_{M_H}^E; M_H(M_{1/2}, M_{3/2}, g, g')) \\ & + \ln P(M_2^E, \sigma_{M_2}^E; M_2(M_{1/2}, M_{3/2}, g, g')), \end{aligned} \quad (\text{B.3.1})$$

where $P(M_i^E, \sigma_{M_i}^E; M_i)$ is Gaussian distributed. We can then maximize this sum and obtain values at the best-fit point

$$\vec{\Theta}^* = \arg \max \mathcal{L}. \quad (\text{B.3.2})$$

To find the goodness of the fit we can now determine the pull value which gives a measure for how good the measurement fits the model

$$\text{pull}_i = \frac{M_i^E - M_i(\vec{\Theta}^*)}{\sigma_{M_i}^E}. \quad (\text{B.3.3})$$

Due to the Gaussian distribution of the measurement the pull value follows a Gaussian as well. We now define the χ^2 of the various masses at the best-fit point

$$\chi_i^2 = \frac{(M_i^E - M_i(\vec{\Theta}^*))^2}{(\sigma_{M_i}^E)^2},$$

and compute the total deviation of the data from the model prediction

$$\overline{\chi^2} \equiv \sum_{i=0,L,H,2} \chi_i^2. \quad (\text{B.3.4})$$

Here, $\overline{\chi^2}$ is the minimal value given at the best-fit point.

From the range $\Delta\chi^2$ around the minimal value of χ^2 we can infer the confidence level interval. For one degree of freedom in the fit we find that the following ranges correspond to certain significances

$$\begin{aligned} \Delta\chi^2 = 1 & \rightarrow 1\sigma \sim 68.3\%, \\ \Delta\chi^2 = 4 & \rightarrow 2\sigma \sim 95.4\%, \\ \Delta\chi^2 = 9 & \rightarrow 3\sigma \sim 99.7\%. \end{aligned} \quad (\text{B.3.5})$$

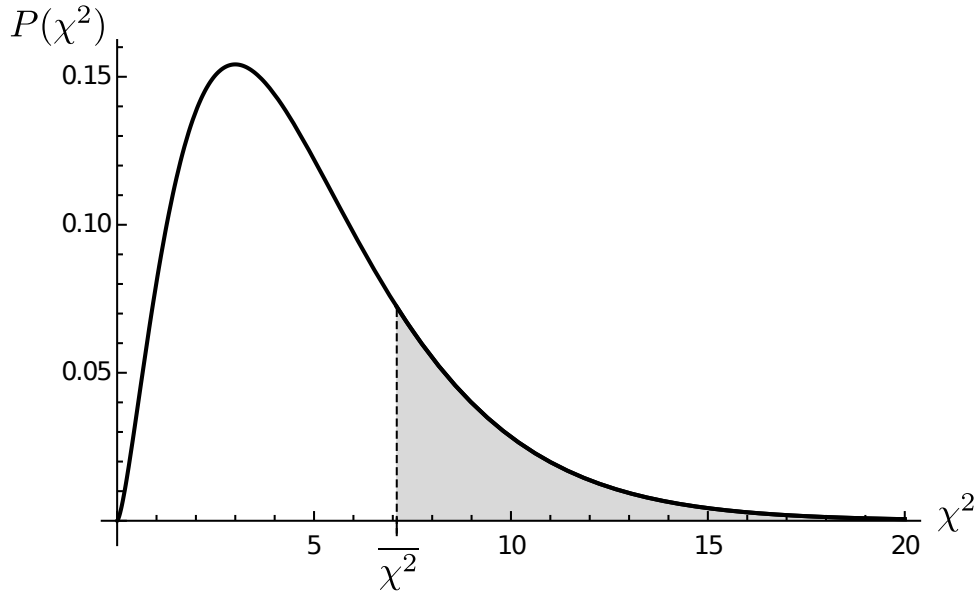


Figure B.3.1.: χ^2 distribution for 5 degrees of freedom. The p -value is the integral over the gray shaded area.

For the value of $\overline{\chi^2}$ we can obtain the p -value. It gives the probability of receiving such a result or an extremem one (higher value for $\overline{\chi^2}$) assuming that the initial model is true. As a threshold we demand the p -value to be $\geq 3\%$ to consider the fit as good. It can be computed using the cumulative distribution function (CDF)

$$p\text{-value} = 1 - \text{CDF}_{\chi^2}(\#\text{d.o.f.}, \overline{\chi^2}). \quad (\text{B.3.6})$$

Here, the number of degrees of freedom is given by the difference of the number of measurements and fit parameters

$$\#\text{d.o.f.} = \#\text{measurements} - \#\text{parameters}$$

The p -value is the integral over the gray shaded area shown in Figure B.3.1.

For the likelihood we have a Gaussian distribution

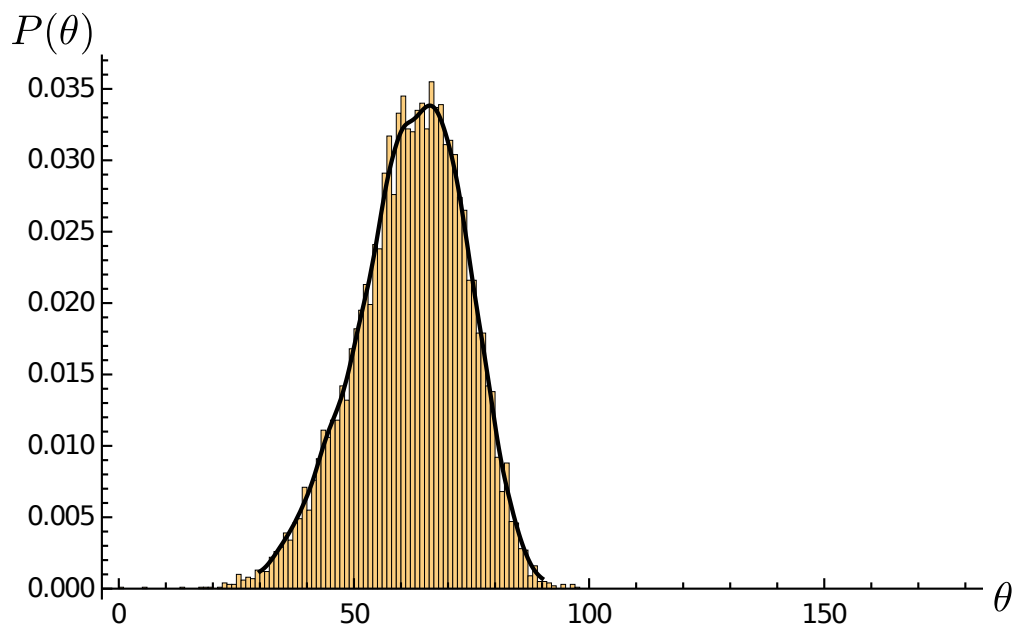
$$\mathcal{L} \sim e^{-\frac{1}{2} \sum_i \left(\frac{M_i^E - M_i(\vec{\Theta}^*)}{\sigma_{M_i}^E} \right)^2} = e^{-\frac{1}{2} \chi^2}, \quad (\text{B.3.7})$$

which means that we get

$$-2 \ln \mathcal{L} = \chi^2 + \text{const.} \quad (\text{B.3.8})$$

We can now compute the uncertainties within the 1σ range, e.g. for $M_{1/2}$. Therefore we take the difference between $\chi^2(M_{1/2})$ at the best-fit point which still depends on the variable whose uncertainty we are interested in and $\overline{\chi^2}$

$$-2[\ln \mathcal{L}(M_{1/2}) - \ln \mathcal{L}^*] = \chi^2(M_{1/2}) - \overline{\chi^2} \equiv \Delta\chi^2(M_{1/2}). \quad (\text{B.3.9})$$

Figure B.3.2.: Histogram for mixing angle θ .

Here, $\ln \mathcal{L}^*$ is the sum of the log-likelihoods at the best-fit point. The constant in Equation (B.3.8) cancels. We can now set this to the inverse CDF of the χ^2 distribution depending on the number of parameters in the fit and on the value for the 1σ level 68.3%

$$\Delta\chi^2(M_{1/2}) \stackrel{!}{=} \text{CDF}_{\chi^2}^{-1}(\#\text{parameters}, 0.683). \quad (\text{B.3.10})$$

We can then solve for $M_{1/2}$ and get an upper and a lower bound. From this we can infer the error

$$1\sigma = \frac{M_{1/2}^{\text{upper}} - M_{1/2}^{\text{lower}}}{2} \quad (\text{B.3.11})$$

With the obtained values for the fit parameters and their errors we can compute the mixing angle. It is distributed asymmetric since the tangent is not a linear function. Therefore, we determine the error using a histogram for the mixing angle (see Figure B.3.2).

C. Details on B - \bar{B} Mixing

C.1. Loop Integrals

Following [58, 177], we can easily find for the massless propagator diagram in QCD

$$\int \frac{d^D k}{[-(k+p)^2]^{n_1} [-k^2]^{n_2}} = i\pi^{\frac{D}{2}} (-p^2)^{\frac{D}{2}-n_1-n_2} G(n_1, n_2),$$

where

$$G(n_1, n_2) = \frac{\Gamma\left(n_1 + n_2 - \frac{D}{2}\right) \Gamma\left(\frac{D}{2} - n_1\right) \Gamma\left(\frac{D}{2} - n_2\right)}{\Gamma(n_1)\Gamma(n_2)\Gamma(D - n_1 - n_2)} \quad (\text{C.1.1})$$

and in the massive case

$$\int \frac{d^D k}{[m^2 - (k+p)^2]^{n_1} [-k^2]^{n_2}} = i\pi^{\frac{D}{2}} m^{D-2(n_1+n_2)} M(n_1, n_2),$$

where

$$M(n_1, n_2) = \frac{\Gamma\left(n_1 + n_2 - \frac{D}{2}\right) \Gamma(D - n_1 - 2n_2)}{\Gamma(n_1)\Gamma(D - n_1 - n_2)}. \quad (\text{C.1.2})$$

For the HQET propagator diagram we find

$$\int \frac{d^D k}{[-v(k+p) - i\epsilon]^{n_1} [-k^2 - i\epsilon]^{n_2}} = i\pi^{\frac{D}{2}} 2^{D-2n_2} (-v \cdot p)^{D-n_1-2n_2} I(n_1, n_2),$$

where

$$I(n_1, n_2) = \frac{\Gamma(n_1 + 2n_2 - D)\Gamma\left(\frac{D}{2} - n_2\right)}{\Gamma(n_1)\Gamma(n_2)}.$$

C.2. Master Integrals

C.2.1. Perturbative Contribution

For the non-factorizable perturbative three-loop contributions in Figure 5.6 we find the topologies shown in Figure C.2.1. Using an integration by parts method [178, 179] (a review can be found e.g. in [180]) the topologies can be reduced to simpler diagrams. There are several packages available for Mathematica that can automatically do this for a given basis. The program LiteRed [127, 128] is one of them and was used here. The required master integrals in Equation (5.37) were computed in [116] and correspond to the diagrams in Table C.2.1. Here, I_n corresponds to the sunset diagram in Equation (5.35).

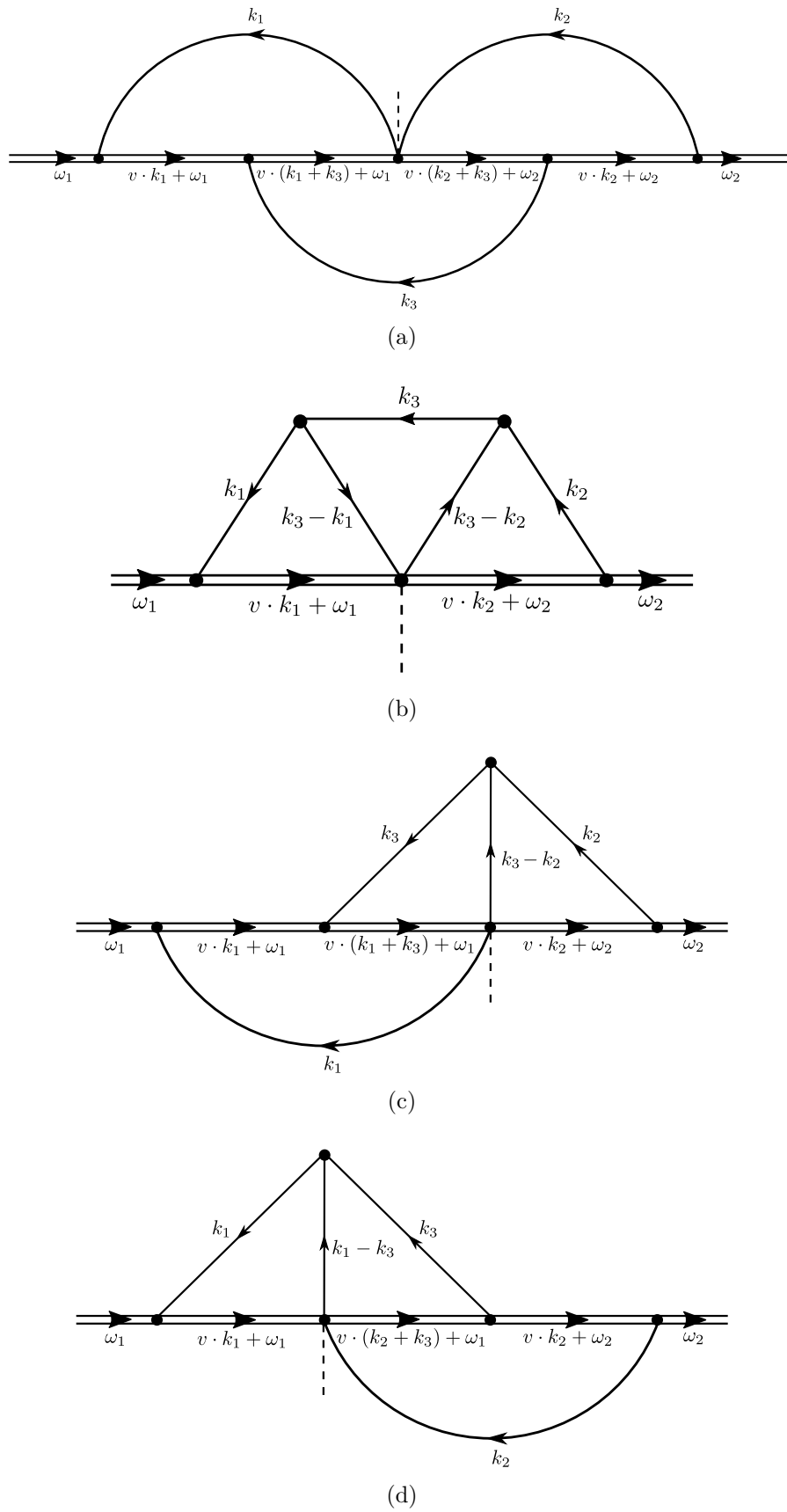


Figure C.2.1.: Topologies of the three-loop diagrams.

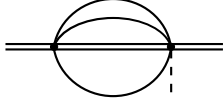
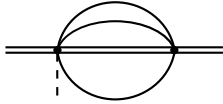
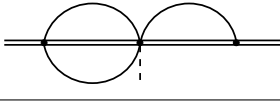
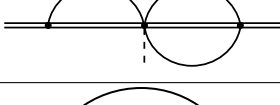
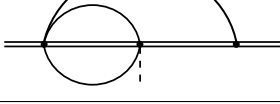

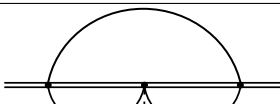
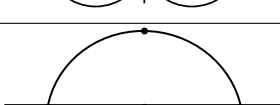
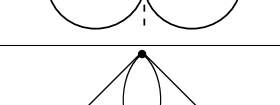
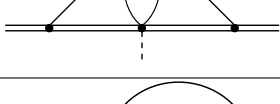
Diagram	Corresponding Master Integrals [116]
	$I_3(-2\omega_1)^{3D-7}$
	$I_3(-2\omega_2)^{3D-7}$
	$I_1 I_2(-2\omega_1)^{2D-5}(-2\omega_2)^{D-3}$
	$I_1 I_2(-2\omega_2)^{2D-5}(-2\omega_1)^{D-3}$
	$M_1(\omega_1, \omega_2)$
	$M_1(\omega_2, \omega_1)$
	$M_2(\omega_1, \omega_2) = M_2(\omega_2, \omega_1)$
	$M'_2(\omega_1, \omega_2) = M'_2(\omega_2, \omega_1)$
	$M_3(\omega_1, \omega_2) = M_3(\omega_2, \omega_1)$
	$M_4(\omega_1, \omega_2) = M_4(\omega_2, \omega_1)$

Table C.2.1.: Corresponding master diagrams for the three-loop topologies.

C.2.2. Quark Condensate Contribution

For the quark condensate contribution there is only one relevant topology shown in Figure C.2.2. This corresponds to the master integrals given in Table C.2.2.

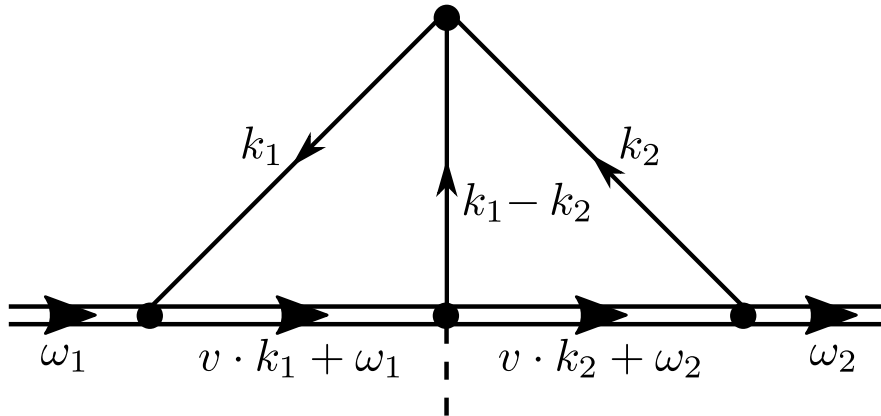


Figure C.2.2.: Topology of the two-loop diagram.

Diagram	Corresponding Master Integrals [97]
	$M(\omega_1, \omega_2)$
	$M(\omega_2, \omega_1)$

Table C.2.2.: Corresponding master diagrams for the two-loop topology.

D. Details on CP Violation in Three-Body-Decays

D.1. Dalitz Distribution

This section will give a brief introduction to Dalitz plots based on [16,30]. The partial decay rate for a three-body decay can be written in terms of the invariants $m_{ij}^2 = p_{ij}^2$, where $p_{ij} = p_i + p_j$ and the variables are defined in Figure D.1.1. Momentum conservation requires $m_{12}^2 + m_{23}^2 + m_{13}^2 = M^2 + m_1^2 + m_2^2 + m_3^2$, such that the decay rate only depends on two variables [16]

$$d\Gamma = \frac{1}{(2\pi)^3} \frac{1}{32M^2} |\mathcal{A}(m_{12}^2, m_{23}^2)|^2 dm_{12}^2 dm_{23}^2. \quad (\text{D.1.1})$$

Usually, this form is used to make a scatter plot in m_{12}^2 and m_{23}^2 , which we call a Dalitz plot [181]. Usually it adopts a triangular shape as seen in Figure D.1.2, where we display the shape of a Dalitz plot for the decay $B^0 \rightarrow \pi^+ \pi^0 \pi^-$. The gray area shows the phase space to which the events are restricted. The boundaries for this shape are given by the range of the variable m_{23}^2 depending on m_{12}^2 . We have

$$\begin{aligned} (m_{23}^2)_{\min} &= (E_2^* + E_3^*)^2 - (\vec{p}_2^* - \vec{p}_3^*)^2 \\ &= (E_2^* + E_3^*)^2 - \left(\sqrt{E_2^{*2} - m_2^{*2}} + \sqrt{E_3^{*2} - m_3^{*2}} \right)^2, \end{aligned} \quad (\text{D.1.2})$$

$$(m_{23}^2)_{\max} = (E_2^* + E_3^*)^2 - \left(\sqrt{E_2^{*2} - m_2^{*2}} - \sqrt{E_3^{*2} - m_3^{*2}} \right)^2, \quad (\text{D.1.3})$$

where

$$E_2^* = \frac{m_{12}^2 - m_1^2 + m_2^2}{2m_{12}}, \quad E_3^* = \frac{M^2 - m_{12}^2 - m_3^2}{2m_{12}} \quad (\text{D.1.4})$$

are the energies of particle 2 and 3 in the rest frame of particles 1 and 2.

The Dalitz plot directly provides insight into the dynamics of the transition amplitude \mathcal{A} . A squared amplitude which is constant would result in a uniform population of the Dalitz plot as seen in Figure D.1.3(a). This, on the other hand, implicates that the amplitude is not constant if we observe some structures in the Dalitz plot. Three-body decays predominantly proceed through resonant two-body decays, where one of the final states decays once again. These resonances manifest themselves as bands in the Dalitz plot as shown in Figure D.1.3. From the shape of the band we

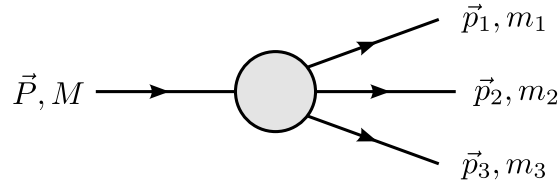


Figure D.1.1.: Definition of the variables for the decay of one particle into three particles.

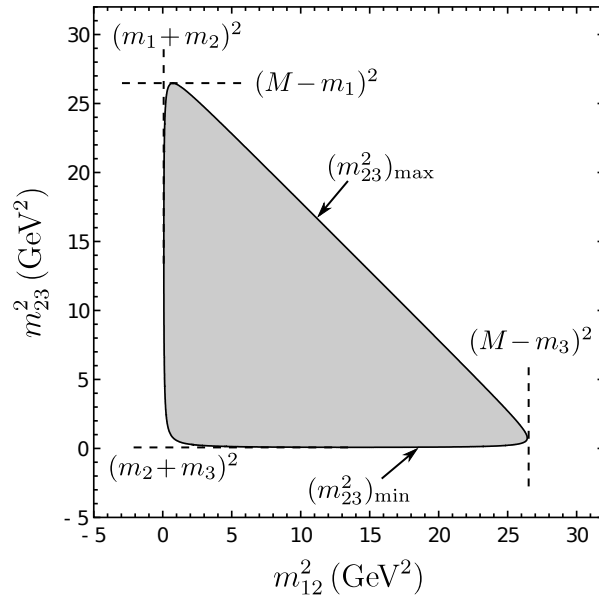


Figure D.1.2.: Shape of the Dalitz Plot for $B^0 \rightarrow \pi^+ \pi^0 \pi^-$.

can infer the type of the resonance, namely if it is a scalar (b), vector (c) or tensor (d) resonance. This is due to the fact that the amplitude is proportional to the corresponding Legendre polynomial. The number of gaps is then directly linked to the number of respective zeros in the Legendre polynomials

$$\begin{aligned}
 P_0(x) &= 1, \\
 P_1(x) &= x, \\
 P_2(x) &= \frac{1}{2}(3x^2 - 1).
 \end{aligned}
 \tag{D.1.5}$$

Another advantage of Dalitz plots is that we can obtain some information on the phase differences when studying overlapping resonances, which is also schematically shown in Figure D.1.3(e) and (f). This allows for studies of CP violation as e.g. in [137].

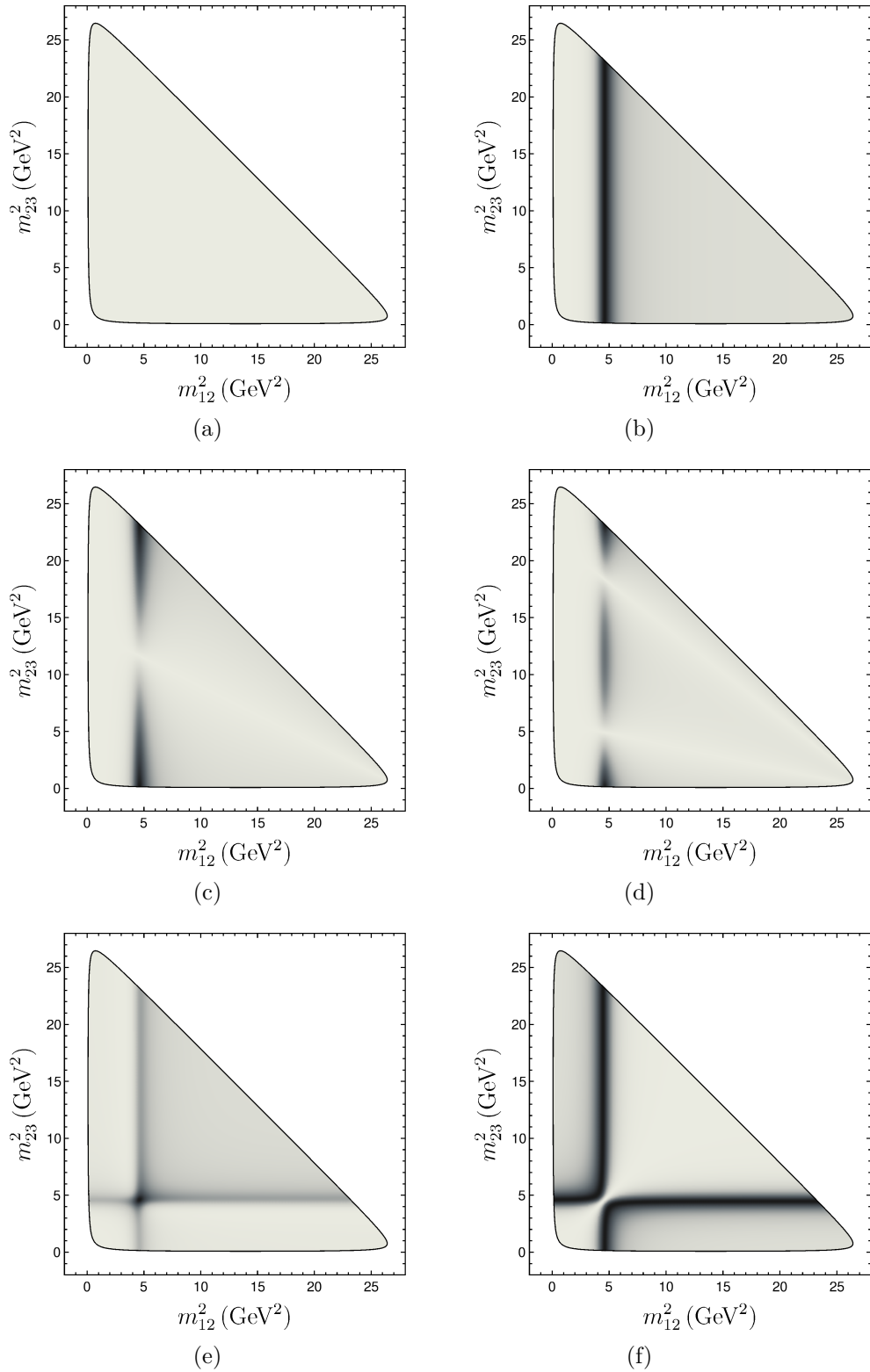


Figure D.1.3.: Examples for Dalitz plots for a (a) phase-space decay, (b) scalar resonance, (c) vector resonance and (d) tensor resonance as well as (e) constructive interference and (f) destructive interference.

D.2. Calculation of the QCD-Factorized Effective Hamiltonian

From [152] we have the effective Hamiltonian

$$\mathcal{H}_{\text{eff}} = \frac{G_F}{\sqrt{2}} \sum_{p=u,c} \lambda_p \left(C_1 Q_1^p + C_2 Q_2^p + \sum_{i=3,\dots,6} C_i Q_i \right) \quad (\text{D.2.1})$$

with

$$\begin{aligned} Q_1^p &= (\bar{p}_i b_j)_{V-A} (\bar{d}_j p_i)_{V-A}, \\ Q_2^p &= (\bar{p} b)_{V-A} (\bar{d} p)_{V-A}, \\ Q_3 &= (\bar{d} b)_{V-A} \sum_{q=u,c} (\bar{q} q)_{V-A}, \\ Q_4 &= (\bar{d}_i b_j)_{V-A} \sum_{q=u,c} (\bar{q}_j q_i)_{V-A}, \\ Q_5 &= (\bar{d} b)_{V-A} \sum_{q=u,c} (\bar{q} q)_{V+A}, \\ Q_6 &= (\bar{d}_i b_j)_{V-A} \sum_{q=u,c} (\bar{q}_j q_i)_{V+A}, \end{aligned} \quad (\text{D.2.2})$$

where $(\bar{q} q)_{V\pm A} = \bar{q} \gamma_\mu (1 \pm \gamma_5) q$.

We can now find the factorized Hamiltonian. For naive factorization we have

$$\langle \pi \pi | j_1 \otimes j_2 | B \rangle = \langle \pi | j_1 | B \rangle \langle \pi | j_2 | 0 \rangle + \langle \pi | j_1 | 0 \rangle \langle \pi | j_2 | B \rangle. \quad (\text{D.2.3})$$

So we need to find the factorized operators $Q = j_1 \otimes j_2$. We start with Q_1^u and Q_2^p . To get all different possibilities we sum the operator and the Fierz transformed operator (see Appendix A)

$$(\bar{p}_i b_j)_{V-A} (\bar{d}_j p_i)_{V-A} = (\bar{p}_i p_i)_{V-A} (\bar{d}_j b_j)_{V-A}.$$

In addition, note that

$$\langle \pi | \bar{u} u | B \rangle = \langle \pi | \bar{d} d | B \rangle = \langle \pi | \bar{d} u | B \rangle = 0. \quad (\text{D.2.4})$$

We then find

$$\begin{aligned}
& C_1 \langle \pi \pi | (\bar{u}_i b_j)_{V-A} (\bar{d}_j u_i)_{V-A} | B \rangle + C_1 \langle \pi \pi | (\bar{u}_i u_i)_{V-A} (\bar{d}_j b_j)_{V-A} | B \rangle \\
& + C_2 \langle \pi \pi | (\bar{u}_i b_i)_{V-A} (\bar{d}_j u_j)_{V-A} | B \rangle + C_2 \langle \pi \pi | (\bar{u}_i u_j)_{V-A} (\bar{d}_j b_i)_{V-A} | B \rangle \\
& = C_1 \langle \pi | \underbrace{(\bar{u}_i b_j)_{V-A}}_{=\frac{\delta_{ij}}{N_C} (\bar{u}b)_{V-A}} | B \rangle \langle \pi | (\bar{d}_j u_i)_{V-A} | 0 \rangle + C_1 \langle \pi | (\bar{d}_j b_j)_{V-A} | B \rangle \langle \pi | (\bar{u}_i u_i)_{V-A} | 0 \rangle \\
& + C_2 \langle \pi | (\bar{u}_i b_i)_{V-A} | B \rangle \langle \pi | (\bar{d}_j u_j)_{V-A} | 0 \rangle + C_2 \langle \pi | (\bar{d}_j b_i)_{V-A} | B \rangle \langle \pi | \underbrace{(\bar{u}_i u_j)_{V-A}}_{=\frac{\delta_{ij}}{N_C} (\bar{u}u)_{V-A}} | 0 \rangle \\
& = \frac{C_1}{N_C} \langle \pi | (\bar{u}b)_{V-A} | B \rangle \langle \pi | (\bar{d}u)_{V-A} | 0 \rangle + C_1 \langle \pi | (\bar{d}b)_{V-A} | B \rangle \langle \pi | (\bar{u}u)_{V-A} | 0 \rangle \\
& + C_2 \langle \pi | (\bar{u}b)_{V-A} | B \rangle \langle \pi | (\bar{d}u)_{V-A} | 0 \rangle + \frac{C_2}{N_C} \langle \pi | (\bar{d}b)_{V-A} | B \rangle \langle \pi | (\bar{u}u)_{V-A} | 0 \rangle \\
& = a_1^u \langle \pi | (\bar{u}b)_{V-A} | B \rangle \langle \pi | (\bar{d}u)_{V-A} | 0 \rangle + a_2^u \langle \pi | (\bar{d}b)_{V-A} | B \rangle \langle \pi | (\bar{u}u)_{V-A} | 0 \rangle, \quad (D.2.5)
\end{aligned}$$

where $a_1^u = C_2 + \frac{C_1}{N_C}$ and $a_2^u = C_1 + \frac{C_2}{N_C}$.

Analogously, we find for C_3 and C_4 with $q = u, c$

$$\begin{aligned}
& C_3 \langle \pi \pi | (\bar{d}_i b_i)_{V-A} (\bar{q}_j q_j)_{V-A} | B \rangle + C_3 \langle \pi \pi | (\bar{d}_i q_j)_{V-A} (\bar{q}_j b_i)_{V-A} | B \rangle \\
& + C_4 \langle \pi \pi | (\bar{d}_i b_j)_{V-A} (\bar{q}_j q_i)_{V-A} | B \rangle + C_4 \langle \pi \pi | (\bar{d}_i q_i)_{V-A} (\bar{q}_j b_j)_{V-A} | B \rangle \\
& = C_3 \langle \pi | (\bar{d}_i b_i)_{V-A} | B \rangle \langle \pi | (\bar{q}_j q_j)_{V-A} | 0 \rangle + C_3 \langle \pi | (\bar{q}_j b_i)_{V-A} | B \rangle \langle \pi | \underbrace{(\bar{d}_i q_j)_{V-A}}_{=\frac{\delta_{ij}}{N_C} (\bar{d}q)_{V-A}} | 0 \rangle \\
& + C_4 \langle \pi | \underbrace{(\bar{d}_i b_j)_{V-A}}_{=\frac{\delta_{ij}}{N_C} (\bar{d}b)_{V-A}} | B \rangle \langle \pi | (\bar{q}_j q_i)_{V-A} | 0 \rangle + C_4 \langle \pi | (\bar{q}_j b_j)_{V-A} | B \rangle \langle \pi | (\bar{d}_i q_i)_{V-A} | 0 \rangle \\
& = C_3 \langle \pi | (\bar{d}b)_{V-A} | B \rangle \langle \pi | (\bar{q}q)_{V-A} | 0 \rangle + \frac{C_3}{N_C} \langle \pi | (\bar{q}b)_{V-A} | B \rangle \langle \pi | (\bar{d}q)_{V-A} | 0 \rangle \\
& = a_3 \langle \pi | (\bar{d}b)_{V-A} | B \rangle \langle \pi | (\bar{q}q)_{V-A} | 0 \rangle + a_4 \langle \pi | (\bar{q}b)_{V-A} | B \rangle \langle \pi | (\bar{d}q)_{V-A} | 0 \rangle, \quad (D.2.6)
\end{aligned}$$

with $a_3 = C_3 + \frac{C_4}{N_C}$ and $a_4 = C_4 + \frac{C_3}{N_C}$.

For C_5 and C_6 we need to apply the Fierz transformation (see Appendix A)

$$(\bar{d}b)_{V-A} (\bar{q}q)_{V+A} = -2(\bar{d}q)_{S+P} (\bar{q}b)_{S-P},$$

where $(\bar{q}q)_{V\pm A} = \bar{q}(1 \pm \gamma_5)q$ and obtain

$$\begin{aligned}
& C_5 \langle \pi\pi | (\bar{d}_i b_i)_{V-A} (\bar{q}_j q_j)_{V+A} | B \rangle - 2C_5 \langle \pi\pi | (\bar{d}_i q_j)_{S+P} (\bar{q}_j b_i)_{S-P} | B \rangle \\
& + C_6 \langle \pi\pi | (\bar{d}_i b_j)_{V-A} (\bar{q}_j q_i)_{V-A} | B \rangle - 2C_6 \langle \pi\pi | (\bar{d}_i q_i)_{S+P} (\bar{q}_j b_j)_{S-P} | B \rangle \\
& = C_5 \langle \pi | (\bar{d}_i b_i)_{V-A} | B \rangle \langle \pi | (\bar{q}_j q_j)_{V-A} | 0 \rangle + C_5 \underbrace{\langle \pi | (\bar{q}_j q_j)_{V-A} | B \rangle}_{=0} \langle \pi | (\bar{d}_i b_i)_{V-A} | 0 \rangle \\
& \quad - 2C_5 \langle \pi | (\bar{q}_j b_i)_{S-P} | B \rangle \langle \pi | \underbrace{(\bar{d}_i q_j)_{S-P} | 0 \rangle}_{= \frac{\delta_{ij}}{N_C} (\bar{d}q)_{S+P}} + C_6 \langle \pi | \underbrace{(\bar{d}_i b_j)_{V-A} | B \rangle}_{= \frac{\delta_{ij}}{N_C} (\bar{d}b)_{V-A}} \langle \pi | (\bar{q}_j q_i)_{V-A} | 0 \rangle \\
& \quad - 2C_6 \langle \pi | (\bar{q}_j b_j)_{S-P} | B \rangle \langle \pi | (\bar{d}_i q_i)_{S+P} | 0 \rangle \\
& = C_5 \langle \pi | (\bar{d}_i b_i)_{V-A} | B \rangle \langle \pi | (\bar{q}_j q_j)_{V-A} | 0 \rangle - 2C_5 \langle \pi | (\bar{q}_j b_i)_{S-P} | B \rangle \langle \pi | \underbrace{(\bar{d}_i q_j)_{S+P} | 0 \rangle}_{= \frac{\delta_{ij}}{N_C} (\bar{d}q)_{S+P}} \\
& \quad + C_6 \langle \pi | \underbrace{(\bar{d}_i b_j)_{V-A} | B \rangle}_{= \frac{\delta_{ij}}{N_C} (\bar{d}b)_{V-A}} \langle \pi | (\bar{q}_j q_i)_{V-A} | 0 \rangle - 2C_6 \langle \pi | (\bar{q}_j b_j)_{S-P} | B \rangle \langle \pi | (\bar{d}_i q_i)_{S+P} | 0 \rangle \\
& = C_5 \langle \pi | (\bar{d}b)_{V-A} | B \rangle \langle \pi | (\bar{q}q)_{V-A} | 0 \rangle - 2C_5 \langle \pi | (\bar{q}b)_{S-P} | B \rangle \langle \pi | (\bar{d}q)_{S+P} | 0 \rangle \\
& \quad + C_6 \langle \pi | (\bar{d}b)_{V-A} | B \rangle \langle \pi | (\bar{q}q)_{V-A} | 0 \rangle - 2C_6 \langle \pi | (\bar{q}b)_{S-P} | B \rangle \langle \pi | (\bar{d}q)_{S+P} | 0 \rangle \\
& = a_5 \langle \pi | (\bar{d}b)_{V-A} | B \rangle \langle \pi | (\bar{q}q)_{V-A} | 0 \rangle - 2a_6 \langle \pi | (\bar{q}b)_{S-P} | B \rangle \langle \pi | (\bar{d}q)_{S+P} | 0 \rangle, \quad (\text{D.2.7})
\end{aligned}$$

where $a_5 = C_5 + \frac{C_6}{N_C}$ and $a_6 = C_6 + \frac{C_5}{N_C}$.

Finally, this gives us the QCD factorized Hamiltonian for $B \rightarrow \pi\pi$ from Equation (6.14)

$$\mathcal{H}_{\text{eff}} = \frac{G_F}{\sqrt{2}} (\lambda_u T_u + \lambda_c T_c), \quad (\text{D.2.8})$$

with

$$\begin{aligned}
T_u &= a_1^u \left[(\bar{u}b)_{V-A} \otimes (\bar{d}u)_{V-A} \right] + a_2^u \left[(\bar{d}b)_{V-A} \otimes (\bar{u}u)_{V-A} \right] \\
& \quad + a_3 \sum_q \left[(\bar{d}b)_{V-A} \otimes (\bar{q}q)_{V-A} \right] + a_4^u \sum_q \left[(\bar{q}b)_{V-A} \otimes (\bar{d}q)_{V-A} \right] \\
& \quad + a_5 \sum_q \left[(\bar{d}b)_{V-A} \otimes (\bar{q}q)_{V+A} \right] - 2a_6^u \sum_q \left[(\bar{q}b)_{S-P} \otimes (\bar{d}q)_{S+P} \right]
\end{aligned}$$

and

$$\begin{aligned}
T_c &= a_3 \sum_q \left[(\bar{d}b)_{V-A} \otimes (\bar{q}q)_{V-A} \right] + a_4^c \sum_q \left[(\bar{q}b)_{V-A} \otimes (\bar{d}q)_{V-A} \right] \\
& \quad + a_5 \sum_q \left[(\bar{d}b)_{V-A} \otimes (\bar{q}q)_{V+A} \right] - 2a_6^c \sum_q \left[(\bar{q}b)_{S-P} \otimes (\bar{d}q)_{S+P} \right].
\end{aligned}$$

D.3. New Non-Perturbative Input

Here, we discuss in more detail the new non-perturbative input that we use in Chapter 6 for our QCDF approach for three-body decays.

D.3.1. Generalized Form Factor

For the generalized form factor in Equation (6.24) we can make a decomposition into an isospin singlet and triplet

$$F_{t,ij}^{ab} = \langle \pi^a \pi^b | \bar{q}_j b | B_i \rangle = F_t^{I=0} \delta_{ij} \delta^{ab} + F_t^{I=1} i \varepsilon^{abc} \sigma_{ij}^c,$$

where $a, b = 1, \dots, 3$ are isospin indices and $i, j = 1, 2$ are $SU(2)$ flavor indices, where $q_1 = u$ and $q_2 = d$. Here, ε^{abc} is the antisymmetric Levi-Civita tensor and σ^c are the Pauli matrices

$$\sigma^1 = \begin{pmatrix} 0 & 1 \\ 1 & 0 \end{pmatrix}, \quad \sigma^2 = \begin{pmatrix} 0 & -i \\ i & 0 \end{pmatrix}, \quad \sigma^3 = \begin{pmatrix} 1 & 0 \\ 0 & -1 \end{pmatrix}. \quad (\text{D.3.1})$$

Focussing on $B^- \rightarrow \pi^- \pi^+ \pi^-$ we have $i = j = 1$ and using that the physical pions are superpositions of the flavor eigenstates

$$\Rightarrow \pi^+ = \frac{1}{\sqrt{2}} (\pi^1 - i\pi^2), \quad \pi^- = \frac{1}{\sqrt{2}} (\pi^1 + i\pi^2), \quad \pi^0 = \pi^3 \quad (\text{D.3.2})$$

we find that

$$\begin{aligned} F_t &= \langle \pi^- \pi^+ | \bar{u} b | B^- \rangle = \frac{1}{2} \langle (\pi^1 + i\pi^2)(\pi^1 - i\pi^2) | \bar{u} b | B^- \rangle \\ &= \frac{1}{2} \left[\langle \pi^1 \pi^1 | \bar{u} b | B^- \rangle - i \langle \pi^1 \pi^2 | \bar{u} b | B^- \rangle + i \langle \pi^2 \pi^1 | \bar{u} b | B^- \rangle + \langle \pi^2 \pi^2 | \bar{u} b | B^- \rangle \right] \\ &= \frac{1}{2} \left[(F_t^{I=0} \underbrace{\delta^{11}}_{=1} + F_t^{I=1} i \underbrace{\varepsilon^{12c}}_{=1 \text{ if } c=3} \sigma_{11}^c) + F_t^{I=1} i \underbrace{\varepsilon^{21c}}_{=-1 \text{ if } c=3} \sigma_{11}^c + (F_t^{I=0} \underbrace{\delta^{22}}_{=1}) \right] \\ &= \frac{1}{2} \left[F_t^{I=0} - i F_t^{I=1} i \underbrace{\sigma_{11}^3}_{=1} - i F_t^{I=1} i \underbrace{\sigma_{11}^3}_{=1} + F_t^{I=0} \right] \\ &= \frac{1}{2} [2F_t^{I=0} + 2F_t^{I=1}] \\ &= F_t^{I=0} + F_t^{I=1}. \end{aligned}$$

D.3.2. Two-Pion Generalized Distribution Amplitude (GDA)

The two-pion distribution amplitude can be locally defined as

$$\langle \pi^a(k_1) \pi^b(k_2) | \bar{q}_{i,\beta} q_{j,\alpha} | 0 \rangle = \frac{1}{4} (\not{k})_{\alpha\beta} \int_0^1 du \Phi_{\parallel ij}^{ab}(u, \zeta, k^2), \quad (\text{D.3.3})$$

where $k = k_1 + k_2$ and α, β are Dirac indices. For the 2π LCDA, we can also make a flavor decomposition into an isosinglet and isovector component

$$\Phi_{\parallel ij}^{ab} = \Phi_{\parallel}^{I=0} \delta_{ij} \delta^{ab} + \Phi_{\parallel}^{I=1} i \varepsilon^{abc} \sigma_{ij}^c. \quad (\text{D.3.4})$$

From C-parity it follows that $\Phi_{\parallel}^{I=0}$ is antisymmetric with respect to the interchange of u and $\bar{u} = (1 - u)$. Thus we have

$$\int_0^1 du \Phi_{\parallel}^{I=0}(u, \zeta, k_{12}^2) = 0. \quad (\text{D.3.5})$$

The isovector contribution is normalized as follows [155]

$$\int_0^1 du \Phi_{\parallel}^{I=1}(u, \zeta, k_{12}^2) = (2\zeta - 1)F_{\pi}(k_{12}^2), \quad (\text{D.3.6})$$

where ζ is the light-cone momentum fraction of the two pions in the final state $\zeta = \frac{k_1^+}{k^+} = \frac{k_{13}^2}{m_B^2 - k_{12}^2}$ [155, 156].

We then find that

$$\begin{aligned} \langle \pi^- \pi^+ | \bar{u}u | 0 \rangle &= \frac{1}{2} \langle (\pi^1 + i\pi^2) (\pi^1 - i\pi^2) | \bar{u}u | 0 \rangle \\ &= \frac{1}{2} [\langle \pi^1 \pi^1 | \bar{u}u | 0 \rangle - i \langle \pi^1 \pi^2 | \bar{u}u | 0 \rangle + i \langle \pi^2 \pi^1 | \bar{u}u | 0 \rangle + \langle \pi^2 \pi^2 | \bar{u}u | 0 \rangle] \\ &= \frac{1}{2} \frac{\not{k}}{4} \int_0^1 du [\Phi_{\parallel}^{I=0} + \Phi_{\parallel}^{I=1} + \Phi_{\parallel}^{I=1} + \Phi_{\parallel}^{I=0}] \\ &= \frac{\not{k}}{4} \int_0^1 du [\Phi_{\parallel}^{I=0} + \Phi_{\parallel}^{I=1}] \\ &= \frac{\not{k}}{4} (2\zeta - 1) F_{\pi}(k_{12}^2) \end{aligned} \quad (\text{D.3.7})$$

and analogously

$$\langle \pi^- \pi^+ | \bar{d}d | 0 \rangle = -\frac{\not{k}}{4} (2\zeta - 1) F_{\pi}(k_{12}^2),$$

where we omitted the Dirac indices for simplicity.

At leading order we do not have an isoscalar contribution to the matrix element $\langle \pi\pi | \bar{q}_i q_i | 0 \rangle$ since the pions need to have the same angular momentum to form $I = 0$ and this is forbidden by Bose symmetry.

D.4. Calculation of the Amplitude for $B \rightarrow \pi\pi\pi$

Using the effective Hamiltonian from Equation (6.14) we now discuss in detail how to obtain the amplitude in Equation (6.44).

We define

$$\begin{aligned} \langle \pi^-(k_3) | (\bar{d}u)_{V-A} | 0 \rangle &= i f_{\pi} k_{3\mu}, \\ \langle \pi^-(k_3) | (\bar{u}u)_{V-A} | 0 \rangle &= \pi^-(k_3) | (\bar{d}d)_{V-A} | 0 \rangle = 0, \end{aligned} \quad (\text{D.4.1})$$

where the latter is zero because of charge conservation, and following Appendix D.3.2

$$\begin{aligned}\langle \pi^-(k_1)\pi^+(k_2)|(\bar{u}u)_{V-A}|0\rangle &= -\langle \pi^-(k_1)\pi^+(k_2)|(\bar{d}d)_{V-A}|0\rangle = (k_1 - k_2)_\mu F_\pi^{\text{em}} \\ &= \bar{k}_\mu F_\pi^{\text{em}}, \\ \langle \pi^-(k_1)\pi^+(k_2)|(\bar{d}u)_{V-A}|0\rangle &= 0.\end{aligned}\tag{D.4.2}$$

Further, we obtain for the $B \rightarrow \pi$ and $B \rightarrow \pi\pi$ form factors

$$\begin{aligned}\langle \pi^-(k_3)|\bar{k} \cdot (\bar{d}b)_{V-A}|B^-\rangle &= \langle \pi^-(k_3)|\bar{d}\bar{k}b|B^-\rangle = 2k_3 \cdot \bar{k}f_+(k^2), \\ \langle \pi^-(k_3)|(\bar{u}b)_{V-A}|B^-\rangle &= 0\end{aligned}\tag{D.4.3}$$

as well as

$$\begin{aligned}\langle \pi^-(k_1)\pi^+(k_2)|k_3 \cdot (\bar{u}b)_{V-A}|B^-\rangle &= -im_\pi F_t(k^2, k_3 \cdot \bar{k}), \\ \langle \pi^-(k_1)\pi^+(k_2)|(\bar{d}b)_{V-A}|B^-\rangle &= 0.\end{aligned}\tag{D.4.4}$$

We can then calculate our amplitude

$$\begin{aligned}&a_1 \langle \pi^-(k_1)\pi^+(k_2)\pi^-(k_3)|(\bar{u}b)_{V-A} \otimes (\bar{d}u)_{V-A}|B^-\rangle \\ &= a_1 \langle \pi^-(k_1)\pi^+(k_2)|(\bar{u}b)_{V-A}|B^-\rangle \underbrace{\langle \pi^-(k_3)|(\bar{d}u)_{V-A}|0\rangle}_{=if_\pi k_{3\mu}} \\ &= a_1 if_\pi \langle \pi^-(k_1)\pi^+(k_2)|k_3 \cdot (\bar{u}b)_{V-A}|B^-\rangle \\ &= a_1 f_\pi m_\pi F_t, \\ &a_2 \langle \pi^-(k_1)\pi^+(k_2)\pi^-(k_3)|(\bar{d}b)_{V-A} \otimes (\bar{u}u)_{V-A}|B^-\rangle \\ &= a_2 \langle \pi^-(k_3)|(\bar{d}b)_{V-A}|B^-\rangle \underbrace{\langle \pi^-(k_1)\pi^+(k_2)|(\bar{u}u)_{V-A}|0\rangle}_{=\bar{k}_\mu F_\pi^{\text{em}}} \\ &= a_2 F_\pi^{\text{em}} \langle \pi^-(k_3)|\bar{k} \cdot (\bar{d}b)_{V-A}|B^-\rangle \\ &= a_2 2k_3 \cdot \bar{k}f_+ F_\pi^{\text{em}}, \\ &a_4 \langle \pi^-(k_1)\pi^+(k_2)\pi^-(k_3)|(\bar{u}b)_{V-A} \otimes (\bar{d}u)_{V-A}|B^-\rangle \\ &\quad + a_4 \langle \pi^-(k_1)\pi^+(k_2)\pi^-(k_3)|(\bar{d}b)_{V-A} \otimes (\bar{d}d)_{V-A}|B^-\rangle \\ &= a_4 \langle \pi^-(k_1)\pi^+(k_2)|(\bar{u}b)_{V-A}|B^-\rangle \underbrace{\langle \pi^-(k_3)|(\bar{d}u)_{V-A}|0\rangle}_{=if_\pi k_{3\mu}} \\ &\quad + a_4 \langle \pi^-(k_3)|(\bar{d}b)_{V-A}|B^-\rangle \underbrace{\langle \pi^-(k_1)\pi^+(k_2)|(\bar{d}d)_{V-A}|0\rangle}_{=-\bar{k}F_\pi^{\text{em}}} \\ &= a_4 if_\pi \underbrace{\langle \pi^-(k_1)\pi^+(k_2)|k_3 \cdot (\bar{u}b)_{V-A}|B^-\rangle}_{-im_\pi F_t} \\ &\quad - a_4 F_\pi^{\text{em}} \underbrace{\langle \pi^-(k_3)|\bar{k} \cdot (\bar{d}b)_{V-A}|B^-\rangle}_{=2k_3 \cdot \bar{k}f_+} \\ &= a_4 \left(f_\pi m_\pi F_t - 2k_3 \cdot \bar{k}f_+ F_\pi^{\text{em}} \right).\end{aligned}$$

Due to charge conservation and Equation (D.4.2) the matrix elements of a_3 , a_5 and a_6 vanish and only contribute at higher orders.

Finally end up with

$$\mathcal{A} = \frac{G_F}{\sqrt{2}} \left[(\lambda_u(a_2^u - a_4^u) - \lambda_c a_4^c) m_B^2 (1 - s_{+-}^{\text{low}} - 2s_{+-}^{\text{high}}) f_+(s_{+-}^{\text{low}}) F_\pi^{\text{em}}(s_{+-}^{\text{low}}) \right. \\ \left. + (\lambda_u(a_1^u + a_4^u) + \lambda_c a_4^c) f_\pi m_\pi (F_t^{I=0}(s_{+-}^{\text{low}}, s_{+-}^{\text{high}}) + F_t^{I=1}(s_{+-}^{\text{low}}, s_{+-}^{\text{high}})) \right],$$

where $2k_3 \cdot \bar{k} = m_B^2(1 - s_{+-}^{\text{low}} - 2s_{+-}^{\text{high}})$ (cf. Equation (6.44)).

D.5. Computation of the Helicity Angle θ_π

We want to transform the momenta in the B meson rest frame into the helicity angle θ_π defined in Figure D.5.1.

In the B meson rest frame we have

$$\vec{p}_B = 0 = \vec{k} + \vec{k}_3 \quad \Rightarrow \quad \vec{k} = -\vec{k}_3 \quad \Rightarrow \quad |\vec{k}| = |\vec{k}_3|, \quad (\text{D.5.1})$$

where $k = k_1 + k_2$ and in the dipion rest frame we have

$$\vec{k}^* = 0 = \vec{k}_1^* + \vec{k}_2^* \quad \Rightarrow \quad \vec{k}_1^* = -\vec{k}_2^* \quad \Rightarrow \quad |\vec{k}_1^*| = |\vec{k}_2^*|. \quad (\text{D.5.2})$$

Hence, we find in the B rest frame

$$p_B = \begin{pmatrix} m_B \\ 0 \\ 0 \\ 0 \end{pmatrix}, \quad k = \begin{pmatrix} k_0 \\ 0 \\ 0 \\ |\vec{k}| \end{pmatrix}, \quad k_3 = \begin{pmatrix} k_{3,0} \\ 0 \\ 0 \\ -|\vec{k}_3| \end{pmatrix} = \begin{pmatrix} m_B - k_0 \\ 0 \\ 0 \\ -|\vec{k}| \end{pmatrix} \quad (\text{D.5.3})$$

and in the dipion rest frame

$$k_1^* = \begin{pmatrix} k_{1,0}^* \\ k_{1,1}^* \\ 0 \\ k_{1,3}^* \end{pmatrix} = \begin{pmatrix} \sqrt{m_\pi^2 + |\vec{k}_1^*|^2} \\ -|\vec{k}_1^*| \sin \theta \\ 0 \\ |\vec{k}_1^*| \cos \theta \end{pmatrix}, \quad (\text{D.5.4})$$

$$k_2^* = \begin{pmatrix} k_{2,0}^* \\ k_{2,1}^* \\ 0 \\ k_{2,3}^* \end{pmatrix} = \begin{pmatrix} \sqrt{m_\pi^2 + |\vec{k}_2^*|^2} \\ +|\vec{k}_2^*| \sin \theta \\ 0 \\ -|\vec{k}_2^*| \cos \theta \end{pmatrix} = \begin{pmatrix} \sqrt{m_\pi^2 + |\vec{k}_1^*|^2} \\ +|\vec{k}_1^*| \sin \theta \\ 0 \\ -|\vec{k}_1^*| \cos \theta \end{pmatrix}, \quad (\text{D.5.5})$$

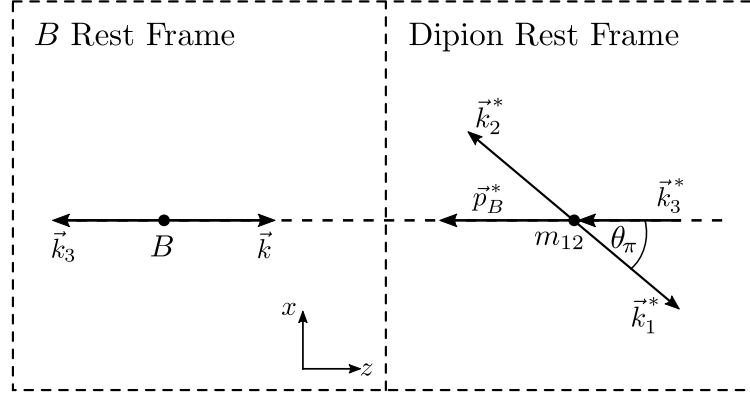


Figure D.5.1.: Definition of the helicity angle as the polar angle θ_π of the π^- in the dipion rest frame.

where we used $p^2 = m^2 = p_0^2 - \vec{p}^2 \Rightarrow p_0 = \sqrt{m^2 + \vec{p}^2}$.

Using $k^2 = k^{*2}$ we can express

$$k^* = \vec{k}_1^* + \vec{k}_2^* = \begin{pmatrix} 2\sqrt{m_\pi^2 + |\vec{k}_1^*|^2} \\ 0 \\ 0 \\ 0 \end{pmatrix} = \begin{pmatrix} \sqrt{k^2} \\ 0 \\ 0 \\ 0 \end{pmatrix}. \quad (\text{D.5.6})$$

With

$$k_0 = \frac{m_B^2 - m_\pi^2 + k^2}{2m_B} \quad (\text{D.5.7})$$

$$(\text{D.5.8})$$

and $k^2 = k_0^2 - |\vec{k}|^2$ we find that

$$|\vec{k}| = \frac{\sqrt{\lambda}}{2m_B}, \quad (\text{D.5.9})$$

where $\lambda(a, b, c) = a^2 + b^2 + c^2 - 2(ab + bc + ac)$ is the Källén function and $\lambda \equiv \lambda(m_B^2, m_\pi^2, k^2)$.

We can then find the Lorentz transformation to boost from the dipion rest frame into the B meson rest frame

$$\Lambda k^* = k \Rightarrow \begin{pmatrix} \gamma & 0 & 0 & -\beta\gamma \\ 0 & 1 & 0 & 0 \\ 0 & 0 & 1 & 0 \\ -\beta\gamma & 0 & 0 & \gamma \end{pmatrix} \begin{pmatrix} \sqrt{k^2} \\ 0 \\ 0 \\ 0 \end{pmatrix} = \begin{pmatrix} k_0 \\ 0 \\ 0 \\ -|\vec{k}| \end{pmatrix}$$

leading to

$$\gamma = \frac{k_0}{\sqrt{k^2}} \quad \text{and} \quad -\beta\gamma = \frac{|\vec{k}|}{\sqrt{k^2}}, \quad (\text{D.5.10})$$

and finally

$$\Lambda = \frac{1}{\sqrt{k^2}} \begin{pmatrix} k_0 & 0 & 0 & |\vec{k}| \\ 0 & \sqrt{k^2} & 0 & 0 \\ 0 & 0 & \sqrt{k^2} & 0 \\ |\vec{k}| & 0 & 0 & k_0 \end{pmatrix}. \quad (\text{D.5.11})$$

In the dipion rest frame we find that

$$\vec{k}^* = \vec{k}_1^* - \vec{k}_2^* = 2 \begin{pmatrix} 0 \\ -|\vec{k}_1^*| \sin \theta \\ 0 \\ |\vec{k}_1^*| \cos \theta \end{pmatrix} = \beta_\pi \sqrt{k^2} \begin{pmatrix} 0 \\ -\sin \theta \\ 0 \\ \cos \theta \end{pmatrix}, \quad (\text{D.5.12})$$

where we used

$$|\vec{k}_1^*| = \frac{1}{2} \sqrt{k^2 - 4m_\pi^2} = \frac{1}{2} \beta_\pi \sqrt{k^2}, \quad (\text{D.5.13})$$

with

$$\beta_\pi^2 = \frac{k^2 - 4m_\pi^2}{k^2}. \quad (\text{D.5.14})$$

Using Equation (D.5.11) we then find

$$\begin{aligned} \bar{k} &= k_1 - k_2 = \Lambda \vec{k}^* \\ &= \beta_\pi \begin{pmatrix} k_0 & 0 & 0 & |\vec{k}| \\ 0 & \sqrt{k^2} & 0 & 0 \\ 0 & 0 & \sqrt{k^2} & 0 \\ |\vec{k}| & 0 & 0 & k_0 \end{pmatrix} \begin{pmatrix} 0 \\ -\sin \theta \\ 0 \\ \cos \theta \end{pmatrix} = \beta_\pi \begin{pmatrix} |\vec{k}| \cos \theta \\ -\sqrt{k^2} \sin \theta \\ 0 \\ k_0 \cos \theta \end{pmatrix} \end{aligned} \quad (\text{D.5.15})$$

and

$$\begin{aligned} k_3 \cdot \bar{k} &= \beta_\pi \begin{pmatrix} m_B - k_0 \\ 0 \\ 0 \\ -|\vec{k}| \end{pmatrix} \cdot \begin{pmatrix} |\vec{k}| \cos \theta \\ -\sqrt{k^2} \sin \theta \\ 0 \\ k_0 \cos \theta \end{pmatrix} = \beta_\pi [(m_B - k_0) + k_0] |\vec{k}| \cos \theta \\ &= \beta_\pi m_B |\vec{k}| \cos \theta \\ &= \frac{\beta_\pi}{2} \sqrt{\lambda} \cos \theta, \end{aligned} \quad (\text{D.5.16})$$

which is the relation from Equation (6.45) and from [158].

Bibliography

- [1] J. J. Thomson. Cathode rays. *Phil. Mag. Ser.5*, 44:293–316, 1897.
- [2] Murray Gell-Mann. A Schematic Model of Baryons and Mesons. *Phys. Lett.*, 8:214–215, 1964.
- [3] G. Zweig. An SU(3) model for strong interaction symmetry and its breaking. Version 1. 1964.
- [4] S. L. Glashow. Partial Symmetries of Weak Interactions. *Nucl. Phys.*, 22:579–588, 1961.
- [5] Abdus Salam. Weak and Electromagnetic Interactions. *Conf. Proc.*, C680519:367–377, 1968.
- [6] Steven Weinberg. A Model of Leptons. *Phys. Rev. Lett.*, 19:1264–1266, 1967.
- [7] A. D. Sakharov. Violation of CP Invariance, c Asymmetry, and Baryon Asymmetry of the Universe. *Pisma Zh. Eksp. Teor. Fiz.*, 5:32–35, 1967. [Usp. Fiz. Nauk161,61(1991)].
- [8] J. F. Donoghue, E. Golowich, and Barry R. Holstein. Dynamics of the standard model. *Camb. Monogr. Part. Phys. Nucl. Phys. Cosmol.*, 2:1–540, 1992. [Camb. Monogr. Part. Phys. Nucl. Phys. Cosmol.35(2014)].
- [9] Michael E. Peskin and Daniel V. Schroeder. *An Introduction to quantum field theory*. Westview Press, 1995.
- [10] Matthew D. Schwartz. *Quantum Field Theory and the Standard Model*. Cambridge University Press, 2014.
- [11] Steven Weinberg. *The Quantum theory of fields. Vol. 1: Foundations*. Cambridge University Press, 2005.
- [12] Steven Weinberg. *The quantum theory of fields. Vol. 2: Modern applications*. Cambridge University Press, 2013.
- [13] Howard Georgi. Lie algebras in particle physics. *Front. Phys.*, 54:1–320, 1999.
- [14] Siegmund Brandt. *The Harvest of a Century*. Oxford University Press, 2009.
- [15] David Griffiths. *Introduction to elementary particles*. 2008.

-
- [16] C. Patrignani et al. Review of Particle Physics. *Chin. Phys.*, C40(10):100001, 2016.
- [17] Peter W. Higgs. Broken Symmetries and the Masses of Gauge Bosons. *Phys. Rev. Lett.*, 13:508–509, 1964.
- [18] Peter W. Higgs. Spontaneous Symmetry Breakdown without Massless Bosons. *Phys. Rev.*, 145:1156–1163, 1966.
- [19] Georges Aad et al. Observation of a new particle in the search for the Standard Model Higgs boson with the ATLAS detector at the LHC. *Phys. Lett.*, B716:1–29, 2012, [arXiv:1207.7214 \[hep-ex\]](#).
- [20] Serguei Chatrchyan et al. Observation of a new boson at a mass of 125 GeV with the CMS experiment at the LHC. *Phys. Lett.*, B716:30–61, 2012, [arXiv:1207.7235 \[hep-ex\]](#).
- [21] C. S. Wu, E. Ambler, R. W. Hayward, D. D. Hoppes, and R. P. Hudson. Experimental Test of Parity Conservation in Beta Decay. *Phys. Rev.*, 105:1413–1414, 1957.
- [22] Nicola Cabibbo. Unitary Symmetry and Leptonic Decays. *Phys. Rev. Lett.*, 10:531–533, 1963. [[648\(1963\)](#)].
- [23] Makoto Kobayashi and Toshihide Maskawa. CP Violation in the Renormalizable Theory of Weak Interaction. *Prog. Theor. Phys.*, 49:652–657, 1973.
- [24] Lincoln Wolfenstein. Parametrization of the Kobayashi-Maskawa Matrix. *Phys. Rev. Lett.*, 51:1945, 1983.
- [25] Andrzej J. Buras, Markus E. Lautenbacher, and Gaby Ostermaier. Waiting for the top quark mass, $K^+ \rightarrow \pi^+ \nu \bar{\nu}$, $B_s^0 - \bar{B}_s^0$ mixing and CP asymmetries in B decays. *Phys. Rev.*, D50:3433–3446, 1994, [arXiv:hep-ph/9403384 \[hep-ph\]](#).
- [26] J. Charles, Andreas Hocker, H. Lacker, S. Laplace, F. R. Le Diberder, J. Malcles, J. Ocariz, M. Pivk, and L. Roos. CP violation and the CKM matrix: Assessing the impact of the asymmetric B factories. *Eur. Phys. J.*, C41(1):1–131, 2005, [arXiv:hep-ph/0406184 \[hep-ph\]](#).
- [27] J. H. Christenson, J. W. Cronin, V. L. Fitch, and R. Turlay. Evidence for the 2π Decay of the K_2^0 Meson. *Phys. Rev. Lett.*, 13:138–140, 1964.
- [28] Ikaros I. Y. Bigi and A. I. Sanda. CP violation. *Camb. Monogr. Part. Phys. Nucl. Phys. Cosmol.*, 9:1–382, 2000.
- [29] K. Anikeev et al. B physics at the Tevatron: Run II and beyond. In *Workshop on B Physics at the Tevatron: Run II and Beyond Batavia, Illinois, September 23-25, 1999*, 2001, [arXiv:hep-ph/0201071 \[hep-ph\]](#).

- [30] A. J. Bevan et al. The Physics of the B Factories. *Eur. Phys. J.*, C74:3026, 2014, [arXiv:1406.6311 \[hep-ex\]](#).
- [31] T. Muta. Foundations of quantum chromodynamics: An Introduction to perturbative methods in gauge theories. *World Sci. Lect. Notes Phys.*, 5:1–409, 1987.
- [32] Walter Greiner, Stefan Schramm, and Eckart Stein. *Quantum chromodynamics*. 2007.
- [33] David J. Gross and Frank Wilczek. Ultraviolet Behavior of Nonabelian Gauge Theories. *Phys. Rev. Lett.*, 30:1343–1346, 1973.
- [34] H. David Politzer. Reliable Perturbative Results for Strong Interactions? *Phys. Rev. Lett.*, 30:1346–1349, 1973.
- [35] Tobias Huber, Enrico Lunghi, Mikolaj Misiak, and Daniel Wyler. Electromagnetic logarithms in $\bar{B} \rightarrow X_s l^+ l^-$. *Nucl. Phys.*, B740:105–137, 2006, [arXiv:hep-ph/0512066 \[hep-ph\]](#).
- [36] Thomas Appelquist and J. Carazzone. Infrared Singularities and Massive Fields. *Phys. Rev.*, D11:2856, 1975.
- [37] Enrico Fermi. Tentativo di una teoria dell'emissione dei raggi beta. *Ric. Sci.*, 4:491–495, 1933.
- [38] E. Fermi. An attempt of a theory of beta radiation. 1. *Z. Phys.*, 88:161–177, 1934.
- [39] K. G. Wilson and John B. Kogut. The Renormalization group and the epsilon expansion. *Phys. Rept.*, 12:75–200, 1974.
- [40] Estia Eichten and Brian Russell Hill. An Effective Field Theory for the Calculation of Matrix Elements Involving Heavy Quarks. *Phys. Lett.*, B234:511–516, 1990.
- [41] Matthias Neubert. Heavy quark symmetry. *Phys. Rept.*, 245:259–396, 1994, [arXiv:hep-ph/9306320 \[hep-ph\]](#).
- [42] Aneesh V. Manohar and Mark B. Wise. *Heavy quark physics*, volume 10. 2000.
- [43] T. Mannel. *Effective Field Theories in Flavor Physics*, volume 203. 2004.
- [44] A. G. Grozin. Heavy quark effective theory. *Springer Tracts Mod. Phys.*, 201:1–213, 2004.
- [45] F. Bloch and A. Nordsieck. Note on the Radiation Field of the electron. *Phys. Rev.*, 52:54–59, 1937.

-
- [46] Howard Georgi. An Effective Field Theory for Heavy Quarks at Low-energies. *Phys. Lett.*, B240:447–450, 1990.
- [47] Thomas Mannel, Winston Roberts, and Zbigniew Ryzak. A Derivation of the heavy quark effective Lagrangian from QCD. *Nucl. Phys.*, B368:204–220, 1992.
- [48] Adam F. Falk, Howard Georgi, Benjamin Grinstein, and Mark B. Wise. Heavy Meson Form-factors From QCD. *Nucl. Phys.*, B343:1–13, 1990.
- [49] Nathan Isgur and Mark B. Wise. Weak Decays of Heavy Mesons in the Static Quark Approximation. *Phys. Lett.*, B232:113–117, 1989.
- [50] Nathan Isgur and Mark B. Wise. WEAK TRANSITION FORM-FACTORS BETWEEN HEAVY MESONS. *Phys. Lett.*, B237:527–530, 1990.
- [51] Michael E. Luke and Aneesh V. Manohar. Reparametrization invariance constraints on heavy particle effective field theories. *Phys. Lett.*, B286:348–354, 1992, [arXiv:hep-ph/9205228](#) [hep-ph].
- [52] Yu-Qi Chen. On the reparametrization invariance in heavy quark effective theory. *Phys. Lett.*, B317:421–427, 1993.
- [53] Michael E. Luke. Effects of subleading operators in the heavy quark effective theory. *Phys. Lett.*, B252:447–455, 1990.
- [54] Adam F. Falk and Matthias Neubert. Second order power corrections in the heavy quark effective theory. 1. Formalism and meson form-factors. *Phys. Rev.*, D47:2965–2981, 1993, [arXiv:hep-ph/9209268](#) [hep-ph].
- [55] Peter L. Cho and Benjamin Grinstein. Heavy hadron form-factor relations for $m_c \neq \infty$ and $\alpha_s(m_c) \neq 0$. *Phys. Lett.*, B285:153–159, 1992, [arXiv:hep-ph/9204237](#) [hep-ph].
- [56] M. Ademollo and Raoul Gatto. Nonrenormalization Theorem for the Strangeness Violating Vector Currents. *Phys. Rev. Lett.*, 13:264–265, 1964.
- [57] C. G. Bollini and J. J. Giambiagi. Lowest order divergent graphs in n-dimensional space. *Phys. Lett.*, 40B:566–568, 1972.
- [58] Andrey Grozin. Lectures on QED and QCD. In *3rd Dubna International Advanced School of Theoretical Physics Dubna, Russia, January 29-February 6, 2005*, pages 1–156, 2005, [arXiv:hep-ph/0508242](#) [hep-ph].
- [59] Gerhard Buchalla. Renormalization of $\Delta B = 2$ transitions in the static limit beyond leading logarithms. *Phys. Lett.*, B395:364–368, 1997, [arXiv:hep-ph/9608232](#) [hep-ph].

-
- [60] Marco Ciuchini, E. Franco, and V. Gimenez. Next-to-leading order renormalization of the $\Delta B = 2$ operators in the static theory. *Phys. Lett.*, B388:167–172, 1996, [arXiv:hep-ph/9608204](#) [hep-ph].
- [61] Jonathan M. Flynn, Oscar F. Hernandez, and Brian Russell Hill. Renormalization of four fermion operators determining $B - \bar{B}$ mixing on the lattice. *Phys. Rev.*, D43:3709–3714, 1991.
- [62] Andrzej J. Buras, Matthias Jamin, and Peter H. Weisz. Leading and Next-to-leading QCD Corrections to ϵ Parameter and $B^0 - \bar{B}^0$ Mixing in the Presence of a Heavy Top Quark. *Nucl. Phys.*, B347:491–536, 1990.
- [63] Nikolai Uraltsev. Heavy quark expansion in beauty: Recent successes and problems. In *Continuous advances in QCD. Proceedings, Conference, Minneapolis, USA, May 13-16, 2004*, pages 100–114, 2004, [arXiv:hep-ph/0409125](#) [hep-ph].
- [64] Florian U. Bernlochner, Zoltan Ligeti, and Sascha Turczyk. A Proposal to solve some puzzles in semileptonic B decays. *Phys. Rev.*, D85:094033, 2012, [arXiv:1202.1834](#) [hep-ph].
- [65] Ming Lu, Mark B. Wise, and Nathan Isgur. Heavy quark symmetry and $D_1(2420) \rightarrow D^* \pi$ decay. *Phys. Rev.*, D45:1553–1556, 1992.
- [66] Adam K. Leibovich, Zoltan Ligeti, Iain W. Stewart, and Mark B. Wise. Semileptonic B decays to excited charmed mesons. *Phys. Rev.*, D57:308–330, 1998, [arXiv:hep-ph/9705467](#) [hep-ph].
- [67] Adam F. Falk and Thomas Mehen. Excited heavy mesons beyond leading order in the heavy quark expansion. *Phys. Rev.*, D53:231–240, 1996, [arXiv:hep-ph/9507311](#) [hep-ph].
- [68] Ulrich Kilian, Jurgen G. Korner, and Dan Pirjol. Excited charmed mesons in chiral perturbation theory. *Phys. Lett.*, B288:360–366, 1992.
- [69] P. Colangelo, F. De Fazio, G. Nardulli, N. Di Bartolomeo, and Raoul Gatto. Strong coupling of excited heavy mesons. *Phys. Rev.*, D52:6422–6434, 1995, [arXiv:hep-ph/9506207](#) [hep-ph].
- [70] Rebecca Klein, Thomas Mannel, Farnoush Shahriaran, and Danny van Dyk. $1/m$ Corrections for Orbitally Excited Heavy Mesons and the $1/2 - 3/2$ Puzzle. *Phys. Rev.*, D91(9):094034, 2015, [arXiv:1503.00569](#) [hep-ph].
- [71] Nathan Isgur and Mark B. Wise. Spectroscopy with heavy quark symmetry. *Phys. Rev. Lett.*, 66:1130–1133, 1991.
- [72] K. A. Olive et al. Review of Particle Physics. *Chin. Phys.*, C38:090001, 2014.

- [73] Bernard Aubert et al. Dalitz Plot Analysis of $B^- \rightarrow D^+\pi^-\pi^-$. *Phys. Rev.*, D79:112004, 2009, arXiv:0901.1291 [hep-ex].
- [74] Kazuo Abe et al. Study of $B^- \rightarrow D^{**0}\pi^- (D^{**0} \rightarrow D^{(*)+}\pi^-)$ decays. *Phys. Rev.*, D69:112002, 2004, arXiv:hep-ex/0307021 [hep-ex].
- [75] J. M. Link et al. Measurement of masses and widths of excited charm mesons D_2^* and evidence for broad states. *Phys. Lett.*, B586:11–20, 2004, arXiv:hep-ex/0312060 [hep-ex].
- [76] H. Abramowicz et al. Production of the excited charm mesons D_1 and D_2^* at HERA. *Nucl. Phys.*, B866:229–254, 2013, arXiv:1208.4468 [hep-ex].
- [77] P. del Amo Sanchez et al. Observation of new resonances decaying to $D\pi$ and $D^*\pi$ in inclusive e^+e^- collisions near $\sqrt{s} = 10.58$ GeV. *Phys. Rev.*, D82:111101, 2010, arXiv:1009.2076 [hep-ex].
- [78] Kazuo Abe et al. Observation of the $D_1(2420) \rightarrow D\pi^+\pi^-$ decays. *Phys. Rev. Lett.*, 94:221805, 2005, arXiv:hep-ex/0410091 [hep-ex].
- [79] Bernard Aubert et al. Study of the decay $\bar{B}^0 \rightarrow D^{*+}\omega\pi^-$. *Phys. Rev.*, D74:012001, 2006, arXiv:hep-ex/0604009 [hep-ex].
- [80] Pietro Biancofiore, Pietro Colangelo, and Fulvia De Fazio. On the anomalous enhancement observed in $B \rightarrow D^{(*)}\tau\bar{\nu}_\tau$ decays. *Phys. Rev.*, D87(7):074010, 2013, arXiv:1302.1042 [hep-ph].
- [81] Johannes Heinonen and Thomas Mannel. Improved Estimates for the Parameters of the Heavy Quark Expansion. *Nucl. Phys.*, B889:46–63, 2014, arXiv:1407.4384 [hep-ph].
- [82] V. Morenas, A. Le Yaouanc, L. Oliver, O. Pene, and J. C. Raynal. Quantitative predictions for B semileptonic decays into D , D^* and the orbitally excited D^{**} in quark models à la Bakamjian-Thomas. *Phys. Rev.*, D56:5668–5680, 1997, arXiv:hep-ph/9706265 [hep-ph].
- [83] S. Godfrey and Nathan Isgur. Mesons in a Relativized Quark Model with Chromodynamics. *Phys. Rev.*, D32:189–231, 1985.
- [84] Sinisa Veseli and Isard Dunietz. Decay constants of p and d wave heavy light mesons. *Phys. Rev.*, D54:6803–6810, 1996, arXiv:hep-ph/9607293 [hep-ph].
- [85] P. Cea, P. Colangelo, L. Cosmai, and G. Nardulli. Decay Constants of Heavy Mesons From a QCD Relativistic Potential Model. *Phys. Lett.*, B206:691–695, 1988.
- [86] P. Colangelo, G. Nardulli, and M. Pietroni. Relativistic bound state effects in heavy meson physics. *Phys. Rev.*, D43:3002–3010, 1991.

- [87] Nathan Isgur, Daryl Scora, Benjamin Grinstein, and Mark B. Wise. Semileptonic B and D Decays in the Quark Model. *Phys. Rev.*, D39:799–818, 1989.
- [88] Ikaros I. Y. Bigi, Mikhail A. Shifman, and N. Uraltsev. Aspects of heavy quark theory. *Ann. Rev. Nucl. Part. Sci.*, 47:591–661, 1997, [arXiv:hep-ph/9703290](#) [hep-ph].
- [89] Y. Amhis et al. Averages of b -hadron, c -hadron, and τ -lepton properties as of summer 2014. 2014, [arXiv:1412.7515](#) [hep-ex].
- [90] R Aaij et al. Precision measurement of the B_s^0 - \bar{B}_s^0 oscillation frequency with the decay $B_s^0 \rightarrow D_s^- \pi^+$. *New J. Phys.*, 15:053021, 2013, [arXiv:1304.4741](#) [hep-ex].
- [91] Murray Gell-Mann and A. Pais. Behavior of neutral particles under charge conjugation. *Phys. Rev.*, 97:1387–1389, 1955.
- [92] S. L. Glashow, J. Iliopoulos, and L. Maiani. Weak Interactions with Lepton-Hadron Symmetry. *Phys. Rev.*, D2:1285–1292, 1970.
- [93] S. W. Herb et al. Observation of a Dimuon Resonance at 9.5-GeV in 400-GeV Proton-Nucleus Collisions. *Phys. Rev. Lett.*, 39:252–255, 1977.
- [94] C. Albajar et al. Search for $B^0 - \bar{B}^0$ Oscillations at the CERN Proton - anti-Proton Collider. 2. *Phys. Lett.*, B186:247–254, 1987. [Erratum: *Phys. Lett.*B197,565(1987)].
- [95] H. Albrecht et al. Observation of $B^0 - \bar{B}^0$ Mixing. *Phys. Lett.*, B192:245–252, 1987.
- [96] A. Abulencia et al. Observation of $B_s^0 - \bar{B}_s^0$ Oscillations. *Phys. Rev. Lett.*, 97:242003, 2006, [arXiv:hep-ex/0609040](#) [hep-ex].
- [97] Andrey G. Grozin, Rebecca Klein, Thomas Mannel, and Alexei A. Pivovarov. $B^0 - \bar{B}^0$ mixing at next-to-leading order. *Phys. Rev.*, D94(3):034024, 2016, [arXiv:1606.06054](#) [hep-ph].
- [98] Alexander Lenz and Ulrich Nierste. Theoretical update of $B_s - \bar{B}_s$ mixing. *JHEP*, 06:072, 2007, [arXiv:hep-ph/0612167](#) [hep-ph].
- [99] Ulrich Nierste. Three Lectures on Meson Mixing and CKM phenomenology. In *Heavy quark physics. Proceedings, Helmholtz International School, HQP08, Dubna, Russia, August 11-21, 2008*, pages 1–38, 2009, [arXiv:0904.1869](#) [hep-ph].
- [100] A. Lenz, U. Nierste, J. Charles, S. Descotes-Genon, A. Jantsch, C. Kaufhold, H. Lacker, S. Monteil, V. Niess, and S. T’Jampens. Anatomy of New Physics in $B - \bar{B}$ mixing. *Phys. Rev.*, D83:036004, 2011, [arXiv:1008.1593](#) [hep-ph].

- [101] Ulrich Nierste. B Mixing in the Standard Model and Beyond. In *7th International Workshop on the CKM Unitarity Triangle (CKM 2012) Cincinnati, Ohio, USA, September 28-October 2, 2012*, 2012, arXiv:1212.5805 [hep-ph].
- [102] Alexander Lenz. Theoretical update of B -Mixing and Lifetimes. In *2012 Electroweak Interactions and Unified Theories: Proceedings of the 47th Rencontres de Moriond on Electroweak Interactions and Unified Theories, La Thuile, March 3-10, 2012*, 2012, arXiv:1205.1444 [hep-ph].
- [103] T. Inami and C. S. Lim. Effects of Superheavy Quarks and Leptons in Low-Energy Weak Processes $K_L \rightarrow \mu\bar{\mu}$, $K^+ \rightarrow \pi^+\nu\bar{\nu}$ and $K^0 \leftrightarrow \bar{K}^0$. *Prog. Theor. Phys.*, 65:297, 1981. [Erratum: *Prog. Theor. Phys.*65,1772(1981)].
- [104] A. Chodos, R. L. Jaffe, K. Johnson, Charles B. Thorn, and V. F. Weisskopf. A New Extended Model of Hadrons. *Phys. Rev.*, D9:3471–3495, 1974.
- [105] K. Johnson. The M.I.T. Bag Model. *Acta Phys. Polon.*, B6:865, 1975.
- [106] Elvira Gamiz, Christine T. H. Davies, G. Peter Lepage, Junko Shigemitsu, and Matthew Wingate. Neutral B Meson Mixing in Unquenched Lattice QCD. *Phys. Rev.*, D80:014503, 2009, arXiv:0902.1815 [hep-lat].
- [107] N. Carrasco et al. B-physics from $N_f = 2$ tmQCD: the Standard Model and beyond. *JHEP*, 03:016, 2014, arXiv:1308.1851 [hep-lat].
- [108] Yasumichi Aoki, Tomomi Ishikawa, Taku Izubuchi, Christoph Lehner, and Amarjit Soni. Neutral B meson mixings and B meson decay constants with static heavy and domain-wall light quarks. *Phys. Rev.*, D91(11):114505, 2015, arXiv:1406.6192 [hep-lat].
- [109] R. J. Dowdall, C. T. H. Davies, R. R. Horgan, G. Peter Lepage, C. J. Monahan, and J. Shigemitsu. B-meson mixing from full lattice QCD with physical u, d, s and c quarks. 2014, arXiv:1411.6989 [hep-lat].
- [110] S. Aoki et al. Review of lattice results concerning low-energy particle physics. *Eur. Phys. J.*, C77(2):112, 2017, arXiv:1607.00299 [hep-lat].
- [111] A. Bazavov et al. $B_{(s)}^0$ -mixing matrix elements from lattice QCD for the Standard Model and beyond. *Phys. Rev.*, D93(11):113016, 2016, arXiv:1602.03560 [hep-lat].
- [112] A. A. Ovchinnikov and A. A. Pivovarov. Estimate of the hadronic matrix element of $B^0 - \bar{B}^0$ mixing using the method of QCD sum rules. *Phys. Lett.*, B207:333–337, 1988. [*Yad. Fiz.*48,189(1988)].
- [113] L. J. Reinders and S. Yazaki. A QCD Sum Rule Calculation of the $B\bar{B}$ Mixing Matrix Element $\langle \bar{B}^0 | O_{\Delta B=2} | B^0 \rangle$. *Phys. Lett.*, B212:245–250, 1988.

- [114] J. G. Korner, A. I. Onishchenko, Alexey A. Petrov, and A. A. Pivovarov. $B^0 - \bar{B}^0$ mixing beyond factorization. *Phys. Rev. Lett.*, 91:192002, 2003, [arXiv:hep-ph/0306032](#) [hep-ph].
- [115] T. Mannel, B. D. Pecjak, and A. A. Pivovarov. Sum rule estimate of the subleading non-perturbative contributions to $B_s - \bar{B}_s$ mixing. *Eur. Phys. J.*, C71:1607, 2011, [arXiv:hep-ph/0703244](#) [HEP-PH].
- [116] Andrey G. Grozin and Roman N. Lee. Three-loop HQET vertex diagrams for $B^0 - \bar{B}^0$ mixing. *JHEP*, 02:047, 2009, [arXiv:0812.4522](#) [hep-ph].
- [117] E. Bagan, Patricia Ball, Vladimir M. Braun, and Hans Gunter Dosch. QCD sum rules in the effective heavy quark theory. *Phys. Lett.*, B278:457–464, 1992.
- [118] Xiang-Dong Ji and M. J. Musolf. Subleading logarithmic mass dependence in heavy meson form-factors. *Phys. Lett.*, B257:409–413, 1991.
- [119] David J. Broadhurst and A. G. Grozin. Two loop renormalization of the effective field theory of a static quark. *Phys. Lett.*, B267:105–110, 1991, [arXiv:hep-ph/9908362](#) [hep-ph].
- [120] V. Gimenez. Two loop calculation of the anomalous dimension of the axial current with static heavy quarks. *Nucl. Phys.*, B375:582–622, 1992.
- [121] Mikhail A. Shifman and M. B. Voloshin. On Annihilation of Mesons Built from Heavy and Light Quark and $\bar{B}^0 \leftrightarrow B^0$ Oscillations. *Sov. J. Nucl. Phys.*, 45:292, 1987. [*Yad. Fiz.*45,463(1987)].
- [122] H. David Politzer and Mark B. Wise. Leading Logarithms of Heavy Quark Masses in Processes with Light and Heavy Quarks. *Phys. Lett.*, B206:681–684, 1988.
- [123] V. Gimenez. Two loop calculation of the anomalous dimension of four fermion operators with static heavy quarks. *Nucl. Phys.*, B401:116–167, 1993.
- [124] K. G. Chetyrkin, A. L. Kataev, A. B. Krasulin, and A. A. Pivovarov. CALCULATION OF THE $K^0 - \bar{K}^0$ MIXING PARAMETER VIA THE QCD SUM RULES AT FINITE ENERGIES. *Phys. Lett.*, B174:104, 1986, [arXiv:hep-ph/0103230](#) [hep-ph].
- [125] Stephan Narison and A. A. Pivovarov. QSSR estimate of the B_B parameter at next-to-leading order. *Phys. Lett.*, B327:341–346, 1994, [arXiv:hep-ph/9403225](#) [hep-ph].
- [126] Matthias Neubert. Heavy meson form-factors from QCD sum rules. *Phys. Rev.*, D45:2451–2466, 1992.
- [127] R. N. Lee. Presenting LiteRed: a tool for the Loop InTEgrals REDuction. 2012, [arXiv:1212.2685](#) [hep-ph].

- [128] Roman N. Lee. LiteRed 1.4: a powerful tool for reduction of multiloop integrals. *J. Phys. Conf. Ser.*, 523:012059, 2014, [arXiv:1310.1145](#) [hep-ph].
- [129] David J. Broadhurst and A. G. Grozin. Operator product expansion in static quark effective field theory: Large perturbative correction. *Phys. Lett.*, B274:421–427, 1992, [arXiv:hep-ph/9908363](#) [hep-ph].
- [130] V. A. Novikov, L. B. Okun, Mikhail A. Shifman, A. I. Vainshtein, M. B. Voloshin, and Valentin I. Zakharov. Sum Rules for Charmonium and Charmed Mesons Decay Rates in Quantum Chromodynamics. *Phys. Rev. Lett.*, 38:626, 1977. [Erratum: *Phys. Rev. Lett.* 38,791(1977)].
- [131] A. A. Ovchinnikov and A. A. Pivovarov. QCD sum rule calculation of the quark gluon condensate. *Sov. J. Nucl. Phys.*, 48:721–723, 1988. [*Yad. Fiz.* 48,1135(1988)].
- [132] A. A. Pivovarov. Determination of the numerical magnitude of the mixed quark - gluon vacuum condensate. *Bull. Lebedev Phys. Inst.*, 5:1–3, 1991. [Kratk. Soobshch. *Fiz.* 5,3(1991)].
- [133] Andrey G. Grozin, Thomas Mannel, and Alexei A. Pivovarov. Towards a Next-to-Next-to-Leading Order analysis of matching in B^0 - \bar{B}^0 mixing. 2017, [arXiv:1706.05910](#) [hep-ph].
- [134] Patrick Gelhausen, Alexander Khodjamirian, Alexei A. Pivovarov, and Denis Rosenthal. Decay constants of heavy-light vector mesons from QCD sum rules. *Phys. Rev.*, D88:014015, 2013, [arXiv:1305.5432](#) [hep-ph]. [Erratum: *Phys. Rev.* D91,099901(2015)].
- [135] M. Beneke, G. Buchalla, M. Neubert, and Christopher T. Sachrajda. QCD factorization for $B \rightarrow \pi\pi$ decays: Strong phases and CP violation in the heavy quark limit. *Phys. Rev. Lett.*, 83:1914–1917, 1999, [arXiv:hep-ph/9905312](#) [hep-ph].
- [136] M. Beneke, G. Buchalla, M. Neubert, and Christopher T. Sachrajda. QCD factorization for exclusive, nonleptonic B meson decays: General arguments and the case of heavy light final states. *Nucl. Phys.*, B591:313–418, 2000, [arXiv:hep-ph/0006124](#) [hep-ph].
- [137] Roel Aaij et al. Measurements of CP violation in the three-body phase space of charmless B^\pm decays. *Phys. Rev.*, D90(11):112004, 2014, [arXiv:1408.5373](#) [hep-ex].
- [138] J. P. Lees et al. Evidence for CP violation in $B^+ \rightarrow K^*(892)^+\pi^0$ from a Dalitz plot analysis of $B^+ \rightarrow K_S^0\pi^+\pi^0$ decays. 2015, [arXiv:1501.00705](#) [hep-ex].
- [139] Bernard Aubert et al. Dalitz Plot Analysis of $B^\pm \rightarrow \pi^\pm\pi^\pm\pi^\mp$ Decays. *Phys. Rev.*, D79:072006, 2009, [arXiv:0902.2051](#) [hep-ex].

-
- [140] R Aaij et al. Measurement of CP violation in the phase space of $B^\pm \rightarrow K^\pm \pi^+ \pi^-$ and $B^\pm \rightarrow K^\pm K^+ K^-$ decays. *Phys. Rev. Lett.*, 111:101801, 2013, [arXiv:1306.1246](#) [hep-ex].
- [141] Roel Aaij et al. Measurement of CP violation in the phase space of $B^\pm \rightarrow K^+ K^- \pi^\pm$ and $B^\pm \rightarrow \pi^+ \pi^- \pi^\pm$ decays. *Phys. Rev. Lett.*, 112(1):011801, 2014, [arXiv:1310.4740](#) [hep-ex].
- [142] A. Garmash et al. Evidence for large direct CP violation in $B^\pm \rightarrow \rho(770)^0 K^\pm$ from analysis of the three-body charmless $B^\pm \rightarrow K^\pm \pi^\pm \pi^\mp$ decay. *Phys. Rev. Lett.*, 96:251803, 2006, [arXiv:hep-ex/0512066](#) [hep-ex].
- [143] R. M. Sternheimer and S. J. Lindenbaum. Extension of the Isobaric Nucleon Model for Pion Production in Pion-Nucleon, Nucleon-Nucleon, and Antinucleon-Nucleon Interactions. *Phys. Rev.*, 123:333–376, 1961.
- [144] D. Herndon, P. Soding, and R. J. Cashmore. A GENERALIZED ISOBAR MODEL FORMALISM. *Phys. Rev.*, D11:3165, 1975.
- [145] Eugene P. Wigner. Resonance Reactions and Anomalous Scattering. *Phys. Rev.*, 70:15–33, 1946.
- [146] S. U. Chung, J. Brose, R. Hackmann, E. Klempt, S. Spanier, and C. Strassburger. Partial wave analysis in K matrix formalism. *Annalen Phys.*, 4:404–430, 1995.
- [147] Nicolas Rey-Le Lorier, Maxime Imbeault, and David London. Diagrammatic Analysis of Charmless Three-Body B Decays. *Phys. Rev.*, D84:034040, 2011, [arXiv:1011.4972](#) [hep-ph].
- [148] Maxime Imbeault and David London. SU(3) Breaking in Charmless B Decays. *Phys. Rev.*, D84:056002, 2011, [arXiv:1106.2511](#) [hep-ph].
- [149] Chuan-Hung Chen and Hsiang-nan Li. Three body nonleptonic B decays in perturbative QCD. *Phys. Lett.*, B561:258–265, 2003, [arXiv:hep-ph/0209043](#) [hep-ph].
- [150] Susanne Kränkl, Thomas Mannel, and Javier Virto. Three-body nonleptonic B decays and QCD factorization. *Nucl. Phys.*, B899:247–264, 2015, [arXiv:1505.04111](#) [hep-ph].
- [151] Rebecca Klein, Thomas Mannel, Javier Virto, and K. Keri Vos. CP Violation in Multibody B Decays from QCD Factorization. 2017, [arXiv:1708.02047](#) [hep-ph].
- [152] Gerhard Buchalla, Andrzej J. Buras, and Markus E. Lautenbacher. Weak decays beyond leading logarithms. *Rev. Mod. Phys.*, 68:1125–1144, 1996, [arXiv:hep-ph/9512380](#) [hep-ph].

- [153] G. Peter Lepage and Stanley J. Brodsky. Exclusive Processes in Perturbative Quantum Chromodynamics. *Phys. Rev.*, D22:2157, 1980.
- [154] A. V. Efremov and A. V. Radyushkin. Factorization and Asymptotical Behavior of Pion Form-Factor in QCD. *Phys. Lett.*, 94B:245–250, 1980.
- [155] Maxim V. Polyakov. Hard exclusive electroproduction of two pions and their resonances. *Nucl. Phys.*, B555:231, 1999, [arXiv:hep-ph/9809483](#) [hep-ph].
- [156] M. Diehl, T. Gousset, B. Pire, and O. Teryaev. Probing partonic structure in $\gamma^*\gamma \rightarrow \pi\pi$ near threshold. *Phys. Rev. Lett.*, 81:1782–1785, 1998, [arXiv:hep-ph/9805380](#) [hep-ph].
- [157] M. Diehl. Generalized parton distributions. *Phys. Rept.*, 388:41–277, 2003, [arXiv:hep-ph/0307382](#) [hep-ph].
- [158] Sven Faller, Thorsten Feldmann, Alexander Khodjamirian, Thomas Mannel, and Danny van Dyk. Disentangling the Decay Observables in $B^- \rightarrow \pi^+\pi^-\ell^-\bar{\nu}_\ell$. *Phys. Rev.*, D89(1):014015, 2014, [arXiv:1310.6660](#) [hep-ph].
- [159] J. P. Dedonder, A. Furman, R. Kaminski, L. Lesniak, and B. Loiseau. S-, P- and D-wave $\pi\pi$ final state interactions and CP violation in $B^\pm \rightarrow \pi^\pm\pi^\mp\pi^\pm$ decays. *Acta Phys. Polon.*, B42:2013, 2011, [arXiv:1011.0960](#) [hep-ph].
- [160] M. Beneke, G. Buchalla, M. Neubert, and Christopher T. Sachrajda. QCD factorization in $B \rightarrow \pi K, \pi\pi$ decays and extraction of Wolfenstein parameters. *Nucl. Phys.*, B606:245–321, 2001, [arXiv:hep-ph/0104110](#) [hep-ph].
- [161] O. Shekhovtsova, T. Przedzinski, P. Roig, and Z. Was. Resonance chiral Lagrangian currents and τ decay Monte Carlo. *Phys. Rev.*, D86:113008, 2012, [arXiv:1203.3955](#) [hep-ph].
- [162] C. Hanhart. A New Parameterization for the Pion Vector Form Factor. *Phys. Lett.*, B715:170–177, 2012, [arXiv:1203.6839](#) [hep-ph].
- [163] J. P. Lees et al. Precise Measurement of the $e^+e^- \rightarrow \pi^+\pi^-(\gamma)$ Cross Section with the Initial-State Radiation Method at BABAR. *Phys. Rev.*, D86:032013, 2012, [arXiv:1205.2228](#) [hep-ex].
- [164] E. Arganda, M. J. Herrero, and J. Portoles. Lepton flavour violating semileptonic tau decays in constrained MSSM-seesaw scenarios. *JHEP*, 06:079, 2008, [arXiv:0803.2039](#) [hep-ph].
- [165] Alejandro Celis, Vincenzo Cirigliano, and Emilie Passemar. Lepton flavor violation in the Higgs sector and the role of hadronic τ -lepton decays. *Phys. Rev.*, D89:013008, 2014, [arXiv:1309.3564](#) [hep-ph].

- [166] J. T. Daub, C. Hanhart, and B. Kubis. A model-independent analysis of final-state interactions in $\bar{B}_{d/s}^0 \rightarrow J/\psi\pi\pi$. *JHEP*, 02:009, 2016, [arXiv:1508.06841](#) [hep-ph].
- [167] M. Beneke and T. Feldmann. Symmetry breaking corrections to heavy to light B meson form-factors at large recoil. *Nucl. Phys.*, B592:3–34, 2001, [arXiv:hep-ph/0008255](#) [hep-ph].
- [168] I. Sentitemsu Imsong, Alexander Khodjamirian, Thomas Mannel, and Danny van Dyk. Extrapolation and unitarity bounds for the $B \rightarrow \pi$ form factor. *JHEP*, 02:126, 2015, [arXiv:1409.7816](#) [hep-ph].
- [169] Christian Hambrock and Alexander Khodjamirian. Form factors in $\bar{B}^0 \rightarrow \pi\pi\ell\bar{\nu}_\ell$ from QCD light-cone sum rules. *Nucl. Phys.*, B905:373–390, 2016, [arXiv:1511.02509](#) [hep-ph].
- [170] Shan Cheng, Alexander Khodjamirian, and Javier Virto. $B \rightarrow \pi\pi$ Form Factors from Light-Cone Sum Rules with B -meson Distribution Amplitudes. *JHEP*, 05:157, 2017, [arXiv:1701.01633](#) [hep-ph].
- [171] Shan Cheng, Alexander Khodjamirian, and Javier Virto. Timelike-helicity $B \rightarrow \pi\pi$ form factor from light-cone sum rules with dipion distribution amplitudes. *Phys. Rev.*, D96(5):051901, 2017, [arXiv:1709.00173](#) [hep-ph].
- [172] Martin Beneke and Matthias Neubert. QCD factorization for $B \rightarrow PP$ and $B \rightarrow PV$ decays. *Nucl. Phys.*, B675:333–415, 2003, [arXiv:hep-ph/0308039](#) [hep-ph].
- [173] Aoife Bharucha, David M. Straub, and Roman Zwicky. $B \rightarrow V\ell^+\ell^-$ in the Standard Model from light-cone sum rules. *JHEP*, 08:098, 2016, [arXiv:1503.05534](#) [hep-ph].
- [174] Patricia Ball and Roman Zwicky. $B_{d,s} \rightarrow \rho, \omega, K^*, \phi$ decay form-factors from light-cone sum rules revisited. *Phys. Rev.*, D71:014029, 2005, [arXiv:hep-ph/0412079](#) [hep-ph].
- [175] Hai-Yang Cheng, Chun-Khiang Chua, and Kwei-Chou Yang. Charmless hadronic B decays involving scalar mesons: Implications to the nature of light scalar mesons. *Phys. Rev.*, D73:014017, 2006, [arXiv:hep-ph/0508104](#) [hep-ph].
- [176] Patrick Koppenburg and Sébastien Descotes-Genon. The CKM Parameters. 2017, [arXiv:1702.08834](#) [hep-ex].
- [177] A. G. Grozin. Lectures on perturbative HQET.1. 2000, [arXiv:hep-ph/0008300](#) [hep-ph].

-
- [178] K. G. Chetyrkin and F. V. Tkachov. Integration by Parts: The Algorithm to Calculate beta Functions in 4 Loops. *Nucl. Phys.*, B192:159–204, 1981.
- [179] F. V. Tkachov. A Theorem on Analytical Calculability of Four Loop Renormalization Group Functions. *Phys. Lett.*, 100B:65–68, 1981.
- [180] Andrey G. Grozin. Lectures on multiloop calculations. *Int. J. Mod. Phys.*, A19:473–520, 2004, [arXiv:hep-ph/0307297](https://arxiv.org/abs/hep-ph/0307297) [hep-ph].
- [181] R. H. Dalitz. On the analysis of tau-meson data and the nature of the tau-meson. *Phil. Mag. Ser. 7*, 44:1068–1080, 1953.

Danksagung

An dieser Stelle möchte ich mich bei einigen Leuten bedanken die zu dieser Arbeit beigetragen haben.

Zuerst möchte ich mich bei Prof. Dr. Thomas Mannel für die Unterstützung bedanken und dafür, dass er es mir überhaupt erst ermöglicht hat diese Arbeit zu schreiben. Desweiteren möchte ich Prof. Dr. Alexander Khodjamirian dafür danken, dass er sich bereit erklärt hat Zweitgutachter zu sein.

Ein ganz besonderer Dank gilt PD Dr. Tobias Huber, der geduldig die gesamte Arbeit Korrektur gelesen hat und immer ein offenes Ohr für meine Fragen hatte. Zusätzlich bedanke ich mich für die Unterstützung von Dr. Danny van Dyk und Dr. K. Keri Vos.

Mein Dank geht des Weiteren an die Arbeitsgruppe der Theoretischen Physik I in Siegen, die mir in den letzten Jahren ein Zuhause gegeben hat. Insbesondere möchte ich mich bei Dr. Björn O. Lange bedanken, der immer offen für Fragen war. Zusätzlich geht mein Dank an alle Freunde, Kommilitonen und meine WG, die mich während des Studiums begleitet haben.

Ich möchte mich außerdem bei Michael J. Bowman, Ed.D., bedanken, der vor langer Zeit mein Interesse an Physik geweckt hat. Ohne ihn wäre ich womögliche einen anderen Weg eingeschlagen.

Zu guter Letzt geht der größte Dank an meine Familie und meinen Freund Marcus. Ohne ihre Unterstützung während meines Studiums wäre diese Arbeit nicht möglich gewesen.